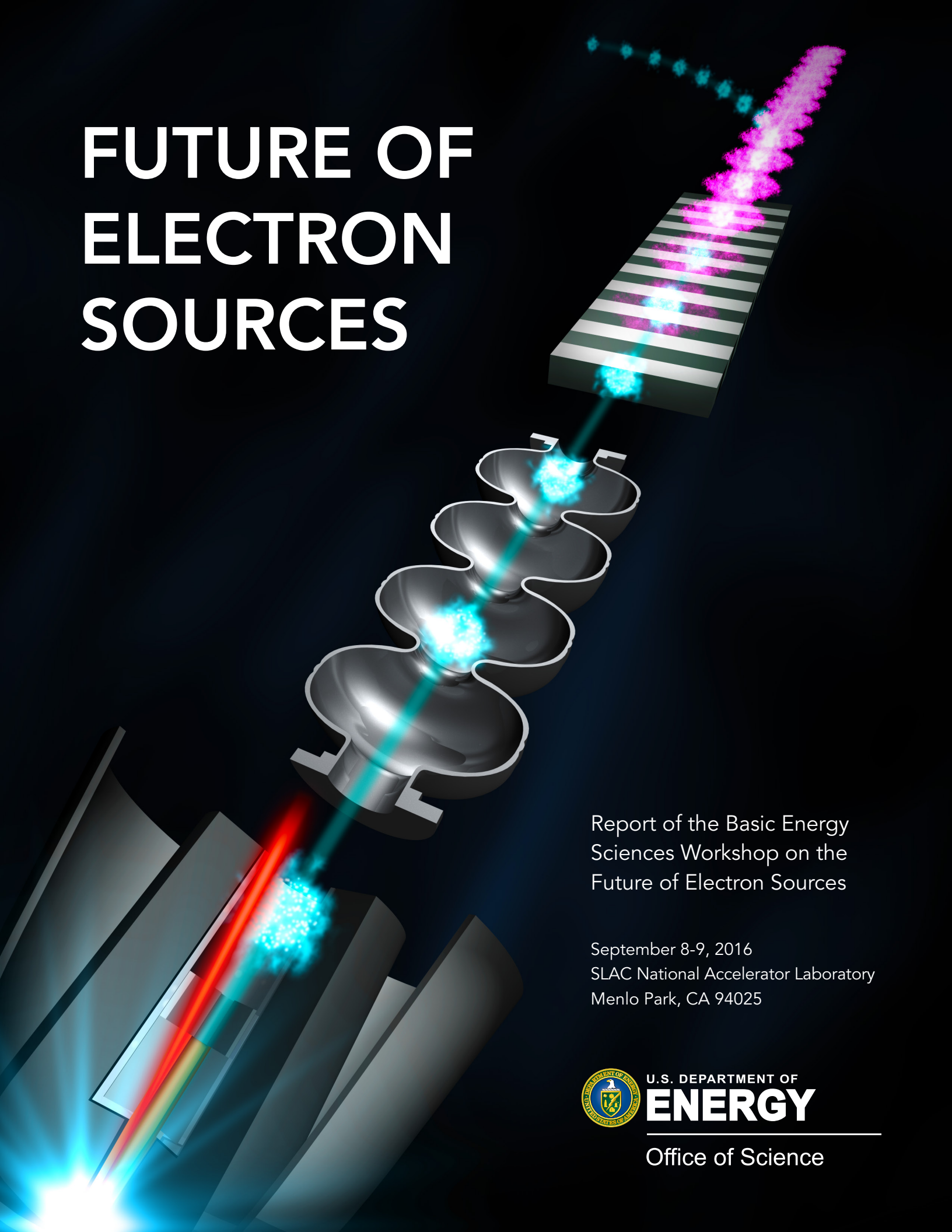


# FUTURE OF ELECTRON SOURCES



Report of the Basic Energy  
Sciences Workshop on the  
Future of Electron Sources

September 8-9, 2016  
SLAC National Accelerator Laboratory  
Menlo Park, CA 94025



U.S. DEPARTMENT OF  
**ENERGY**

Office of Science

# FUTURE ELECTRON SOURCES

---

## Report of the Basic Energy Sciences Workshop on the Future of Electron Sources

September 8-9, 2016

SLAC National Accelerator Laboratory, 2575 Sand Hill Road, Menlo Park, CA 94025

### **Workshop Co-Chairs:**

Xijie Wang, SLAC National Accelerator Laboratory

Pietro Musumeci, University of California - Los Angeles

### **DOE/BES Contacts:**

Eliane Lessner, U.S. Department of Energy, Basic Energy Sciences

**Administrative and Editorial Assistance:** Julia Goldstein, SLAC Office of Communications

**Cover Design:** Courtesy of SLAC

### **Disclaimer**

This report was prepared as an account of work sponsored by an agency of the United States Government. Neither the United States Government nor any agency thereof, nor any of their employees, makes any warranty, express or implied, or assumes any legal liability or responsibility for the accuracy, completeness, or usefulness of any information, apparatus, product, or process disclosed, or represents that its use would not infringe privately owned rights. Reference herein to any specific commercial product, process, or service by trade name, trademark, manufacturer, or otherwise, does not necessarily constitute or imply its endorsement, recommendation, or favoring by the United States Government or any agency thereof. The views and opinions of authors expressed herein do not necessarily state or reflect those of the United States Government or any agency thereof.

# TABLE OF CONTENTS

Executive Summary .....	1
1. Electron Sources Scientific Needs for BES X-ray and Electron Scattering Facilities ..	4
1.0. Scientific need for high-repetition hard X-ray FELs and ultrafast electron probes.	4
1.1. Future electron source R&D .....	10
1.2. Technical requirements and brightness scaling law.....	14
2. Panel 1: Science and technology of electron generation.....	24
2.0. Overview .....	24
2.1. Materials development and discovery for reduced transverse emittance .....	27
2.2. Nano-emitters for coherent electron sources .....	31
2.3. Photocathode materials by design.....	34
2.4. Cross-cutting technologies and issues .....	37
3. Panel 2: Continuous Wave Electron Sources.....	41
3.0. Overview .....	41
3.1. VHF NCRF guns.....	45
3.2. High frequency SRF guns .....	47
3.3. VHF SRF guns .....	52
3.4. DC Electron Guns .....	55
4. Panel 3: Pulsed RF photocathode guns .....	59
4.0. Overview .....	59
4.1. Very high gradient injector R&D .....	63
4.2. Injector design and demonstration for advanced applications.....	68
5. Panel 4: Novel Electron Sources.....	73
5.0. Overview .....	73
5.1. Ultra-high gradient (>GV/m) acceleration .....	73
5.2. Advanced beam-manipulation concepts .....	79

5.3. Sources approaching quantum degeneracy .....	83
References .....	89
Appendix A: List of Participants .....	103
Appendix B: Workshop Agenda .....	106

## LIST OF FIGURES

---

Figure 1-1: A unique feature of XFELs is the ability to probe the fastest time scales, providing over three orders of magnitude higher temporal resolution than a synchrotron source. Courtesy of SLAC.....	4
Figure 1-2: The broad scientific reach & impact of XFEL.....	5
Figure 1-3. XFEL output as a function of X-ray photo energy for a charge of 100 pC and 5 different normalized emittance values. ....	7
Figure 1-4: Electron microscopy, exploiting the reduction in electron wavelength with increasing beam voltage, showed steady increases in resolving power for over 70 years. ....	8
Figure 1-5: Elements of an X-ray FEL. ....	15
Figure 1-6: Elements of a relativistic UED beamline. ....	18
Figure 1-7: Schematic of typical ICS.....	20
Figure 1-8: X-ray brightness for proposed U.S. synchrotron radiation sources upgrade. ....	22
Figure 2-1: QE and MTE of alkali antimonide photocathodes operated close to threshold at ambient and cryogenic temperatures. ....	28
Figure 2-2: DFT-evaluated photoemission from Nb(001).....	30
Figure 2-3: (a) Distorted equipotential lines (red) due to varying surface potential and consequently distorted electron trajectories (black). ....	31
Figure 2-4: Configuration of a photo-electron source for microscopy applications with the photocathode back illuminated to produce a sub-micron size electron source.....	33
Figure 2-5: Lensed nano-emitter. Reprinted with permission from [Tsuji, 2016].....	33
Figure 2-6: Micro lenses rotate each of the beamlets in phase space to form a beam with very small volume in phase space implying very low intrinsic emittance. Courtesy of LBNL. ....	34
Figure 2-7: QE vs. response time for photocathodes.....	35
Figure 2-8: Plasmonic structures in the form of nanorods, nanocavities. Courtesy of LANL. ....	36
Figure 2-9: Spatial profile of the UV laser beam for the LCLS photoinjector before and after spatial shaping. Courtesy of SLAC.....	38
Figure 2-10: Quasi-flat-top laser temporal profiles generated through nonlinear spectral phase control of a 1030nm seed oscillator with a transform limited pulse duration of ~300fs. .	38

Figure 3-1: Cornell injector emittance results at 20, 100, and 300 pC. ....	41
Figure 3-2: Superfish simulation showing the electric field distribution inside APEX-2 cavity (left), and the on-axis electric field profile (right). Courtesy of LBNL. ....	46
Figure 3-3: CAD views of APEX, the existing VHF-Gun (top), and of APEX-2, the proposed dual-cell upgraded version (bottom). Courtesy of LBNL. ....	46
Figure 3-4: Drawing of 3.5-cell DC Pierce gun. Courtesy of Peking University. ....	48
Figure 3-5: CAD drawing showing a cross section of the gun at the ELBE facility, with cathode exchanger. Courtesy of HZDR. ....	49
Figure 3-6: Multilayer KEK cathode concept (left, not to scale). ....	50
Figure 3-7: Drawing of the gun with superconducting cathode and picture of the cavity. Courtesy of DESY. ....	51
Figure 3-8: A 3.5-cell cavity with a higher frequency in the final cell for focusing (left). An SRF gun installed at HZDR (right). Courtesy of HZDR. ....	51
Figure 3-9: Drawing of the WiFEL SRF gun, left, and BNL SRF gun, right. ....	53
Figure 3-10 Simulated emittance and bunch length Pareto front of APEX and SRF gun-based injectors, with a conservative assumed intrinsic emittance of 1.0 $\mu\text{m}/\text{mm}$ rms spot size. Courtesy of SLAC. ....	54
Figure 3-11: Measured values of breakdown voltage versus contact gap ....	56
Figure 3-12: A sketch of a gun geometry with an intermediate electrode. Courtesy of KEK and JAEA. ....	56
Figure 3-13: Two 500 kV photoemission DC guns, the compact ERL gun developed at JAEA (left) and the second DC gun developed at KEK (right). Courtesy of KEK and JAEA. ...	57
Figure 4-1: Shot-by-shot beam energy and phase stability from SLAC MeV-UED facility. Courtesy of SLAC. ....	62
Figure 4-2: Pulse length dependence of the achievable gradient in X-band structures (left). Pulse length dependence of the maximum surface field for different materials (right). ....	64
Figure 4-3: Breakdown probability as a function of peak electric field in single cell X-band accelerating structure tests. ....	65
Figure 4-4: (left) RF surface resistance of two different S-band test cavities, manufactured at SLAC (blue) and UCLA (green). (right) Quality factor in SLAC test cavity. Reprinted with permission from [Rosenzweig, 2017]. ....	66

Figure 4-5: Feeding of injection gun by external RF sources (top) and E-field structures of modes in three-mode RF gun cavity.....	68
Figure 4-6: Comparison of slice emittance of 200 pC beam with 20 A peak current for different laser distributions and thermal meittance. ....	69
Figure 4-7: Mechanical concept for TW photoinjector .....	70
Figure 4-8: Longitudinal phase space control in a 1.5-cell S-band photoinjector: higher-order term reduction at high bunch charge (left); chirp control at low bunch charge (right). ...	71
Figure 4-9: 1.4 cell RF gun Cavity profile (left).....	72
Figure 5-1: Performance of and structure of photoinjectors. ....	75
Figure 5-2: Schematic of an X-ray FEL driven by a laser-plasma accelerated electron source. Courtesy of LBNL. ....	77
Figure 5-3: Laser pulse interacting with electron pulses. ....	80
Figure 5-4: Electrons diffracted in grating to produce nanopatterned beamlets.....	83
Figure 5-5: Principle of the cold-atom electron source. ....	85
Figure 5-6: Principle of a quantum-degenerate electron source based on ionization of Cs atoms in a high Rydberg state. Courtesy of LBNL. ....	86
Figure 5-7: SEM images of DFEA samples fabricated at Vanderbilt University shown at four different magnifications. ....	87

## LIST OF TABLES

---

Table 1-1: Electron beam parameters required for future XFEL and ultrafast electron probe applications. ....	12
Table 1-2: Characteristics of the electron beam after the injector, for different X-ray FEL scenarios using current technology (i.e. current state-of-the-art) and desired. ....	17
Table 1-3: Required parameters for new electron scattering modalities. ....	19
Table 2-1: Panel 1 Research Focus Areas.....	26
Table 2-2: Photocathode metrics .....	27
Table 3-1: Present performance level for high-brightness CW electron guns [Sannibale, 2016].	44
Table 3-2: Preliminary parameters for the APEX and APEX-2 guns .....	47
Table 4-1: Beam parameters obtained from S-band cryogenic photoinjector simulation studies, for UEM and FEL scenarios. ....	67

## EXECUTIVE SUMMARY

---

Electron sources represent an enabling technology for all cutting-edge applications of electron accelerators, two of the most notable ones being the X-ray free electron laser (FEL) and the electron microscope. FELs were enabled by the development of high-brightness electron sources, and they have changed the paradigm for a broad spectrum of scientific research. Electron microscopes have achieved sub-Å spatial resolution through the introduction of a cold field-emitter and aberration correction optics. Further development of these tools to atomic spatial and temporal resolutions is needed to advance atomic and molecular sciences to new levels of precision.

The introduction of a photocathode electron source for ultrafast electron diffraction (UED) in the early 1980s [Mourou, 1982], and the invention of the photocathode radio frequency (RF) gun [Fraser, 1987] laid a solid foundation for the X-ray free electron laser (XFEL). Successful operation of the first XFEL in 2009 ushered in a new era of X-ray science. This singularly powerful “microscope” has generated molecular movies, glimpsed the birth of a chemical bond, traced electrons moving through materials, and creating 3-D images of proteins that are a key to drug discovery [Bostedt, 2016].

The Basic Energy Sciences Advisory Committee (BESAC) sub-committees outlined five transformative opportunities for discovery science [BESAC, 2015]. To address these scientific grand challenges, it is necessary to develop brighter X-ray photon sources with better temporal resolution and higher energy and to develop novel, time-resolved electron scattering instrumentation. The future of the next generation of X-ray and electron instruments, from hard X-ray FELs to ultrafast electron scattering instrumentation, will strongly depend on breakthrough advances in electron sources. The scientific community has expressed a strong desire for a new generation of BES facilities through a series of Basic Research Need (BRN) reports. In all instances, the path forward involves improving the brightness of the electron source.

The Basic Energy Science (BES) Report on Future of Electron Scattering recommended development of UED and ultrafast electron microscopy (UEM) instrumentation capable of nano-diffraction with 10 fs temporal resolution in stroboscopic mode, and better than 100 fs temporal resolution in single shot mode. It also called for a single-shot real-space imaging system with spatial/temporal resolution of 10 nm/10 ps. This represents a thousand-fold improvement over

current state-of-the-art instruments. Such microscopes require electron beam bunches with more than 10 million electrons, nanometer normalized emittance, and relative energy spread smaller than ten parts per million (ppm). The peak current of such an electron source is at least nine orders of magnitude higher than the sources in current electron microscopes.

The BESAC Report on Facility Upgrades recently identified The Linear Coherent Light Source II High Energy Upgrade (LCLS II-HE) as “*absolutely central to contribute to world leading science.*” LCLS II-HE will provide X-ray energies above 5 keV. Even harder X-rays would be desirable to study atomic structure dynamics, electronic and nuclear coupling in biological and chemical processes, and energy materials in situ. LCLS II-HE could potentially reach 20 keV, but it requires a factor of ten improvement in electron beam brightness (a factor of three to four in emittance).

Though the field of electron sources is quite mature, both revolutionary and evolutionary advances in electron sources are needed. On September 8-9, 2016, BES sponsored a *Workshop on the Future of the Electron Source* at SLAC National Accelerator Laboratory. The goal of the workshop was to define the electron source requirements for future XFELs, UED and UEM, and to identify future research and development (R&D) opportunities. More than sixty participants from U.S. national laboratories, academia, and international institutions attended the workshop.

The workshop explored the frontiers of electron source R&D with the following goals:

- (1) Identify needs and opportunities for research in novel electron sources.
- (2) Seek transformational advances in peak and average electron beam brightness that could expand the scientific capabilities of X-ray and electron scattering instruments.
- (3) Explore novel applications such as shorter wavelength FELs, single shot UEM, femtosecond nano-diffraction, high average flux Compton scattering sources, and compact light sources.

The workshop started with four plenary talks covering the status of electron sources, and highlighting the most urgent needs of future X-ray and electron scattering facilities. The talks made it evident that significant progress in electron sources will not only maximize the impact of current facilities, but also enable novel capabilities that can help maintain the U.S. leadership in X-ray and electron-based scattering instrumentation.

Four breakout panels addressed the major technical areas of electron sources: (1) science and technology of electron generation, (2) continuous wave (CW) electron sources, (3) pulsed electron sources, and (4) exotic electron sources. Prior to the workshop, the panel co-chairs polled the panelists and other experts in the field and invited them to make recommendations on the most promising ways to advance the field of electron sources. During the workshop, each panel reviewed the proposals and novel ideas submitted. These summaries of the discussions on scientific needs and instrument requirements and their recommendations form the basis of this report.

The consensus from the workshop is that advances in all major technical areas of electron sources are required to meet future X-ray and electron scattering instrument needs. Nanotechnology and materials by design hold great promise in revolutionizing photocathodes. Progress in gun technology is needed to preserve the initial beam brightness. The panel identified the following priority research directions (PRDs):

- I. Next generation cathode R&D for high brightness beams.
- II. CW injector R&D to significantly increase accelerating gradients on the cathode and output beam energy.
- III. High-gradient R&D for next generation electron sources.
- IV. R&D in advanced accelerator and beam manipulation concepts.

In addition to the PRDs listed above, research in beam diagnostics, beam dynamics, and laser technology should also be pursued. Though the ultimate limit of beam brightness is set by the laws of quantum mechanics and the fermionic nature of the electron, this limit is four to five orders of magnitude beyond capabilities at current state-of-the-art facilities. By combining progress from several research directions, for example by pairing a much smaller thermal emittance with higher gradient guns, the small improvements interact multiplicatively, and a transformational advance (by more than one order of magnitude) in output beam brightness can be achieved. The community has identified that such an increase in source performance could be within reach in the next three to five years. Advances in electron sources and related technology will enable novel instruments and facilities with unprecedented characteristics to investigate matter at the fundamental spatial and temporal scale, leading once more to a revolution in X-ray and electron scattering science.

# 1. ELECTRON SOURCES SCIENTIFIC NEEDS FOR BES X-RAY AND ELECTRON SCATTERING FACILITIES

## 1.0. Scientific need for high-repetition hard X-ray FELs and ultrafast electron probes

Electron sources represent an enabling technology for both X-ray and electron probes. High-brightness electron beams efficiently generate bright X-rays and determine the fundamental resolution limits of electron probes (see Sections 1.2.2 and 1.2.4). X-rays and electrons are two of the most fundamental probes of matter. They provide the ability to map the atomic composition and structure of molecules, materials, and devices. X-rays and electron probes have revolutionized our fundamental understanding of matter and, thereby, redefined chemistry, physics, biology, and many related fields of science and technology. X-rays and electrons are complementary tools. Electrons have a larger scattering cross-section compared to X-rays but cause relatively smaller sample damage (i.e. have a smaller ratio between elastic and inelastic scattering) cross section. X-rays are well suited for studying electronic structure of the materials while electrons are known for real-space imaging. The small de Broglie wavelength of electrons allows them broad coverage of reciprocal space, whereas X-rays offer generally higher reciprocal space resolution with deeper sample penetration.

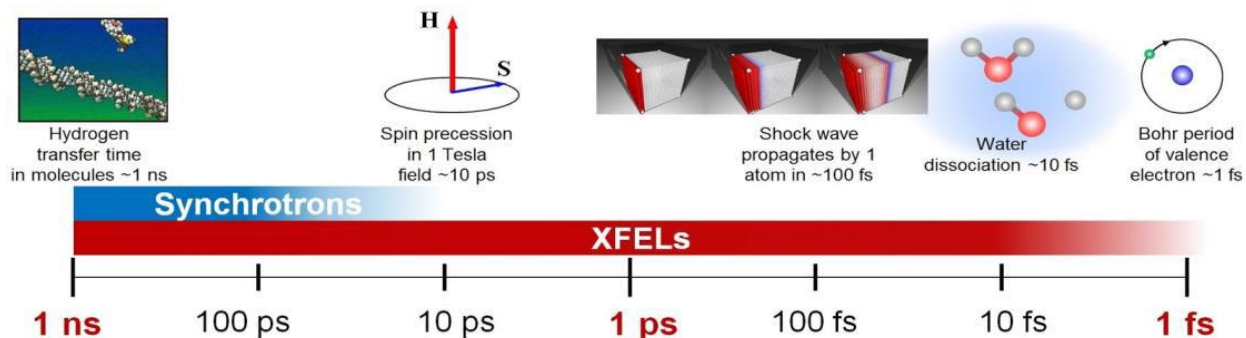


Figure 1-1: A unique feature of XFELs is the ability to probe the fastest time scales, providing over three orders of magnitude higher temporal resolution than a synchrotron source. Courtesy of SLAC.

The development of synchrotron-based X-ray sources over the past 60 years has led to the modern age of X-ray science (and five Nobel Prizes since 1997) by harnessing high-energy electron accelerator technology to provide X-ray beams that are intense and tunable over a wide

wavelength range. However, the quantum fluctuations of the synchrotron radiation process limit the temporal resolution and coherence of the X-rays (see Figure 1-1). Both atomic spatial resolution and femtosecond temporal resolution are required to understand and ultimately control the interplay between spin, charge and lattice degrees of freedom in quantum materials, the chemical dynamics of molecular systems, and the evolution of complexity in mesoscale systems.

Successful operation of the linear coherent light source (LCLS) at SLAC in 2009 ushered in a new era of X-ray science. This singularly powerful “microscope” has generated molecular movies, provided a glimpse of the birth of a chemical bond, traced electrons moving through materials, and created 3-D images of proteins that are key to drug discovery (Figure 1-2) [Bostedt, 2016].

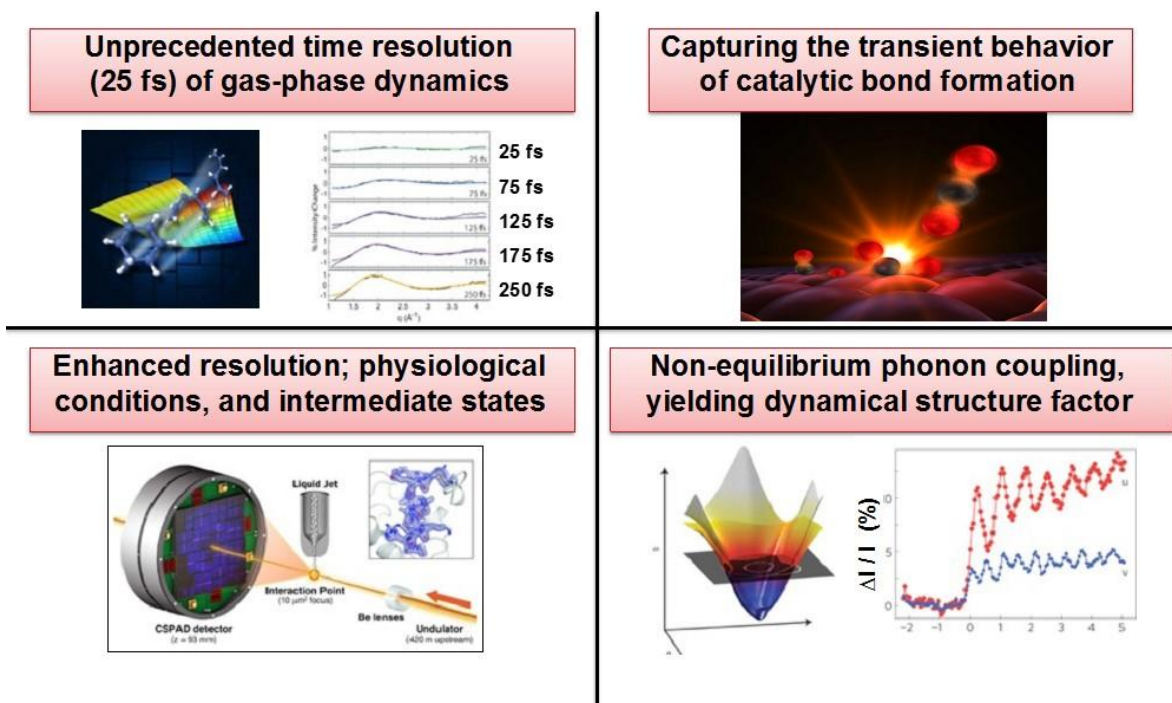


Figure 1-2: The broad scientific reach & impact of XFEL. Imaging molecular motion (top left, courtesy of SLAC). Reaction sequence for catalytic Co oxidation on Ru surface (top right, courtesy of SLAC). LCLS serial crystallography and model of the interface between synaptotagmin-1 and neuronal SNARE complex (bottom left, courtesy of SLAC). Coherent phonon-phonon correlations and acoustic phonon dispersion function (inset) measured in bulk Ge via Fourier transform inelastic X-ray scattering (FT-IXS) (bottom right, Reprinted from [Trigo, 2013] with permission from Macmillan Publishers Ltd).

The early success of LCLS and the future potential of XFEL sources have triggered intense development of XFEL capabilities around the world: up to 16 laser sources in six facilities will soon be operational. Chief among these is the European XFEL, scheduled to

perform its first experiments in 2017. It will exploit pulsed superconducting accelerator technology (pulsed-SCRF) to deliver an average brightness that will exceed the performance of LCLS at 1 Å by more than 1,000-fold, a capability gap with profound implications for science. While LCLS has delivered unprecedented peak brightness, the average brightness is modest, similar to that of a storage ring-based synchrotron source. Many experiments could take advantage of lower peak intensity in order to avoid perturbation of the sample by the X-ray probe. In these cases, signal accumulation times often become prohibitive at 120 Hz, thus rendering many experiments impractical. The next-generation facility, LCLS-II, will be based on advanced superconducting accelerator technology (continuous-wave RF) and tunable magnetic undulators. It will support the latest seeding technologies to provide fully coherent X-rays (at the spatial diffraction limit and at the temporal transform limit) in a uniformly-spaced train of pulses with programmable repetition rate up to 1 MHz, and tunable photon energies from 0.25 to 5 keV. LCLS-II qualitatively changes the way that X-ray scattering, spectroscopy, and imaging will be performed [Schoenlein, 2015].

Hard X-rays above 5 keV are required to study atomic structure dynamics, electronic and nuclear coupling in biological and chemical processes, and energy materials in situ. The hard X-ray regime is where over 75% of LCLS users operate at present [BESAC, 2016].

The availability of hard X-rays in the 20 keV energy range at high repetition rate will provide a powerful new scientific tool for probing both atomic and electronic structure of matter. Such hard X-rays are essential to access scattering at large momentum-transfer for characterizing structure at the atomic scale, such as making molecular movies during chemical and biological processes [Minitti, 2015]. Pair distribution function (PDF) analysis relies on hard X-ray scattering to map the radial distribution function of specific atoms in molecular complexes or heterogeneous materials. High repetition rate is essential to achieve the differential sensitivity to follow changes in X-ray scattering via time-resolved PDF in reactive complexes and dynamic materials. Finally, the penetration power of hard X-rays presents an advantage for probing bulk material properties and buried interfaces. For example, X-rays at 20 keV penetrate ~1 cm of water, or ~1 mm of silicon.

To generate hard X-rays above 5 keV, an electron beam energy higher than 4 GeV is required. The proposed LCLS-II-HE will double the electron beam energy from 4 GeV to 8 GeV. Hard X-rays should reach 20 keV by energy doubling based on simple FEL scaling (see

Section 1.2.1). Nevertheless, start-to-end simulations using the current LCLS-II CW electron source show that the LCLS-II-HE can only extend the hard X-ray energy range from 5 keV to ~12 keV due to brightness limitations [BESAC, 2016]. To enable future hard X-ray FELs, more than an order of magnitude improvement in CW electron source brightness is needed, corresponding to reduction by a factor of three to four in emittance (Figure 1-3).

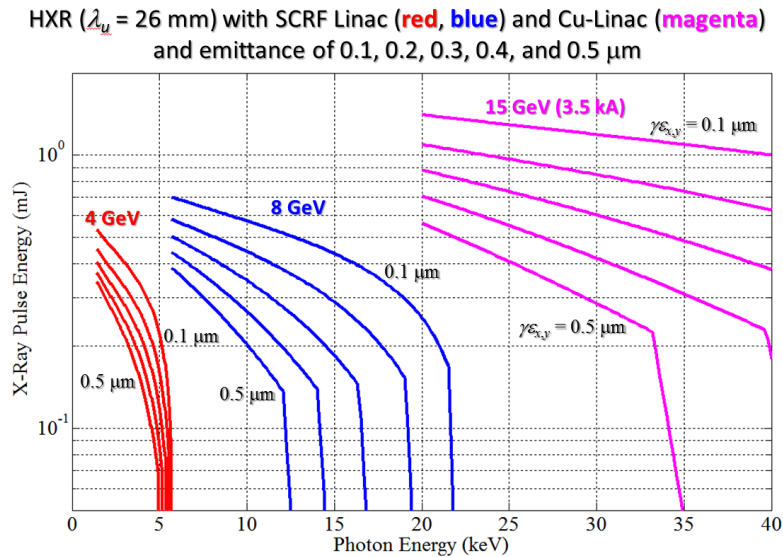


Figure 1-3. XFEL output as a function of X-ray photo energy for a charge of 100 pC and 5 different normalized emittance values. The best emittance demonstrated is ~0.5  $\mu\text{m}$ . Courtesy of SLAC.

Optical microscopy reached its far-field diffraction limit roughly a century ago. To overcome the diffraction limits of light-based microscopes, Max Knoll and Ernst Ruska of Germany introduced the transmission electron microscope (TEM) in 1931. Since then, the resolution of the TEM improved dramatically, from microns to sub-Å. These improvements in TEM resolution are largely due to brighter electron sources and higher electron beam energy (Figure 1-4). The recent development of cold electron sources and aberration correction optics resulted in a new generation of electron microscopes reaching sub-Å resolution [Batson, 2002]. The TEAM project for aberration-corrected TEM and scanning transmission electron microscopy (STEM), funded by the Department of Energy - Basic Energy Sciences (DOE-BES), has achieved atomic spatial resolution, and is now the tool of choice for imaging the ultra-small world. Among the many scientific results enabled by the TEAM microscopes were the direct imaging of live action motion in single graphene sheets, imaging beyond the Bohr radius [Erni, 2009], and the development of atomic electron tomography [Miao, 2016].

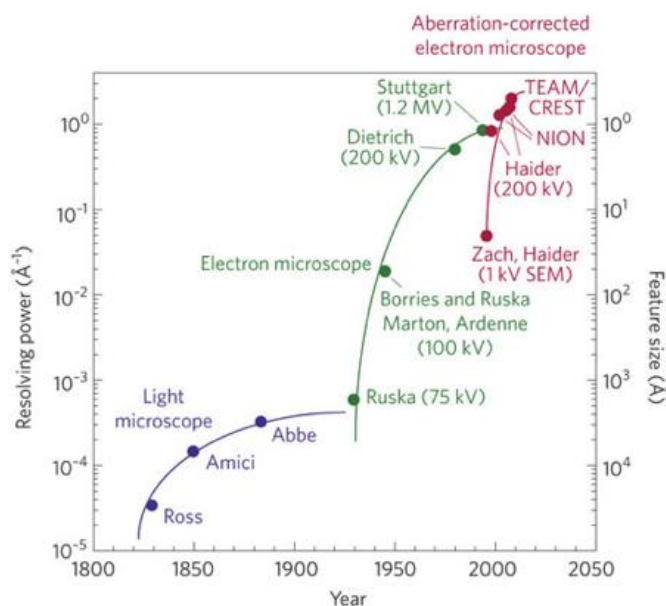


Figure 1-4: Electron microscopy, exploiting the reduction in electron wavelength with increasing beam voltage, showed steady increases in resolving power for over 70 years. Reprinted from [Muller, 2009] with permission from Macmillan Publishers Ltd.

Static structures determined via crystallography and high-resolution TEM mainly represent equilibrium ground states. Static images possess undeniable power, but do not address many of the critical mission needs of the DOE-BES. The core research mission of BES requires characterizing and controlling the transformation and transport of energy from one form and one location to another by intrinsically non-local transient phenomena. Since the introduction of ultrafast electron scattering based on photoelectron sources in early 1980s [Mourou, 1982], these probes have seen tremendous progress in both technological developments and scientific applications.

In reciprocal space, ultrafast electron diffraction (UED) has been used to study ultrafast structure dynamics, strongly correlated electron systems and transient intermediates of chemical reactions [Ewbank, 1999; Cao, 1998; Ihee, 2001; Siwick, 2003]. UED instruments, based on a DC gun, have been improved in stages, including the minimization of gun-sample distance, addition of RF bunch compressor and increase of gun voltage. The temporal resolution is limited to the sub-picosecond range due to the repulsive space charge effects at relatively low beam energies [Sciaini, 2011]. Introduction of MeV photoelectron beams for ultrafast electron scattering [X. Wang, 1996; X. Wang, 2003] made it possible to break the 100-fs time-resolution

barrier [Yang, 2016]. The next frontier is an electron probe capable of 0.1 Å and 10 fs resolution that would, for example, allow scientists to identify the key electronic and nuclear degrees of freedom and their coupling in chemical reactions [Miller, 2014].

In real-space, ultrafast electron microscopy (UEM) was achieved by adding optical access to both cathode and sample chamber of a TEM. UEM is capable of operating in two modes: stroboscopic [Lobastov, 2005] and single-shot (DTEM) [Armstrong, 2007]. A UEM operating in stroboscopic mode employs a single electron per pulse (low charge) and high repetition rate (100 kHz), to eliminate the effects of the Coulomb interactions between particles in the same bunch and maintain ultra-high spatial resolution. The stroboscopic mode UEM can access timescales of hundreds of fs with sub-nm spatial resolution [Plemmons, 2015]. DTEM has demonstrated 10 nm, 10 ns spatial temporal resolution [Browning, 2012].

Capturing irreversible processes in materials science and biology and studying non-equilibrium nanoscale phonon dynamics requires a single-shot UEM with more than a factor of 100 improvement in spatial-temporal resolution compared to existing DTEMs. Improving resolution to this level requires higher beam energy [Armstrong, Reed, 2007; Xiang, 2014; Li, 2014] and nm-scale normalized emittance. An even bolder alternative could be considered if the relative coherence of the beam (a quantity defined as the coherence length divided by the beam size [Carbone, 2012], currently at the  $10^{-4}$  level) could be increased by more than two orders of magnitude, enabling lens-less coherent diffractive imaging. This approach would minimize the space-charge blurring induced by stochastic Coulomb scattering occurring in the imaging cross-overs.

The BES *Report on Future of Electron Scattering* recommended development of UED and ultrafast electron microscopy (UEM) instrumentation capable of nano-diffraction with 10 fs temporal resolution in stroboscopic mode, and better than 100 fs temporal resolution in single-shot mode [Hall, 2014]. Nano-UED will represent a paradigm shift, as it will open up complementary measurements to those performed on LCLS-II using soft X-ray holography for nanoscale lattice and charge/spin dynamics studies. Those measurements can provide deep insights into the mechanisms of the lattice response for a wide range of quantum materials and nanostructures.

## 1.1. Future electron source R&D

The advent of XFELs [Pellegrini, 2016] would not have been possible without the low emittance and high current beams made available by the development of high gradient RF photoguns. The introduction of a photocathode electron source for UED in the early 1980s [Mourou, 1982], and the invention of the photocathode RF gun [Fraser, 1987] laid a solid foundation for the XFEL. The widespread development of fundamentally higher brightness electron beams is the result of two decades of progress during the 1980s and 1990s in studying and understanding the key aspects of beam generation and evolution in high gradient photoinjectors [Kim, 1989; Carlsten, 1989; X. Wang, 1996; Serafini, 1997]. Advances in the quality of electron beams have been so significant that the entire trajectory of science has changed. These sources have permitted the production of intense, cold, relativistic electron beams with small transverse phase space areas (normalized emittances), allowing matching to the radiation-mode size in the undulator and therefore enabling lasing at very short wavelength. In the longitudinal direction, these beams boast ultra-fast time structures, having advanced from the picosecond scale down to femtosecond levels the fundamental temporal scales of material response. This progress has enabled many novel applications of electron accelerators beyond the high-energy physics for which these machines were originally developed.

### 1.1.1. *Important factors influencing future research*

Current electron sources have reached a relatively mature status due to decades of development in accelerator and laser technology, through engineering development, well-benchmarked simulation models, and continuous investments over many years from different U.S. federal funding agencies. Though the field of electron sources is quite mature, both revolutionary and evolutionary advances in electron sources are still needed. Based on improvements to date and ongoing efforts, reaching the required improvements in source performance to enable the novel capabilities of next-generation BES instruments should be feasible in a reasonable amount of time (3-5 years). The *BES Workshop on the Future of the Electron Source* considered the following important elements in formulating future priority research directions (PRDs): the status of existing instruments, the demands of future experiments, and the recent progress in both science and technology.

- Electron sources currently employed in DOE-BES facilities are based on over decade-old designs (both for XFELs and UED/UEM,) which were conceived at a time when the source parameters were based on the luminosity requirements of the high-energy colliders, with working points at 1 nC beam charge and relatively long beams (up to 10 ps) [Ferrario, 2001; Akre, 2008].
- The revolution introduced by femtosecond and sub-femtosecond techniques in ultrafast science has increased the demand for ultrashort electron and X-ray pulses, which in turn have driven the design towards lower charge per bunch. The accompanying advances in detector design [*Neutron*, 2012] and X-ray optics [*X-ray optics*, 2013] have reduced the flux of probe particles (both photons and electrons) needed to acquire statistically significant information from the images. For XFELs, phase space manipulation techniques [Brinkmann, 2001; Cornacchia, 2002] and undulator tapering [X. Wang, 2009; Jiao, 2012] can be used to extract a much larger fraction of energy from the electron beams. This lowers the charge demands for most XFEL applications to 100 pC and below in order to generate the more than  $10^{12}$  photons per pulse required for single molecule imaging. For electron scattering instrumentation, diffraction patterns can be obtained with as low as  $10^6$  electrons per pulse, due to the much larger Rutherford cross-section of interaction with matter. Single shot images require only  $10^8$  electrons per pulse.
- In the last few years there has been steady and measurable progress in RF technology [Grassellino, 2013; Dal Forno, 2016], both superconducting and normal conducting, ranging from a better understanding of the breakdown process to the introduction of novel materials (or materials in specific operating regimes, such as cryogenic temperatures) and surface treatment techniques. This can be exploited in the construction of future electron sources with much larger accelerating gradients and therefore with the promise of much higher beam brightness.
- With the help of material science and solid state physics, and a focused effort in testing and material characterization, many advances have been made in our understanding of photoemission physics. These results, together with the development of technologies such as high average power tunable lasers and surface nanofabrication, have been used to develop advanced photocathode systems with better performance.

- High-gradient advanced accelerator schemes [Limborg, 2016] are becoming more reliable and stable, and there are a variety of novel ideas to apply these to development of new sources with unprecedented brightness, pulse length, or other beam parameters.
- The brightness improvement in future electron sources will lead to a higher charge density, and hence stronger space-charge effects. Preserving gains in electron beam brightness will require electron sources with higher electron beam energy.

All these new elements, coupled to the existing solid base of expertise in synchronization, beam diagnostics, and beam dynamics have the potential for breakthrough advances in the field of electron sources, provided sufficient resources are employed. Table 1-1 lists the electron beam parameters required for electron sources for future XFEL and ultrafast electron probe applications.

*Table 1-1: Electron beam parameters required for future XFEL and ultrafast electron probe applications.*

	<b>XFEL (CW)</b>	<b>XFEL (Pulsed)</b>	<b>UED</b>	<b>UEM</b>
<b>Charge</b>	100 pC	200 pC	10 fC – 0.5 pC	0.5-1 pC
<b>Bunch length</b>	1-10 ps	< 1 ps	10 fs	ns - ps
<b>Energy spread</b>	$10^{-3}$	$10^{-3}$	$10^{-4}$	$10^{-5}$
<b>Emittance</b>	100 nm	50 nm	1 nm	1 nm
<b>Repetition rate</b>	1 MHz	120 Hz	Single-shot to MHz	Single-shot to 100 Hz
<b>Enabling capabilities</b>	20 keV high average power	80 keV lasing multi-TW attosecond X-ray pulses	fs nanodiffraction	Single shot with sub-nm & sub-ns UEM

### **1.1.2. Priority research directions**

The consensus from the workshop participants is that advances in all major technical areas of electron sources are required to produce the electron sources outlined in Table 1-1. Nanotechnology and materials by design hold great promise in revolutionizing photocathodes.

Progress in gun technology is needed to preserve the initial beam brightness. The workshop participants identified the following priority research directions (PRDs):

- I. **Next generation cathode R&D for high brightness beams.** Two key factors for high-brightness beams are small longitudinal and transverse energy spreads at emission. A reduction of more than a factor of 10 in these parameters can be obtained in various ways, including material engineering, cooling the cathode substrate, and laser wavelength tuning. Testing of advanced photocathodes in real gun environments will be critical to translate this research into direct improvement in electron beam quality. In addition, beam coherence can be greatly improved by exploring the use of nanoscale and microscale photoemitters. Ab initio cathode designs could deliver photocathodes with tailored characteristics to enable novel applications of high-brightness beams.
- II. **CW injector R&D to significantly increase accelerating gradients on the cathode and output beam energy.** For CW injectors, more than a factor of two improvement in both accelerating gradient on the cathode and electron beam energy are needed to produce and preserve the high-brightness electron beams required for XFEL and single-shot UEM. Major advances in copper and SRF CW injector technology are needed to meet the challenging requirements. Start-to-end simulations should be pursued to narrow the technological choices.
- III. **High-gradient R&D for next generation electron sources.** Pulsed electron guns are characterized by very high initial accelerating gradients (on the order of 100 MV/m) but relatively low repetition rates (~200 Hz) and average beam currents. Developments in novel structures and materials hold the potential for more than a factor of two larger source electric field and record high peak brightness for the most demanding applications.
- IV. **R&D in advanced accelerator and beam manipulation concepts.** Development of electron guns based on advanced accelerator concepts such as laser or beam plasma wakes or THz waves are recommended as they hold the promise for GV/m injection fields. Application of advanced phase space beam manipulation schemes (emittance exchange and pre-bunching) could mitigate the technology risks and costs of an XFEL by more than one order of magnitude.

Four breakout panels addressed the major technical areas of electron sources representing each PRD: (1) science and technology of electron generation, (2) continuous wave (CW) electron sources, (3) pulsed electron sources, and (4) exotic electron sources. The following chapters in this report describe detailed results from each panel.

## 1.2. Technical requirements and brightness scaling law

### 1.2.1. XFEL electron source requirements

The XFEL stands out in terms of current and near-future impact in the list of applications of high brightness electron beams, as exemplified by the LCLS [Emma, 2010]. The LCLS facility, which introduced coherence and ultrafast properties to high-flux hard X-ray sources, serves as a flagship for DOE-BES and prototype for the fourth generation of X-ray light sources [Altarelli, 2006; Huang, 2012]. The XFEL operation is based on the self-amplified spontaneous emission (SASE) FEL instability, where electrons passing through an undulator magnet emit radiation which can act on the electron beam itself, causing microbunching and hence, due to the coherence effect, an increased emission of radiation (see Figure 1-5). The growth of this instability is made possible by high-brightness electron beams and has yielded X-ray light sources with approximately ten orders of magnitude increase in photon spectral brightness compared to that of synchrotron rings. These extremely bright, coherent light sources have introduced high-impact methods in X-ray based science such as coherent diffraction imaging where X-ray pulses “diffract before destroy” [Chapman, 2011]. LCLS will undergo a significant upgrade starting in 2018 [Schoenlein, 2015], mirroring the investment made worldwide in the XFEL sector.

The fundamental equations describing an XFEL are the synchronism equation for the X-ray wavelength  $\lambda_{x-ray} = \frac{\lambda_{und}}{2\gamma^2} (1 + K^2/2)$  and the equation for the FEL Pierce parameter

$$\rho = \frac{1}{\gamma} \left( \frac{K JJ}{4\sigma k_{und}} \right)^{2/3} \left( \frac{I}{I_A} \right)^{1/3}. \text{ In these equations, } \lambda_{und} \text{ is the XFEL undulator period,}$$

$K = 0.93 \lambda_{und}[\text{cm}] B[\text{T}]$  where  $B$  is the peak undulator magnetic field,  $\gamma = E/m_e c^2$  is the dimensionless relativistic electron energy where  $m_e$  is the electronic mass,  $JJ$  is a factor of order unity coming from the figure-8 motion in the beam’s frame of reference,  $k_{und} = 2\pi/\lambda_{und}$ ,  $\sigma$  is

the electron beam size in the undulator,  $I$  is the electron beam's peak current, and  $I_A$  is about 17 kA. The Pierce parameter is roughly the conversion efficiency from electron beam power to X-ray power, defining the allowable relative energy spread in the electron beam. The gain length also scales inversely with the Pierce parameter [Bonifacio, 1984],  $L_g \propto \rho^{-1}$ . For optimum XFEL performance, the electron beam emittance must be smaller than some fraction of the wavelength,  $\varepsilon < \lambda_{x\text{-ray}} / 4\pi$ .

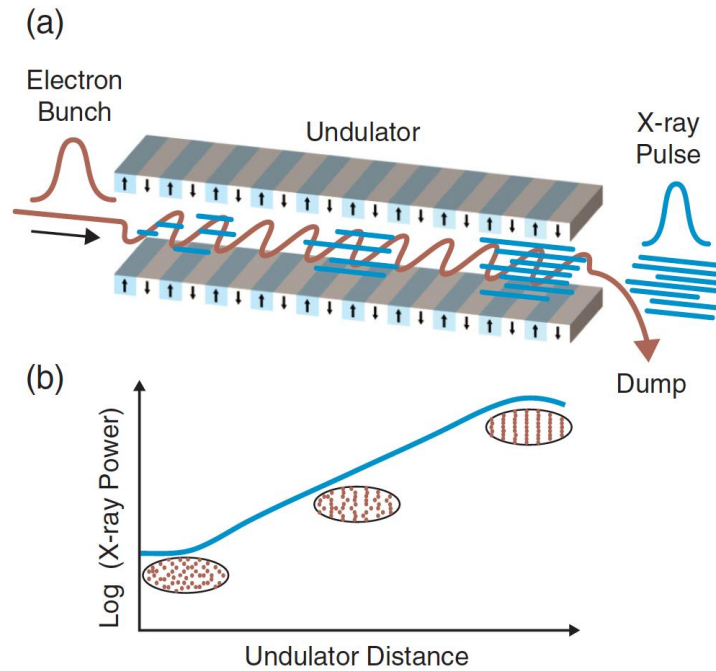


Figure 1-5: Elements of an X-ray FEL. A high brightness beam from the linac/injector interacts with electromagnetic waves in the undulator. The SASE FEL instability grows along the undulator. Reprinted from [Bostedt, 2016] with permission from the American Physical Society.

In practice, there are essentially two key elements to realize a high-gain FEL, the undulator magnet and the high-brightness electron beam. It follows that the quality of the electron beam, and therefore the performance of the electron source, can greatly affect the XFEL performance. This occurs either directly through the  $\rho$  parameter dependence on the peak current  $I$  and the beam transverse size or indirectly through the instability-damping effects of emittance and energy spread [Bonifacio, 1984]. High electron beam brightness, defined as the ratio of the bunch charge to its 6D phase space, is therefore essential to developing new XFEL capabilities.

A large  $\rho$  parameter not only shortens the gain length and therefore the length of the undulator needed to achieve saturation, but it is critical to future advanced XFEL operation

schemes based on seeding and on the generation of ultrashort X-ray pulses. The gain bandwidth scales as  $\rho$  and therefore a higher brightness beam supports lasing with shorter X-ray pulses. Further, tapering of the undulator parameters to increase the fraction of power that can be extracted from the beam beyond saturation is far more efficient when brighter beams are employed [C. Emma, 2014; Duris, 2015].

Since the large final electron beam current is a product of the compression throughout the linac, the improvements in the electron source parameters desired for XFEL operation mainly arise from the demand for lower emittance, and somewhat less so on higher longitudinal phase space density. This viewpoint implicitly places trust in improvements in transport and compression techniques that can preserve the initial beam quality. Indeed, methods such as enhanced SASE [Zholents, 2005] could mitigate the risk associated with reliance on compression; these would rise in importance should very low emittances be achieved at the 100-pC charge level. The FEL peak power is proportional to  $I$ , emphasizing that charge and/or current cannot be sacrificed in pursuing large photon-flux experiments such as single molecule imaging. On the other hand, at reduced charge, the emittance and pulse length may be minimized [X. Wang, 1996; Ding, 2009], allowing access to new FEL regimes, such a sub-fs and/or single spike operation [Rosenzweig, 2008].

It is helpful to describe the current state-of-the-art as well as the desired characteristics of future electron sources for X-ray FELs. State-of-the-art photoinjector designs are based on a family of schemes that utilize a 1.5 to 1.6- cell standing wave geometry in S-band [Palmer, 1998], culminating in the success of the LCLS photoinjector [Akre, 2008]. Table 1-2 lists the characteristics of this device at output, in three different scenarios: (1) nominal operation, (2) low charge, femtosecond FEL, and (3) large charge for high-flux FEL, as developed mostly at SLAC in the last decade, and aiming at applications such as single molecule imaging. XFELs currently in the design stage will require electron beams exceeding these parameters. For example, the Matter-Radiation Interactions in Extremes (MaRIE) XFEL at Los Alamos National Laboratory will require 100 pC at an emittance of 0.15  $\mu\text{m}$ . Future requirements are envisioned that will be even more stringent.

Table 1-2: Characteristics of the electron beam after the injector, for different X-ray FEL scenarios using current technology (i.e. current state-of-the-art) and desired.

Parameter	Nominal operation		Femtosecond FEL		High flux FEL	
<b>Bunch charge</b>	200 pC	$\geq 100$ pC	20 pC	$\sim 10$ pC	500 pC	500 pC
<b>Normalized emittance</b>	0.4 $\mu\text{m}$	$\leq 0.1$ $\mu\text{m}$	0.14 $\mu\text{m}$	$\leq 0.05$ $\mu\text{m}$	1 $\mu\text{m}$	0.3 $\mu\text{m}$
<b>Pulse length (rms)</b>	3 psec	2 psec	2 psec	1 psec	5 psec	3.5 psec
<b>Slice energy spread (rms)</b>	1 keV	1 keV	0.5 keV	.5 keV	2 keV	2 keV

### 1.2.2. Ultra-fast Electron Diffraction/Microscopy source requirements

Complementary to the information that can be obtained using X-rays, ultrafast electron scattering techniques such as diffraction, imaging, and spectroscopy offer a unique opportunity for understanding structural dynamics and the behavior of matter under conditions far away from equilibrium [Carbone, 2012]. Conventional ultrafast electron sources with keV energies suffer from space-charge-induced bunch lengthening and emittance growth, which affects both the spatial and temporal resolution of the instruments [Armstrong, Reed, 2007]. A typical solution is to use stroboscopic methods, where the information is acquired over many cycles of the process under study. Besides significantly alleviating these issues due to the relativistic suppression of space charge effects, high-energy (MeV) electron sources provide access to larger sections of the momentum-space, accessing multiple Brillouin zones at the same time. This minimizes velocity mismatch, the temporal walk-off between pump and probe pulses in the sample [X. Wang, 1996].

Pulsed, high-gradient relativistic sources are ideally suited for experiments that require a high level of pump excitation, and in which the repetition rate of the pump may be inherently limited to  $< 1$  KHz to avoid damage. Such sources are also useful in gas-phase experiments, where the large volume required to increase the signal puts a strong limit on the maximum tolerable velocity mismatch, and for the cases in which nonreversible processes are to be imaged and the information needs to be acquired in a single pulse.

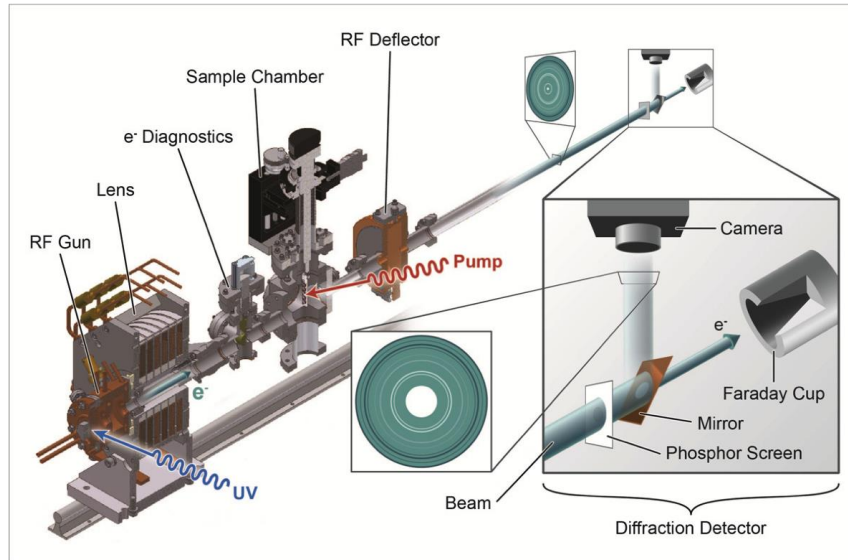


Figure 1-6: Elements of a relativistic UED beamline. The solenoid focuses the beam from the RF gun and allows capturing diffraction patterns like the one shown in the figure. Reprinted from [Zhu, 2015].

The demands on the beam parameters for UED/UEM applications greatly depend on the process under study. The number of electrons determines the signal-to-noise ratio in imaging or diffraction mode. Beam charges of interest vary from the few pC-level to obtain a high contrast, 100x100-pixel image, down to <10 fC for multi-shot diffraction patterns of fully crystalline specimens, which take advantage of the Bragg signal enhancement. Peak current, and therefore bunch length, is also needed to permit a larger number of electrons within a certain relevant measurement time — again picoseconds to femtoseconds — in observing, e.g., dynamic changes in material properties revealed through diffraction. The intrinsic spread in angles of the beam must be smaller than a few mrad, the diffraction angle associated with the electrons' de Broglie wavelength (0.25 pm for 5 MeV electrons). The spot size depends on the relevant spatial scale (either sample dimensions or grain sizes) and is typically below 100  $\mu\text{m}$ , implying a normalized emittance limit of < 100 nm. A state-of-the-art UED beamline, such as the one at the ASTA facility at SLAC, typically runs a 60-fC electron beam of 3.7 MeV beam energy, with normalized emittance of 18 nm. Bunch length of 100 fs is used for stroboscopic diffraction [Weathersby, 2015].

Higher beam brightness opens new opportunities in both UED and UEM. The use of intense, ultra-relativistic electron beams in imaging microscope schemes (UEM), which demands significant improvements in emittance and intensity performance with respect to current state of

the art, has also attracted much recent attention [Li, 2014]. Table 1-3 gives examples of new electron scattering modalities that could be enabled by electron source improvements, with corresponding approximate parameters required.

Table 1-3: Required parameters for new electron scattering modalities.

Parameter	State-of-the-art	Single-digit fs UED	Nano-diffraction	Ps imaging	Ultrafast spectroscopy
Energy	3.7 MeV	4 MeV	4 MeV	5 MeV	4 MeV
Charge	100 fC	50 fC	50 fC	1 pC	$\ll 1$ fC
Bunch length	100 fs	$< 10$ fs	100 fs	10 ps	100 fs
Emittance	20 nm	20 nm	few nm	few nm	20 nm
Spot size	50 $\mu$ m	50 $\mu$ m	3 $\mu$ m	3 $\mu$ m	50 $\mu$ m

**Single-digit fs-resolution UED.** Existing pulsed-photoinjector UED facilities provide small emittance bunches at low charge with sub-ps temporal duration. However, fast processes in materials [Dal Conte, 2015] may exhibit changes requiring temporal resolution of a few fs. This enhanced resolution will require: (1) ultrashort electron bunch and (2) high-resolution time-stamping, or alternatively commensurate timing jitter to provide multishot integration.

**Femtosecond nanodiffraction.** Materials with small grain size require a small, coherent probe to perform successful UED, which places strict requirements on the transverse emittance, and may also require fs-level time resolution. For example, at a few MeV for a probe size of 100 nm, even with the relatively low coherence requirement of  $<1$  mrad divergence (cf. SLAC UED, nominal divergence  $\sim 10$  micro-rad), requires a normalized emittance of  $<1$  nm-rad.

**Single-shot ultrafast electron imaging.** Single-shot TEM requires more than one million electrons. To minimize chromatic effects in the strong imaging lenses required, the relative energy spread should also be kept to  $<10^{-4}$ . The transverse normalized emittances should be  $< 10$  nm-rad for mm-scale lens apertures and object-image distances in the 10s of cm. Successful simulation designs have been performed that show beams with energy spreads in the few 10s of eV. With one order-of-magnitude higher electron beam brightness than the current state-of-the-art (for example, 100 fC at  $\sim 1$  nm-rad normalized emittance), it is possible to employ diffraction contrast, which is of interest for many crystalline materials. Increasing the electron beam brightness further may enable the use of phase contrast in imaging. If the electron beam

brightness can be increased by two orders of magnitude beyond the current state-of-the-art, the coherent fluence may be sufficient to perform coherent diffractive imaging. Coherent diffractive imaging is inherently lens-less, and would bypass stochastic Coulomb scattering at the beam focus, which inherently limits the above lens-based imaging.

**Ultrafast Electron Energy Loss Spectroscopy.** The ability to achieve sub-eV electron energy resolution would unlock the ability to perform ultrafast electron energy loss spectroscopy, which permits the inference of chemical composition information as a function of time. Combined with appropriately designed imaging optics, this provides simultaneous spatial and temporal information about chemical composition. Given its extreme sensitivity to electron energy spread, ultrafast electron energy loss spectroscopy may be ideally operated with single electron packets (absence of Coulomb repulsion at foci). Hence, for pulsed electron sources such spectroscopy may require significant integration times with the repetition rate constraints on high gradient sources. Conversely, the ability to use high gradient can provide improved time resolution compared to high-repetition-rate sources.

### 1.2.3. Physics of Inverse Compton Scattering sources

Inverse Compton Scattering (ICS) is a promising approach to generate narrow-spectrum X-rays using low energy electron beams, and is especially suited for compact university-sized light sources. Additionally, ICS can reach the highest photon energies of interest to basic energy sciences (i.e., up to and exceeding 300 keV) and MeV photons relevant to nuclear physics. Importantly, the photon energy range of ICS sources exceeds that of today's XFELs, and with order-of-magnitude lower energy electron accelerators.

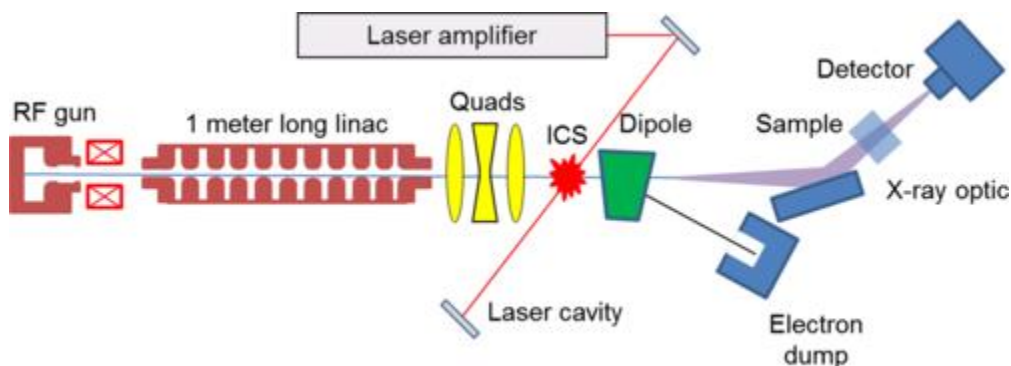


Figure 1-7: Schematic of typical ICS. Reprinted from [Graves, 2014].

Three main formulas describe gamma-ray production from ICS by defining the X-ray energy, the number of X-rays generated per second, and the minimum achievable spectral bandwidth. The X-ray energy  $E_{X\text{-ray}}$  from a single scattering event in terms of the laser photon energy  $E_{laser}$  is  $E_{X\text{-ray}} = E_{laser} \left( 4\gamma^2 / (1 + a_0^2 / 2 + \gamma^2 \theta^2) \right)$ , where  $\gamma$  is the electron's relativistic factor,  $\theta$  is the off-axis observation angle from the electron's trajectory,  $a_0 = 0.85 \times 10^{-5} \lambda_{laser} [m] \sqrt{I_0 [W/m^2]}$  is the normalized laser intensity,  $\lambda_{laser}$  is the wavelength of the laser photons, and  $I_0$  is the laser intensity. The number of X-rays,  $N_{X\text{-ray}}$ , generated per second by  $N_L$  photons of a laser pulse and  $N_e$  electrons of an electron bunch both at a waist is roughly  $N_{X\text{-ray}} = \sigma_T N_L N_e / \pi(\sigma_L^2 + \sigma^2)$ , where  $\sigma_T$  is the Thomson cross-section,  $\sigma_L$  is the transverse rms size of the laser pulse and  $\sigma$  is the transverse rms size of the electron bunch. The minimum achievable spectral bandwidth (on-axis with  $\theta=0$ ) is estimated by adding various growth terms in quadrature,  $\Delta E / E = \sqrt{0.5(k_0 c \Delta t)^{-2} + (k_0 \sigma_L)^{-2} + 4(\Delta\gamma / \gamma)^2 + (\varepsilon_n^4 / \sigma^4) + a_0^4 / 4}$ , where  $k_0 = 2\pi / \lambda_{laser}$  and  $\Delta t$  are the laser light wavenumber and pulse length, respectively;  $\Delta\gamma / \gamma$  and  $\varepsilon_n$  are the electron beam energy spread and normalized emittance, and both the laser light and electron beam have waists at the collision point.

While the number of X-rays only explicitly depends on the electron bunch charge and transverse size, a short electron bunch and high peak current is needed to ensure the electrons interact with the laser photons at their waists, and a small transverse emittance is needed to keep the electron beam waist as small as possible over the laser Rayleigh range. Additionally, a small electron energy spread and emittance is desirable to minimize the energy spread of the generated X-rays.

As an example relevant to BES, an ICS process can produce nearly monochromatic X-rays of 30 keV by colliding a 1  $\mu\text{m}$  laser pulse with a 40 MeV electron beam. This can be compared to needing a 12 to 20 GeV electron beam for a 30 keV XFEL. With the promise of high bunch charge with high peak current, low emittance, and low energy spread, pulsed RF photoinjectors are ideal electron sources for low-average flux ICS machines (Figure 1-7). CW and superconducting (SC) photoinjectors appear more desirable for high-average flux requirements, but at higher cost and overall size. By expanding such systems to slightly higher

electron beam energies, X-ray sources reaching > 70 keV will exceed the flux presently available from bending magnets in storage ring-based sources offering new scientific opportunities. Most synchrotron light sources experience a drop-off in flux at a few 10s of keV (see Figure 1-8).

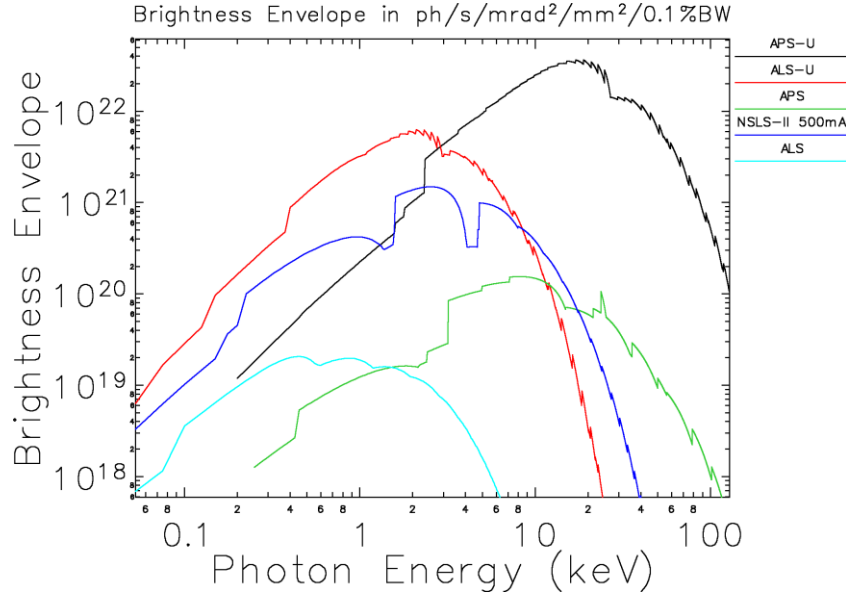


Figure 1-8: X-ray brightness for proposed U.S. synchrotron radiation sources upgrade. Courtesy of ANL.

#### 1.2.4. Brightness scaling laws

The intrinsic transverse beam brightness (5D) is defined as bunch current divided by both transverse phase space areas (emittance), assuming no emittance dilution after emission from the cathode. This expression of brightness is proportional to the axial current density  $J_z$  and inversely proportional to the effective cathode temperature  $T_c$  [Bazarov, 2009; Filippetto, 2014].

$$B_T = \frac{2I}{e_n^2} \gg \frac{8\rho J_z m_0 c^2}{k_B T_c}$$

The parameters  $k_B$  and  $m_0 c^2$  indicate the Boltzmann constant and the electron rest energy, respectively. If this intrinsic brightness is instead cast in its 6D form, it is written as

$$B_{0,6D} = \frac{2I}{\varepsilon_n^2 \delta_\gamma} \approx 8\pi J_z \left[ \frac{m_0 c^2}{k_B T_c} \right]^{3/2},$$

where  $\delta_\gamma$  represents the rms spread in the beam's relativistic mass factor.

For sub-picosecond emission from metallic surfaces,  $k_B T_c$ , is proportional to the difference between the laser photon energy,  $h\nu$ , and the metal's work function,  $W$ . This expression assumes that the transverse and longitudinal temperatures are similar at emission. Thus, either increasing  $J_z$  or lowering  $T_c$  will improve  $B_T$  (or  $B_{0,6D}$ ). Increasing  $J_z$  requires higher effective acceleration field on the cathode while lowering  $T_c$  corresponds to the reduction in mean transverse energy (MTE) of electron emission.

## 2. PANEL 1: SCIENCE AND TECHNOLOGY OF ELECTRON GENERATION

---

### 2.0. Overview

The fundamental limiting element of high brightness electron beam sources is the cathode. Electrons emitted from the cathode can be manipulated in 6D phase space, but the intrinsic quality of the electron beam is fixed once the electrons leave the cathode surface. Therefore, a key aim of modern beam physics is to understand and improve the quality of the electron beam from the cathode itself.

Cathodes currently fall into three basic classes: (1) Thermionic cathodes for injectors to X-ray synchrotron light sources and industry accelerators, (2) Small emitting area, ultra-bright field emission sources for electron microscopes, and (3) Photocathodes for X-ray free electron lasers (XFELs) and ultrafast electron diffraction (UED) and microscopy (UEM).

Injectors for storage rings and industry applications do not require high-brightness sources since the phase space density of the final beam is determined by the ring properties, and memory of the injector characteristics is lost. Thermionic cathodes are chosen for robustness, high average power, and modest emittance requirements. High-resolution electron microscopes require high transverse coherence and very low energy spreads, making the cold field emitter tip the most common source.

Leading edge applications take advantage of laser-driven photoemission electron sources that can generate beams with low transverse momentum and high charge, with a pulse length easily controllable by the laser. Laser technology has advanced to the point where laser pulse shaping can provide full control of the beam distribution. Designing the cathode and the laser together as a system is now becoming essential for improving high-brightness performance.

The quality of the electron beam generated from a photocathode is characterized by the intrinsic emittance, defined as the emittance per unit rms laser spot size on the cathode. Intrinsic emittance is mainly determined by the angular spread of the electrons as they leave the cathode surface. This quantity is closely related to the mean transverse energy (MTE) distribution of emitting particles, i.e.  $\sqrt{MTE/m_0c^2}$ . To set a scale for intrinsic emittance, photocathodes currently used in XFEL or UED sources typically have 200-500 meV MTE and 0.5-1.0 mm-mrad/mm rms normalized intrinsic emittance values [Dowell, 2010].

The most significant advances in cathode physics from the last five years include the demonstration of record high average current from a normal conducting DC photoinjector [Dunham, 2013] and the widespread development and characterization of multi-alkali cathodes [Schubert, 2016], which hold promise for good quantum efficiency with low intrinsic emittances. The Photocathode Physics for Photoinjectors (P3) community is shifting from traditional recipe-based production of cathodes to cathode design based on a much deeper understanding of solid-state physics. Cathodes may no longer be limited to natural materials, but could be designed, guided by computational and analytical methods, and then synthesized [Nemeth, 2010; Droubay, 2014; Velazquez, 2015].

Recent research and experimentation has reduced the risks associated with the development and use of advanced cathodes:

- (1) The gun vacuum quality has been improved with widespread use of load-lock systems, allowing air-sensitive cathodes to be inserted into the gun without being exposed to atmosphere. Examples include Cs<sub>2</sub>Te at ANL/AWA, FNAL/FAST, and DESY/FLASH; CsK<sub>2</sub>Sb at Cornell and JLab DC guns; BNL SRF gun; LBNL APEX gun; and PSI RF gun.
- (2) Exotic cathodes with longer lifetimes and higher yield, such as multi-alkalis, can be more reliably and reproducibly fabricated.
- (3) Cathode technology for electron microscopes has improved with cold field emitters made from LaB<sub>6</sub> [Zhang, 2016] and other materials.

Workshop participants identified three specific research focus areas that could maximize the impact of cathode development on broad applications of bright electron sources including existing and future XFEL and ultrafast electron scattering instrumentation, listed in Table 2-1. These would also benefit broad applications of bright electron sources, and they are summarized in the table. The timeframe for the research is near-term in many cases (1-3 years), but spans mid- to long-term as well. For each focus area, the table lists the scientific and technical challenges and impact.

Table 2-1: Panel 1 Research Focus Areas

Research Focus Area	Scientific & Technical Challenges	Application	Impact on source performance
<b>1. Materials development and discovery</b>	Optimize planar photocathodes for reduced transverse emittance and energy spread	XFEL, UED/UEM	5-10× higher brightness
<b>2. Nano-emitters for coherent electron sources</b>	Increase transverse coherence length by shrinking the source size from $\mu\text{m}$ to nm	UED/UEM	10-100× smaller emittance
<b>3. Photocathode materials by design</b>	Engineer material electronic structure to decouple multiple photocathode metrics, thereby eliminating tradeoffs and allowing simultaneous optimization	XFEL/UEM	10× higher brightness and improved lifetime

Photocathodes in high-brightness superconducting RF guns pose unique performance requirements. The lack of SRF-compatible photocathodes with high quantum efficiency (QE) remains one of the main obstacles to adopting this technology for high average current applications.

To improve (i.e. minimize) intrinsic emittance, near-term research should focus on reducing cathode MTE. This can be achieved by: (1) choosing oriented single-crystal materials in which the electron band structure minimizes transverse momentum, (2) cryo-cooling the bulk photocathode substrate, and (3) using optimized laser wavelengths close to the material work function. These techniques have the potential for an order of magnitude reduction in emittance, but many problems remain to be solved. Factors such as nano-roughness, minute changes in surface potential, and laser-induced heating of the electron system may significantly increase emittance. However, there are many reasons to believe that significant improvements are within reach for applications that require  $\sim 100$  pC beam charge, such as XFELs. Advanced materials development, nanofabrication, computation, and characterization tools from fields such as solid state physics, nanoscience, computational chemistry and materials physics, and surface science hold the promise for a breakthrough in the performance of photocathodes (see Section 2.1).

For even lower beam charges of  $\leq 1$  pC, scaling laws indicate an optimum spot size often smaller than that allowed by optical diffraction of the laser pulse. For UED and UEM applications, an emittance improvement by a factor of 10 could be achieved by dramatically reducing the emission source size to sub-micron levels. This could be done either by restricting the physical dimensions of the emitter or by focusing the laser with a large numerical aperture optical system to diffraction-limited spot sizes (see Section 2.2.1).

Beyond the intrinsic emittance (or MTE), many figures of merit can be used to quantify the photocathode performance. Five of these are listed in Table 2-2, along with the desired goals leading to improved performance of future electron sources. In most photocathode materials, all metrics are connected, so that simultaneous optimization of multiple metrics is impractical or results in undesirable tradeoffs for existing photocathode technologies. One research challenge will be to decouple the linkage between the metrics through tailoring or engineering advanced photocathode systems, through materials exploration and discovery, or through engineering of the bulk material and the surface (see Section 2.3).

*Table 2-2: Photocathode metrics*

<b>Metric</b>	<b>Desired goals</b>	<b>Typical value of relevant parameter</b>
<b>Quantum efficiency, QE</b>	Increase charge yield	10 %
<b>Emittance, <math>\epsilon_n</math>, rms</b>	Reduce transverse emittance	0.5 mm-mrad/mm rms
<b>Response time, <math>\Delta t</math></b>	Enable fast pulse shaping	100 fs
<b>Lifetime</b>	Increase operational duration	Weeks
<b>Robustness</b>	Improve survivability in high field environment	$10^{-8}$ Torr vacuum

## 2.1. Materials development and discovery for reduced transverse emittance

State-of-the-art photocathode MTEs are on the order of 200-500 meV, while the lower limit set by disorder-induced heating in the electron beam is around 1-2 meV [Maxson, Bazarov, 2013]. This leaves significant room for improvement. In principle, a factor of 100 reduction in MTE, and consequently a factor of 10 reduction in emittance, is possible. Reducing the intrinsic

emittance by more than a factor of 5 is a realistic goal for the next 3-5 years. The panel identified three primary research thrusts for achieving these goals.

### 2.1.1. Excess energy tuning

MTE reduction can be accomplished by tuning the laser photon energy to just above the cathode work function. Methods include choosing a cathode with a work function just below the laser photon energy, tuning the cathode work function through materials design and engineering, or tuning the laser itself. The problem with these methods of MTE or emittance reduction in a metal is that the QE also decreases, as it is roughly proportional to the square of the energy above the photoemission threshold (i.e., excess energy). For example, a factor of two reduction in the typical value of 0.5 eV above threshold at room temperature results in almost a factor of four reduction in QE. Thus, much more laser power is required to extract the same charge for cryo-cooled photocathodes.

There is fundamental limit to the MTE related to the temperature of the electrons in a crystal [Feng, 2015]. As a corollary, cryo-cooled photocathodes, when operated with laser wavelengths near the photoemission threshold, can help lower MTE [Cultrera, 2015]. In one example, an MTE as low as 22 meV was obtained by cryo-cooling alkali antimonide photocathodes to 90K (Figure 2-1). In principle, 1 to 2 orders of magnitude reduction in MTE should be possible by operating the photocathode at liquid He temperatures.

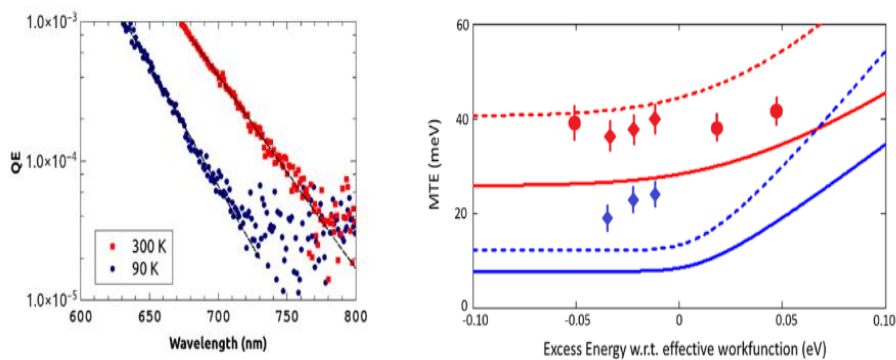


Figure 2-1: QE and MTE of alkali antimonide photocathodes operated close to threshold at ambient and cryogenic temperatures. Reprinted with permission from [Cultrera, 2015].

Development of warm electron guns capable of cryo-cooling the photocathode could serve as a bridge for this activity. Cathode characterization chambers should enable cooling the

cathode material to cryogenic temperature. A cathode load-lock system also needs be designed that cools the cathode to cryogenic temperatures during operation in an NCRF gun. Initial testing in an NCRF gun, rather than an SCRF gun, greatly simplifies the engineering, fabrication, and operation of the test gun. Any success with the NCRF gun could be transferred to SCRF guns using techniques learned from SCRF accelerating cavity development.

### ***2.1.2. Utilizing the band structure and ordered crystals***

Density functional theory (DFT) can be used to calculate the electronic structure of photoemissive materials, determine the work function of crystals in different orientations, evaluate the intrinsic emittance of pristine surfaces, and estimate QE. The results of DFT calculations can also be incorporated into photoemission simulations to predict the transverse momentum distribution of the emitted electrons. A reduction in transverse momentum spread can be achieved by selecting appropriately-oriented single-crystal materials.

DFT-based simulations have already led to significant advances in the understanding of photoemission. Analysis of the polycrystalline copper photocathodes used at LCLS [Vecchione, 2016] indicates that the nominal  $0.6 \mu\text{m}/\text{mm}$  normalized transverse emittance from 253nm laser irradiation can be explained by Cu (110) crystal facets dominating the emission from polycrystalline surfaces. Detailed examination of emission from the (001) face of body-centered cubic metals [T. Li, 2015] has revealed that lower than expected values of MTE are possible when the electronic band structure restricts the maximum transverse momentum of the emitted electrons (Figure 2-2). It turns out that photoemission in certain systems (e.g., group VB metals: V, Nb, and Ta) exhibits a very small effective electron mass [Berger, 2012; Dowell, 2016], whereby higher-energy electrons emit mainly from ‘hole-like’ states with lower transverse momenta. Investigations have found a similar effect in an oriented-crystal system of magnesium oxide layers with silver [Nemeth, 2010; Droubay, 2014]. Single-crystal III-V semiconductors activated to negative electron affinity (NEA) also exhibit extremely low effective electron mass, but the failure of attempts to observe the expected narrow emission cone needs to be explained before a clear path towards sub-thermal MTE emission can be realized [Bradley, 1977; Bazarov, Dunham, et al., 2008].

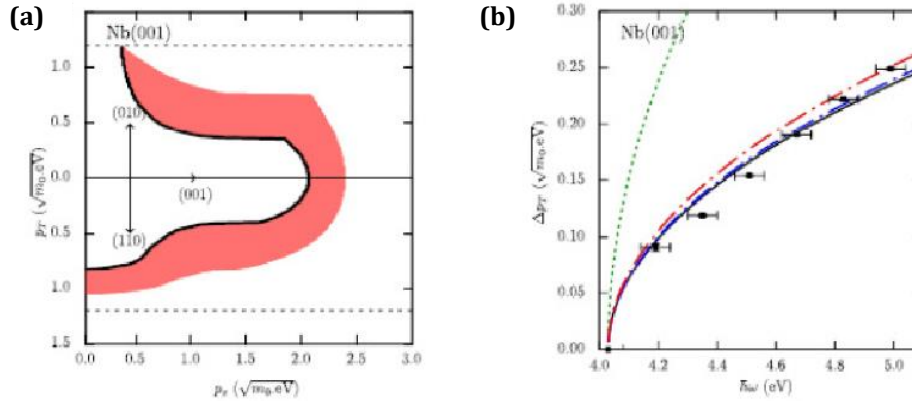


Figure 2-2: DFT-evaluated photoemission from Nb(001). (a) Crystal momentum distribution of the emitting states (red shading) below the Fermi level (black line) for  $\hbar\omega = 4.75\text{eV}$ . (b) Calculated spectral dependence of  $\Delta p_T$  for crystal temperatures of 0K (data points and black line), 300K (blue dot-dashed), and 2750K (red dot-dashed) compared to the dependence calculated assuming a disordered cathode (dashed green line). Reproduced from [T. Li, 2015] with permission from AIP Publishing.

Another interesting possibility for reducing the intrinsic emittance is the use of topological semimetals, which can exhibit a Dirac cone (and zero effective mass) for their quasiparticles near the bottom of a band [Akrap, 2016].

Computational screening of existing single-crystal materials using techniques like DFT should be used to identify candidates that show the potential for delivering small transverse momentum spreads [Camino, 2016; T. Li, 2015]. It will be advantageous to use the high-throughput simulation capabilities developed by the DOE BES Materials Genome Initiative (MGI). Next-generation photoemission simulations should be able to consider the effects of light polarization, surface states and phonon scattering. Such simulations can be used to guide the development of new materials, hetero-structures and ordered over-layers with band-structures chosen to deliver small transverse spreads, high quantum efficiency, low work functions and a prompt response time.

### 2.1.3. Identifying and overcoming limitations

Several factors will limit the minimum possible transverse momentum distribution from photocathodes. It is essential to identify and mitigate these factors when they occur.

One such factor is the physical and chemical surface roughness at micron to Ångstrom length scales [Karkare, Bazarov, 2015; Karkare, Boulet, 2015] (see Figure 2-3a). Photoemission models should consider the effects of such surface variations to identify the limits they impose and to enable their proper inclusion in beam optics simulations. Measurements of such surface

variations should be performed using tools like ultra-high vacuum atomic force microscopy (UHV-AFM, Figure 2-3b), Kelvin force probe microscopy (KPFM), and ultraviolet photoemission electron microscopy (UV-PEEM). The effects of variations should be experimentally verified via in-situ measurements of momentum distributions of photoemitted electrons. Finally, development of atomically smooth photocathode surfaces will be essential.

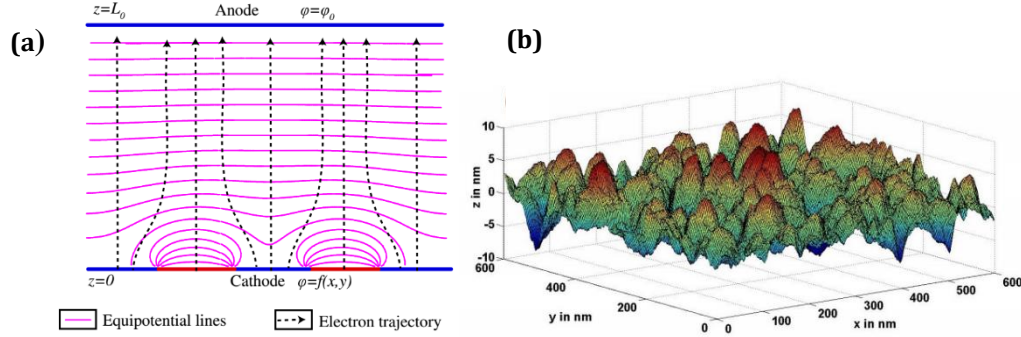


Figure 2-3: (a) Distorted equipotential lines (red) due to varying surface potential and consequently distorted electron trajectories (black). Reprinted with permission from [Karkare, Bazarov, 2015]. Copyright 2015 by the American Physical Society. (b) Surface morphology of an alkali antimonide cathode as measured by an UHV-AFM. Reproduced from [Feng, 2017] with permission from AIP Publishing.

Laser heating of electrons within the photocathode can increase the beam transverse momentum spread [Jensen, 2007; Maxson, 2017] due to the increase in the temperature of the electrons within the material by several thousand degrees Kelvin at a femtosecond time scale. This can be a severe problem, especially for cryo-cooled photocathodes or photocathodes with low QE. Designing high QE photocathodes or using single-crystal photocathodes with emission from filled or partially filled hole-like bands are possible ways of overcoming these limitations.

## 2.2. Nano-emitters for coherent electron sources

The transverse brightness and, therefore, the transverse coherence length of electron beams can be increased by several orders of magnitude by shrinking the source size from millimeters to nanometers. This can be achieved either through electric field enhancement near the cathode surface or by the increase in current density that comes from a smaller source [Filippetto, 2014].

Such increased brightness would have a dramatic impact on time-resolved electron diffraction and microscopy experiments, expanding the scientific breadth of such instruments to nano- and meso-scale systems [Filippetto, 2016]. By increasing the transverse coherence by

more than an order of magnitude, researchers will gain access to the ultrafast dynamics of complex systems, such as nano-machines and biological molecules.

A single nano-emitter can provide enough electrons for diffraction experiments, but due to its limited size, cannot provide the high charge per bunch typical of XFELs. To increase the total amount of deliverable charge, it would be necessary to develop arrays of micron-scale to nanometer-scale emitters.

### ***2.2.1. Single photo-triggered nano-emitters***

Several approaches are possible to reduce the cathode emitting area: (1) using single micro or nano tips on the cathode surface to emit electrons via photo-triggered field emission [Lewellen, 2005], (2) depositing or etching a sub-micron active photo-emitting area onto the cathode surface, or (3) using plasmonic lenses to focus light to sub-wavelength spot sizes.

A small tip provides the electric field enhancement necessary to extract enough electrons for single shot UED from a sub-micron spot size. With a moderate field enhancement of about 10, local surface fields of few tens of MV/m can be produced [Maxson, 2015]. The shape of the tip can be optimized using genetic algorithms to properly tailor the electric field to preserve the electron beam emittance.

The micro-tips can also be coated with a photo-emissive layer so that electrons are produced by illuminating the material in transmission mode. When operated with IR lasers, multi-alkali antimonides have demonstrated simultaneously a sufficient QE of around  $10^{-5}$  and intrinsic emittance close to the thermal limit, and therefore are an immediate candidate for this purpose [Cultrera, 2016; Lee, 2016].

Another approach to reach the sub nm-rad level in electron beam emittance is to operate a high-QE and low-emittance flat photocathode in transmission mode. The laser beam is focused down to sub-micron, diffraction-limited spot sizes using a very short focal length lens placed behind the transmissive substrate. Electron guns in spin-resolved electron microscopes have already developed the technology to illuminate cathodes in transmission mode in high voltage DC guns (see Figure 2-4) [Kuwahara, 2011].

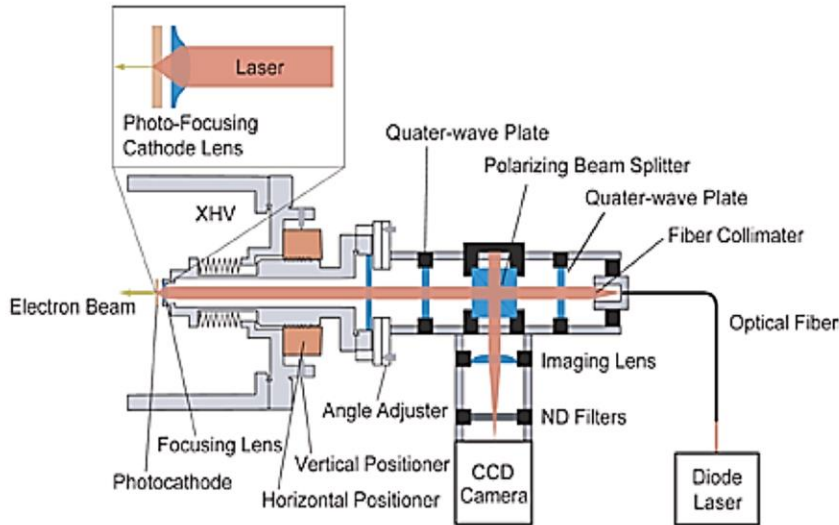


Figure 2-4: Configuration of a photo-electron source for microscopy applications with the photocathode back illuminated to produce a sub-micron size electron source. Reprinted with permission from [Kuwahara, 2011].

### 2.2.2. Lensed nano-emitter arrays

This approach uses a nanostructure consisting of an array of nano-emitters with a micro electrostatic lens placed in front of each nano-emitter [Tsuji no, 2009; Helfen stein, 2013]. A schematic is shown in Figure 2-5. The micro-lenses collimate the beamlets from each nano-emitter, which combine to form a single ultra-low-emittance beam (see Figure 2-6). Several challenges need to be solved in order to make this technology a reality: coupling light to the nano-emitters, fabricating the structure, and biasing the microlenses.

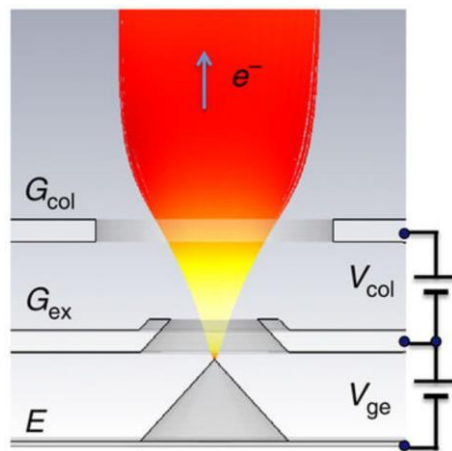


Figure 2-5: Lensed nano-emitter. Reprinted with permission from [Tsuji no, 2016].

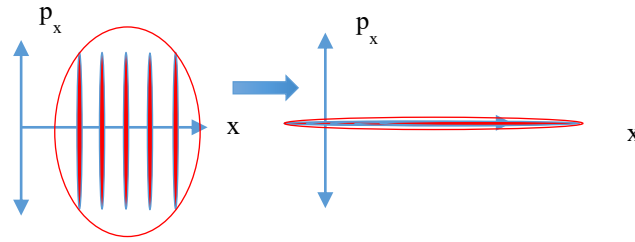


Figure 2-6: Micro lenses rotate each of the beamlets in phase space to form a beam with very small volume in phase space implying very low intrinsic emittance. Courtesy of LBNL.

Plasmonic focusing schemes may be able to couple light to the nano-emitters. The scheme uses an array of plasmonic bow-tie antennae along with back illumination to focus light to less than 10 nm spot sizes. Fairly standard nano-manufacturing capabilities may enable researchers to precisely fabricate such a structure. Lensed arrays will also require new electron guns with the ability to bias the micro lenses. Despite their complexity, lensed nano-emitter arrays present an excellent alternative to current photocathode technologies [Li, 2013; Alexander, 2016] and also enable reduction of transverse emittance below the limit imposed by disorder-induced heating [Maxson, Bazarov, 2013].

### 2.3. Photocathode materials by design

In natural materials, critical parameters such as emittance, QE, lifetime, and temporal response are coupled. For example, thermalization of the electron population to the lattice temperature improves emittance, but because the thermalized tails can take tens of picoseconds (or longer) to be emitted, the response time is greatly increased [Bazarov, Dunham, et al., 2008]. The inclusion of surface layers tends to compromise robustness and lifetime [diBona, 1996; Pavlenko, 2016]. Often the same mechanisms that improve transport and barrier height negatively impact response time and emittance [Jensen, 2011]. Further, the surface condition of a polycrystalline or single crystal material can be a source of increased emittance, with geometric roughness causing emission variation or work function variation [Karkare, 2011; Jensen, 2013].

The goal of this research focus area is to understand, validate, and control the effects of nano-structure on electronic emission [Shabaev, 2013; Maxson, 2017; Savitzky, 2016]. New approaches to material design and electronic engineering can potentially decouple performance parameters, leading to independent application-specific optimization of several metrics. The engineered control of material stoichiometry and structure makes it possible to exploit and

optimize the separate processes governing the absorption of light, facilitating electron transport, and controlling emission of photo-excited electrons. This engineering would rely on processes created for the fabrication of hetero-structures and nano-crystalline technology. Such techniques have not yet been used for enhancing the functionality of photocathodes.

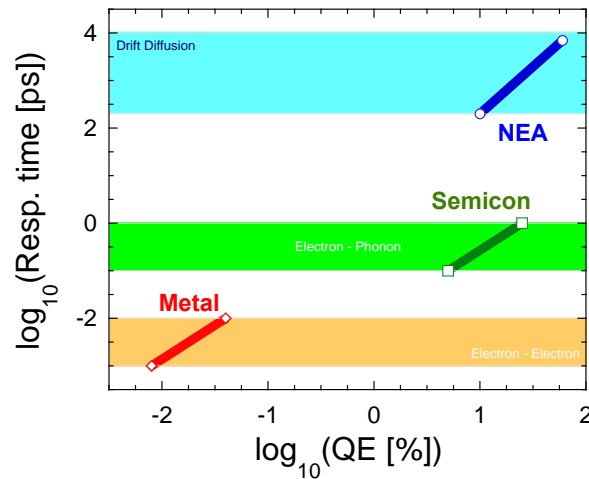


Figure 2-7: QE vs. response time for photocathodes. Dominant scattering mechanisms: electron-electron (metals like Cu); electron-phonon (semiconductors like Cs3 Sb); drift-diffusion (NEA like GaAs). Reprinted with permission after Figure 14 in [Spicer, 1993].

The potential benefits can be grouped into either bulk material modifications or surface structure changes. Modifications to the bulk material include band bending or band gap variation by doping or using graded stoichiometries to modify the cathode optical and transport properties. Superlattices, discrete energy levels associated with resonant structures, quantum dots, and 2D electron gases can all affect surface structure.

### 2.3.1. Computational material physics design and modeling tools

Computational material physics methods can be used to find the effect of material properties, hetero-structures, and applied field on the emission properties of engineered confined-electron structures. Example methods include DFT, DFT-Hartree-Fock (hetero-structure and nano-scale features), molecular dynamics (atomic scale simulations), dissipative particle dynamics, and Lattice Boltzmann or cellular automata methods (mesoscale simulations).

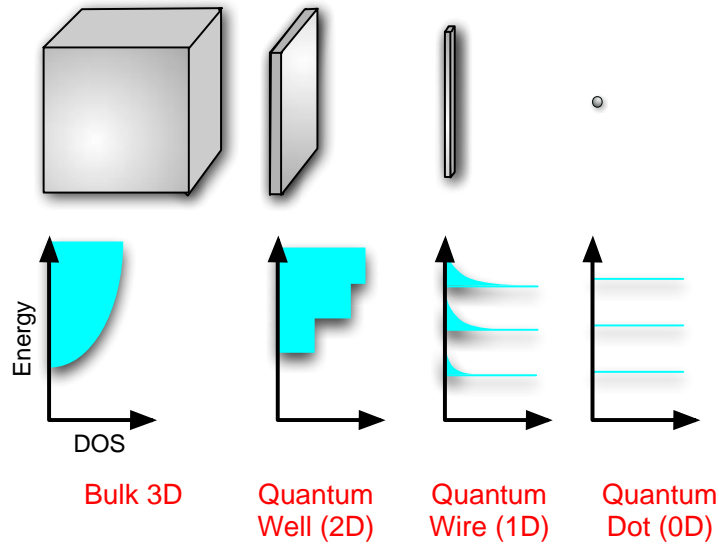


Figure 2-8: Plasmonic structures in the form of nanorods, nanocavities. Courtesy of LANL.

Hetero-structure / superlattice layers and surface distributions introduce discrete energy levels and can exhibit quantum effects such as resonant tunneling. It is possible to fabricate pristine, ordered layers (e.g., graphene) or films at the surface. In addition to modifying transport at the surface, these can also impact surface sensitivity to contamination and degradation. Examples of the tuning and possible optimization of materials and nano-crystalline solids are indicated in the quantum dots of Figure 2-8. These “designer” nanostructure materials exhibit resonant tunneling processes, unlike the usual “over-the-barrier” emission processes that govern most photocathodes and all thermionic cathodes [Jensen, 2013; Karkare, 2014].

Although super-lattices and quantum dots are not new for light emission applications, their use to address photocathode performance and to mitigate between contrary metrics open a new avenue to break the deadlock between those metrics.

### 2.3.2. Materials synthesis and characterization

Atomic Layer Deposition (ALD) or Pulsed Layer Deposition (PLD) can give control over the stoichiometry of a bulk material. Structures such as a lattice of quantum dots can be used to control and decouple the discrete energy levels, tailor the band gap, adjust the effective mass variation, specify the dielectric and optical properties, and thereby control many of the features upon which photo-yield traditionally depends. In the longer term, photocathode characterization

should focus on electronic and emission properties including conductivity, spectral response, transverse momentum spread, and temporal response.

X-ray diffraction (XRD), X-ray fluorescence (XRF), X-ray photoemission spectroscopy (XPS), X-ray reflectivity (XRR), and Auger spectroscopy [Ruiz-Oses, 2014; Schubert, 2016] are the principal tools used to analyze crystal structure, surface structure, and chemical composition. Researchers are beginning to use other tools, such as angle resolved photoemission spectroscopy (ARPES) and momentatron [Vecchione, 2011] to directly measure transverse momentum spread [Lee, 2016]. Advanced materials characterization tools need to be located in the same pristine vacuum environment as material synthesis tools.

## 2.4. Cross-cutting technologies and issues

### 2.4.1. Laser shaping

To minimize the space charge effects and preserve the brightness of the electron beam, beam parameters should remain uniform in all three dimensions. Most photocathodes (Cu, CeTe, Mg) used in the current photoinjectors require a UV drive laser, and transverse beam quality is degraded significantly during the UV conversion. This results in hot spots, which imprint into the electron beam leading to degradation in electron source performance. In addition, the QE of the photocathode is not spatially uniform, so even a spatially uniform laser may lead to a non-uniform distribution of the electron bunch.

Typically, a photocathode drive laser is transversally shaped by expanding the beam to overlap with an iris aperture, which is then imaged onto the cathode to produce either a quasi-uniform “flat top” or “cut Gaussian” beam (see Figure 2-9). The laser beam is longitudinally (temporally) shaped by optically stretching the pulse to a few picoseconds or longitudinally stacking a few shorter pulses to produce an approximately cylindrical distribution, which minimizes the space-charge induced emittance growth.

For transverse shaping, the main challenge so far has been to identify an adaptive optical element that operates in the UV range and can withstand the fluence required to produce the charge needed by the experiments. Efforts to implement adaptive transverse laser profile shaping have been reported by numerous groups, including LCLS using digital micromirror devices [S. Li, 2015], Spring8 using a deformable mirror [Tomizawa, 2004], and Cornell using a liquid-

crystal spatial light modulator [Maxson, Lee, 2013]. Further progress in this effort is likely to require partnering with a manufacturer of spatial light modulators to improve UV compatibility, increase damage threshold, and simplify the optical properties of the device.

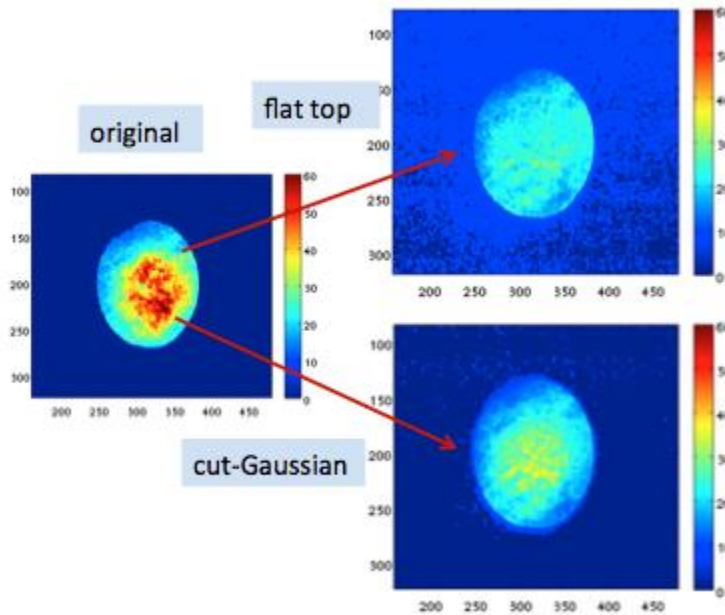


Figure 2-9: Spatial profile of the UV laser beam for the LCLS photoinjector before and after spatial shaping. Courtesy of SLAC.

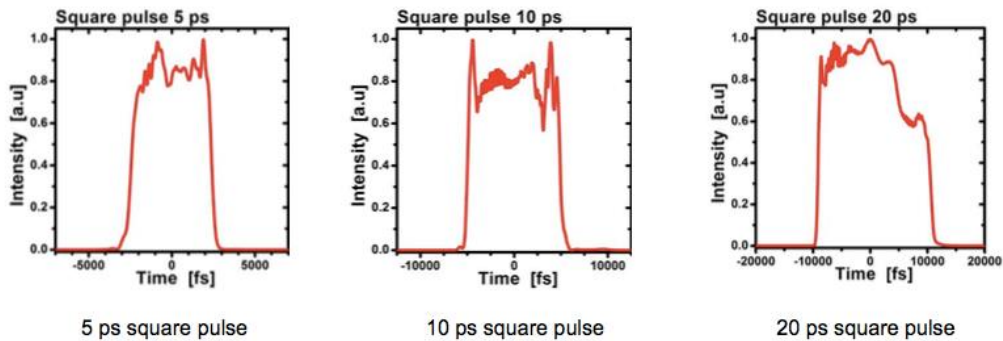


Figure 2-10: Quasi-flat-top laser temporal profiles generated through nonlinear spectral phase control of a 1030nm seed oscillator with a transform limited pulse duration of  $\sim 300$ fs. Courtesy of Amplitude Systèmes. Reprinted with permission.

The longitudinal distribution of electron bunches can be controlled using passive dispersive stretching, free-space or birefringent crystal pulse-stacking techniques [Bazarov, Ouzounov, 2008], or active spectral phase and amplitude control [Weiner, 2000]. A recent

method of non-linear phase-only square-pulse synthesis has been developed [Lozovoy, 2015]; preliminary results are shown in Figure 2-10. Active control has numerous potential advantages, but further R&D of these techniques is required to determine to what extent the pulse shape can be maintained through harmonic conversion, and over what dynamic range the temporal pulse shape can be manipulated to enable future applications. Such applications include multiple bunches or bunches with special temporal structures to compensate or enhance downstream beam dynamics (e.g. coherent synchrotron radiation, micro-bunching, etc.).

A significant improvement in the performance, reliability, and cost of the laser systems for future electron sources would be enabled by the development of photocathodes with lower energy work function, e.g. below 3.1eV (second harmonic of Ti:sapphire 0.8 $\mu$ m (1.55eV) lasers) or 2.3eV (second harmonic of common 1 $\mu$ m (1.15eV) lasers). At visible and IR laser wavelengths, there are numerous robust options for optical materials, diagnostics, and direct spatial and temporal shaping. If wavelength optimization beyond the wavelength coverage of existing laser media is required for optimal performance of a given photocathode, optical parametric amplifiers (OPAs) pumped by Ti:sapphire can produce nearly any visible wavelength through sum frequency mixing. This does, however, increase the complexity of the laser system.

Beyond traditional temporal and spatial beam shaping, programmable 4D field patterns can control the transverse polarization distribution, spatio-temporal shape, and wavefront simultaneously. These novel photon sources are increasingly attracting interest for applications where unconventional optical fields drive processes with spatially varying amplitude, phase and/or polarization within the beam cross-section.

#### ***2.4.2. A new paradigm for accelerating photocathode development***

New BES facility projects have typically chosen highly mature injector and cathode technologies as the baseline. Limited R&D is done for specific projects, with the consequence that progress in advancing novel injector technologies and performance is slow. Many novel photocathode ideas have been developed in the past five years, yet many of these are still in the conceptual or proof-of-concept stage. There is a great need for characterizing and validating photocathode concepts in a realistic injector/gun environment. This development requires significant standardization across the community as well as adoption of best practice distilled from adjacent disciplines (e.g., commercial semiconductor fabrication processes).

The panel recommends that a cohesive, integrated, cooperative effort be established among cathode, laser, and gun research groups and facilities. The goal is to optimize and enable the entire cathode lifecycle: concept, computational materials physics, design, fabrication, characterization, and testing. This effort should encourage collaboration and access between cathode synthesis centers and test facilities. Gun-cathode-laser test facilities that are independent of user operations should be established, and opportunities to test cathodes at electron microscopy (EM) facilities should be explored. It will be particularly important to integrate the findings of such tests in beam optics codes for novel cathode concepts whose operation is outside traditional theory. Finally, the effort should survey and leverage existing design, synthesis, and laboratory test facilities such as those at the DOE nano-centers, synchrotrons, and MGI-funded institutions.

## 3. PANEL 2: CONTINUOUS WAVE ELECTRON SOURCES

### 3.0. Overview

Continuous wave (CW) electron sources have been widely employed in electron accelerators; they are the workhorses for synchrotron light sources, medical accelerators, electron microscopes and nuclear physics machines. The introduction of photocathodes with high quantum efficiency in the 1980s has led to dramatic improvements in beam brightness. Three major types of CW photoinjectors exist: the DC photoinjector (DC), the normal conducting RF photoinjector (NCRF), and the superconducting RF photoinjector (SRF gun).

Over the last few decades, researchers around the world have devoted significant effort to developing CW photoinjectors for energy recovery linac (ERL) and FEL applications. Vigorous research programs at Cornell, Jefferson Lab and KEK/JAEA [Dunham, 2013; Adderley, 2010; Nishimori, 2016] have brought many new advances and have demonstrated that DC guns can provide high quality electron beams. Recent measurements at Cornell showed that a gun operating at 400 kV, followed by a normal conducting buncher cavity and an SRF booster module, could meet the specifications for the LCLS-II program (see Figure 3-1).

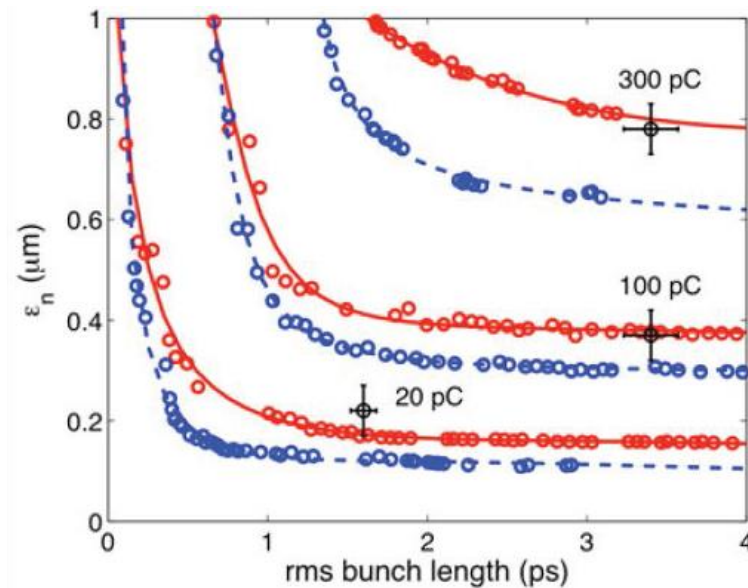


Figure 3-1: Cornell injector emittance results at 20, 100, and 300 pC. Black points are measured, blue points are simulated with ideal laser, red are simulated with measured laser profile. Reprinted with permission from [Bartnik, 2015].

The DC gun is inherently a CW electron source, but both the low electric field strength at the cathode surface and the short accelerating gap limit the maximum extractable bunch charge and maximum energy. DC guns can provide operating voltages up to 500 kV and cathode gradients in the 5 to 10 MV/m range. The DC nature allows for very flexible operation, creating beams ranging from DC to any repetition rate or pulse structure. Average beam currents as high as a 100 mA are possible, with good beam stability. Bunch charges up to 1 nC with emittances of 1  $\mu\text{m}$  have been demonstrated, but it is difficult to raise the charge beyond this without higher gradients. The DC structure is also compatible with extremely high vacuum, which allows use of any type of cathode imaginable, such as the vacuum-sensitive semiconductor cathode GaAs. Cathode load-lock and insertion mechanisms have been routinely used in DC guns.

The main drawbacks of DC guns are the relatively low accelerating gradient, and the resulting lower total beam energy. Because of space charge effects, the weak accelerating field means that for a given charge, a larger laser spot size is required on the cathode, thus limiting the minimum achievable emittance. Another advantage of higher total energy is that the beam can be directly injected into a standard accelerating structure, eliminating the need for bunching and capture sections. The DC gun is a mature technology, with little room to significantly improve its performance.

High gradient NCRF guns are the most advanced type of electron injectors, producing high quality beams. One of the main challenges for a CW NCRF photoinjector is the heat load on the RF cavity. Higher duty cycles can be achieved by using a lower RF frequency, because the resulting larger cavities create lower power density on the structure walls. For example, the Boeing gun has achieved 25% duty cycle operation at 433 MHz [Dowell, 1993], and scientists at Los Alamos National Lab developed a 700 MHz normal-conducting RF gun where a sophisticated cooling system allowed CW RF operation [Nguyen, 2011]. The gun used at the ELSA 19 MeV linac provides an example of a lower frequency NCRF gun that has been proven in operation [Dei-cas, 1990]. This 144 MHz gun has produced high charge, low emittance beams at a ~2% duty cycle.

An LBNL group developed a VHF CW NCRF gun operating at 186 MHz [Sannibale, 2012]. This gun, called 'APEX', is based on conventional mechanical and RF technologies, and produces 750 keV beam with a field gradient 20 MV/m on the cathode. With a gun cavity frequency in the VHF range and a modest field on the cathode, the heat load on the cavity walls

during CW operation is reduced so it can be removed by conventional cooling techniques. Additionally, the long RF wavelength allows for the design of an efficient vacuum system using large pumping slots to provide a high-vacuum conductance path towards external vacuum pumps, with negligible field distortion. This vacuum design provides the extremely low pressures required for using reactive semiconductor cathodes with QE lifetimes compatible with the operation of a user facility.

SRF guns are promising candidates to achieve the high gradient and energy goals for future XFEL and ultrafast electron scattering facilities. By merging the well-established NCRF technology and superconductivity, the dissipated RF power is reduced by several orders of magnitude and CW operation with high average currents becomes possible. Since the first proposed SRF gun in 1989 [Chaloupka, 1989], the technology has made significant progress [Sekutowicz, 2015], achieving fields on the order of 10 MV/m at the cathode during the electron emission phase with superconducting (SC) cathodes. While existing cathodes can be readily used for applications needing relatively low charge per bunch, future CW FELs will require semiconductor cathodes with high quantum efficiency (QE) to deliver hundreds of pC of charge per bunch at repetition rates up to MHz. During the last few decades, several groups have tested such cathodes in SRF guns with mixed results. While the cathode QE degradation and lifetime were mostly acceptable, the insertion of a warm cathode in the SRF cavity induced a significant degradation of the gradient (and consequently also a decrease in beam energy) limiting the best value so far to ~20 MV/m. Table 3-1 summarizes the current performance of the CW photocathode injectors.

The R&D required to develop the CW electron source required for future high-repetition hard X-ray FEL and UED/UEM facilities includes overall system design and optimization, comparison of quarter-wave (SRF and NCRF) and high frequency SRF designs, and evaluation of both multi-frequency and multi-mode concepts. Following these optimization studies and design tradeoffs, the best candidate will be constructed and tested. The following sections present a detailed discussion of various CW electron sources.

Several evolutionary improvements can be combined to meet future FEL and UED/UEM needs. The overall CW injector R&D goal is to significantly increase accelerating gradients on the cathode and thus, output beam energy. More than a factor of two improvement in both gradient and beam energy are needed. Major advances in NCRF and SRF CW injectors are

needed to meet the challenging requirements. Start-to-end simulations should be pursued to narrow the technology choices.

*Table 3-1: Present performance level for high-brightness CW and DC electron guns. Adapted with permission from [Sannibale, 2016].*

Group	Tech- nology	$E_{z,cath}$ at emission, goal	$E_{z,cath}$ at emission, measured	Beam energy, goal	Beam energy, measured	$\epsilon_n$ at charge, measured	Current/ rep rate, measured
		MV/m	MV/m	MeV	MeV	$\mu\text{m}\cdot\text{rad}/\text{pC}$	mA/Hz
Cornell	DC	6	~5	0.5-0.75	~0.4	~0.2 / 20 ~0.3 / 100 ~0.6 / 300	20-65 / $1.3 \times 10^9$
Daresbury (JLab- type Gun)	DC	3.3	3.1	0.35	0.325	5 / 50	8 / $81.25 \cdot 10^6$ 100ms @ 20Hz
KEK/JAEA	DC	6.7	6.7	0.5	0.45-0.5	1.1 / 7.7	1 / $1.3 \cdot 10^9$
JLab	Inverted DC	4.5	~3.9	0.35	~0.3	To be measured	1 / DC
BNL	112 MHz SRF	22.5	15	2	~1.2	2 / 250	0.05 / 5000
DESY Gun 0.2	1.3GHz SRF	40	40/Nb cathode	3.7	To be measured	To be measured	To be measured
HZB/ DESY Gun 0.1	1.3 GHz SRF	40	20 / Pb cathode	3.7	~1.8	2 / 6	$50 \cdot 10^{-9}$ / 8000
HZB	1.3 GHz SRF	24	To be measured	2.3	To be measured	To be measured	To be measured
HZDR	1.3 GHz SRF	30	16 / Cu cathode	9.5	4.5/Cu cathode	3/80 Cs <sub>2</sub> Te cath.	0.4/13·10 <sup>6</sup>
KEK	1.3 GHz SRF	25	To be measured	2	To be measured	To be measured	To be measured
Wisconsin	200 MHz SRF	40	20 MV/m	4	2	1.5 / 100	Not available
LANL	700 MHz NCRF	10	~9.8	2.7	2.5	Not available	Not available
LBNL	186 MHz NCRF	19.5	21	0.75	> 0.8	~0.2 / 20	0.3 / $1 \cdot 10^6$
Peking University	DC/1.3GHz SRF	5	2.6	5	3.4	~2 / 20	0.55 / $81.3 \cdot 10^6$

This panel addressed PRD #2, CW injector R&D to significantly increase accelerating gradients on the cathode and output beam energy, with a focus on NCRF and SRF sources. The panel concluded that DC guns are a relatively mature technology, and any advances in cathodes and lasers resulting from R&D on NCRF and SRF guns could be readily adopted for DC guns to improve their performance. Additional details and secondary research directions are discussed in

Section 3.4. The bulk of this chapter concentrates on the following three focus areas of research on NCRF and SRF guns.

- (1) VHF NCRF gun development. Conduct engineering studies to improve the performance of an NCRF gun with increased gradient on the cathode and total electron beam energy, with a goal of 30 MV/m and greater than 2 MeV beam energy.
- (2) High-frequency SRF gun. Investigate SRF gun designs using new geometries to better utilize the peak field, with a target of 50 MV/m on an installed cathode.
- (3) VHF SRF gun. Capitalize on recent results for this type of gun, which promises to meet the future CW FEL needs. Carry out a design and experimental program to improve the operating gradient to 40 MV/m with total beam energy greater than 2 MeV on an installed cathode, and perform emittance measurements.

### 3.1. VHF NCRF guns

High-repetition-rate, high-brightness electron beam applications such as MHz-class X-ray FELs, UED and UEM rely on electron beams with high 6D brightness to achieve the extreme performance and resolution these applications demand. High 6D brightness requires high accelerating gradients at the gun cathode and high beam energies at the electron gun exit, a challenge for guns operating at high repetition rates. High frequency, normal-conducting (>~1 GHz) RF guns have already widely demonstrated the successful brightness performance at relatively low repetition rates (~100 Hz), but this cannot be scaled up to MHz and GHz rates because of the unrealistically high heat load on the gun cavity walls.

The APEX results have demonstrated that CW guns in the VHF frequency range can represent a low risk, and cost-effective way of achieving the high-gradient, high-energy parameters required by CW FEL machines. Based on these results, a revised version of APEX, APEX-2, has been proposed with higher gradients and beam energies at the gun. APEX-2 would provide the significantly higher brightness demanded by recently proposed upgrades for high repetition rate X-ray FELs and UED/UEM experiments. The new design consists of a two-cell version of the existing VHF gun (see Figure 3-2 and Figure 3-3) that would generate field gradients of up to ~34 MV/m and beam energies of up to ~2 MeV (increases of 1.75 and 2.7 times in gradient and beam energy, respectively, when compared with APEX (Table 3-2)). This is possible by extending the technology demonstrated by APEX. The RF power is provided by

four commercially available conventional RF amplifiers (solid state or tetrode-based), each one providing about 65 kW of CW power. Two of these amplifiers are currently driving APEX reliably at the required power.

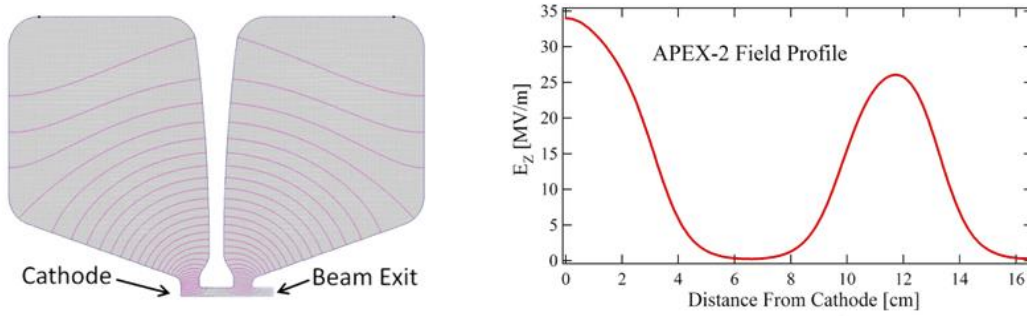


Figure 3-2: Superfish simulation showing the electric field distribution inside APEX-2 cavity (left), and the on-axis electric field profile (right). Courtesy of LBNL.

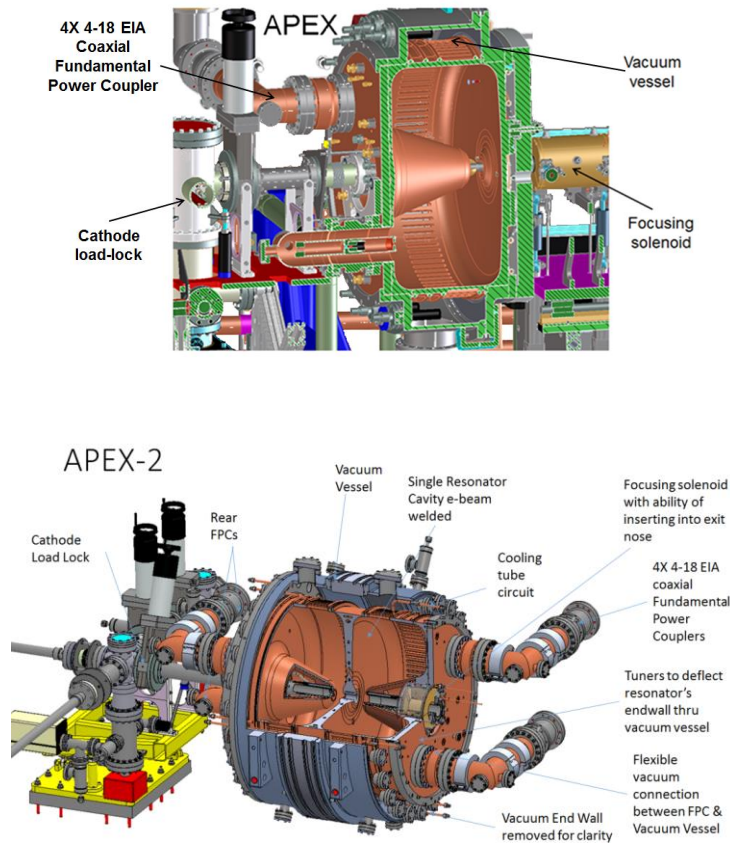


Figure 3-3: CAD views of APEX, the existing VHF-Gun (top), and of APEX-2, the proposed dual-cell upgraded version (bottom). Courtesy of LBNL.

Table 3-2: Preliminary parameters for the APEX and APEX-2 guns

Parameter	APEX	APEX-2
Frequency (MHz)	186.7 (1300/7)	162.5 (1300/8)
Mode of operation	CW	CW
Launching field at photocathode (MV/m)	19.5	34
Beam energy (MeV)	0.75	2
Number of cells	1	2
RMS power per cell (kW)	85	127
Peak wall power density (W/cm <sup>2</sup> )	22	30
Cavity inner radius (cm)	34.7	47.5
Cell length (cm)	35.0	35.0

### 3.2. High frequency SRF guns

Four SRF gun design approaches have been under investigation over the past two decades: (1) a DC gun adjacent to an SC cavity, (2) a choke filter with a non-superconducting cathode, (3) a superconducting cathode integrated into a SC cavity, and (4) quarter-wave, VHF SRF guns.

The first three are high-frequency guns and the last is a relatively low-frequency (VHF) gun. Their present status is discussed below.

#### 3.2.1. DC gun adjacent to SC cavity

The main advantage of using a DC gun coupled to an SRF cavity is that the cathode does not penetrate the interior of the SC gun cavity, which helps to preserve its SRF performance. The main limitation is that low-energy electrons must pass a certain distance before they enter the high electric accelerating field of the cavity. This constrains the beam emittance and/or electron

population per bunch due to the space charge force. This type of gun was initially designed to operate in pulsed mode but can also operate in CW mode. The approach was investigated for many years at Peking University [Hao, 2015]. The gun cavity in the final vertical test reached  $E_{acc}$  of 23.5 MV/m with intrinsic  $Q_0$  of  $10^{10}$ . Later, during the pulsed beam test, the DC voltage of the gun and the cavity gradient were both set to half of their nominal specified values. Nonetheless, the normalized emittance measured at 162.5 kHz bunch repetition rate was  $2 \mu\text{m}$  for 30 pC bunches, very close to the goal of  $1.7 \mu\text{m}$ . This type of system is therefore not likely to provide the low emittance beams needed for X-ray FELs due to the low voltage from the gun.

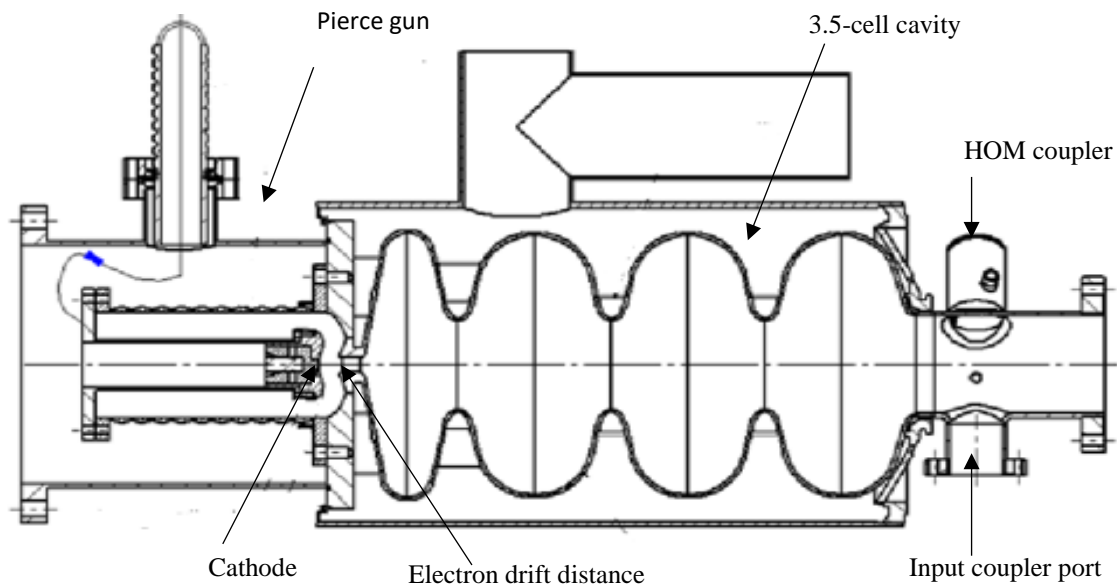


Figure 3-4: Drawing of 3.5-cell DC Pierce gun. Courtesy of Peking University.

### 3.2.2. SRF gun with choke filter

The second type of gun is superior for situations requiring high average current operation. The choke filter allows the use of high-QE cathodes, which are exposed directly to the accelerating field of the gun cavity. This makes low emittances possible even with a high charge per bunch. High QE relaxes the requirements on the irradiating laser, permitting operation with low pulse energy and at a convenient laser wavelength. The near perfect vacuum in an SRF gun is an advantage for cathode lifetime. As already mentioned, detachable cathode plugs and load

lock mechanisms have historically degraded the performance of the SRF cavities attached to them by generating particulates and multipacting near the cathode. This type of high frequency SRF gun operates at HZDR, and a new generation of SRF guns are being developed at KEK in Japan [Konomi, 2015] and HZB in Germany [Burrill, 2015].

The SRF gun program for the ELBE facility at HZDR [Teichart, 2015] is the most advanced among all programs worldwide. The ELBE gun (see Figure 3-5) is designed to operate in two modes: an FEL mode with 80 pC per bunch at a repetition rate of 13 MHz and a high charge mode with 1 nC bunches at 0.5 MHz. In April 2013, the first lasing at ELBE was demonstrated with the electron beam from the first SRF gun at HZDR. The gun operated at 9.6 MV/m with a Cs<sub>2</sub>Te cathode, cooled to 70K. It delivered a 3.5 MeV beam with 3 ps long bunches and a transverse emittance of 3 μm for 80 pC charge. A second gun is in operation with a magnesium cathode and maximum peak field of 12 MV/m. This gun is an excellent demonstration that high frequency SRF guns can work in an accelerator environment, but significant improvement in performance is needed for future facilities.

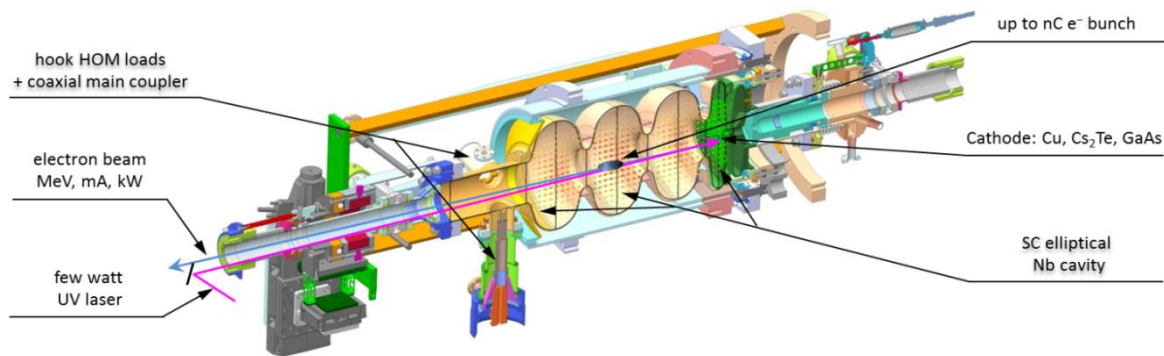


Figure 3-5: CAD drawing showing a cross section of the gun at the ELBE facility, with cathode exchanger. Courtesy of HZDR.

The KEK 1.5-cell, 1.3 GHz gun (see Figure 3-6) is designed to deliver 100 mA average current for the cERL test accelerator. It uses a novel, multi-layer cathode in the Nb cavity, which has not yet been tested in the gun. The cathode, irradiated from the back with 532nm laser light, incorporates a superconducting layer to prevent RF power from leaking towards the cathode exchange mechanism. In the vertical test, with cavity plug and choke filter installed, the cavity reached 25 MV/m on the plug with moderate Q<sub>0</sub> of 10<sup>9</sup>. The initial results are promising, but more work is needed to demonstrate that the gradient can be maintained with a cathode installed.

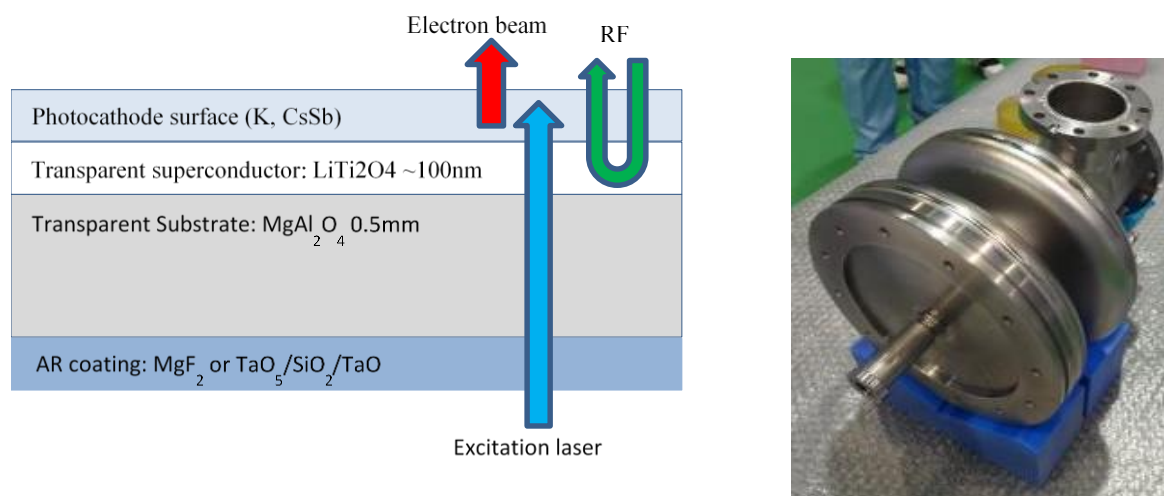


Figure 3-6: Multilayer KEK cathode concept (left, not to scale). An excitation laser (blue arrow) irradiates the structure from the back, while the superconducting layer prevents RF power leakage (green arrow). Photo of the gun cavity (right). Courtesy of KEK.

### 3.2.3. Integrated superconducting cathode

The third type of SRF gun, with a superconducting cathode, is meant for beams operating at low currents (see Figure 3-7). Over the past 10 years, DESY, together with other laboratories, has conducted an R&D program to integrate Pb layers deposited on various versions of Nb cathode plugs [Smedley, 2008]. The SC cathode material significantly simplifies the SRF gun design. Recent progress has been made in both the cooling of the plug and improving the quality of the Pb film.

The gun was successfully tested at DESY with up to 63 MV/m and 33 MV/m on the Nb and Pb-coated cathode, respectively. The Pb film on the DESY-tested plug was later investigated at BNL, and showed a QE of  $3 \times 10^{-4}$  at 258 nm after a moderate laser cleaning. The test confirmed the robustness of the Pb cathode, which after SRF test, shipment from DESY to BNL and exposure to air, still demonstrated reasonable QE. These test results provide valuable information for future SRF gun designs, but are not directly applicable to high repetition rate injectors.

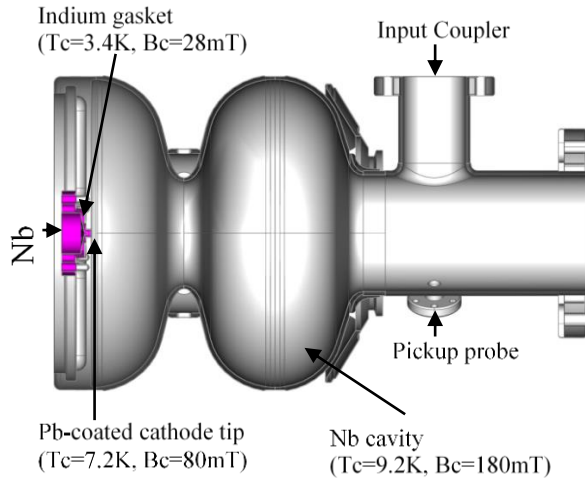


Figure 3-7: Drawing of the gun with superconducting cathode and picture of the cavity. Courtesy of DESY.

In the late 1990's, a group at HZDR proposed using a solenoidal magnetic field of TE modes (see Figure 3-8) to maintain the emittance. Recently, an additional input coupler was added to stably excite a TE mode simultaneously with the fundamental mode  $TM_{010}-\pi$  in a 3.5-cell cavity. HZDR plans to perform a beam experiment with the two excited modes to investigate the influence of the second mode on the beam quality.

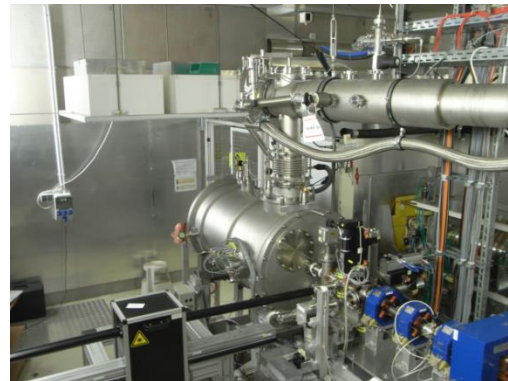
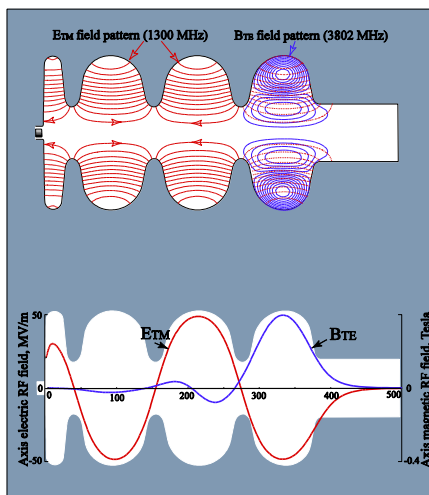


Figure 3-8: A 3.5-cell cavity with a higher frequency in the final cell for focusing (left). An SRF gun installed at HZDR (right). Courtesy of HZDR.

### **3.2.4. Summary and research plan**

The panel recommends the following design approaches for future SRF guns:

- (1) Study new geometries that can better utilize the peak field of the cavity, with a target of 50 MV/m effective gradient.
- (2) Study multi-mode designs with built-in magnetic focusing in the final cell to reduce emittance.
- (3) Develop methods for particle-free cathode insertion, creating guns with excellent RF performance.

To achieve the above goals, the panel proposes a three-pronged research plan:

- (1) Take advantage of upcoming SRF gun tests in Europe and Japan.
- (2) Carry out full system optimization of an injector based on a high-frequency SRF gun. Optimize the gun geometry, RF properties, magnet locations, and beamline layout. Include multi-frequency ideas and new solenoid designs. Compare with quarter-wave simulation results.
- (3) Construct a new cavity and load-lock based on optimization and particle-free insertion techniques. Perform beam tests to confirm reliability and simulations.

## **3.3. VHF SRF guns**

### **3.3.1. Recent developments in VHF guns**

The fourth type of SRF gun (Figure 3-9) is a quarter-wave low frequency gun, similar to the previously described APEX gun. Examples are the guns developed at the University of Wisconsin for the WiFEL project (operating at 199.6 MHz) and at BNL for the coherent electron cooling project (operating at 112 MHz). These guns have similar advantages to the NCRF APEX gun, but with drastically reduced power consumption due to the SC operation. Many scientists in the injector community believe that these guns can be pushed to 40 MV/m on the cathodes by better cavity preparation and by mitigation of particulates deposited in cavities by the cathode exchange mechanism.

The commissioning of the WiFEL gun in 2013 [Bisognano, 2013] showed that the cavity can operate CW at a gradient of 29 MV/m without the cathode inserted. With the cathode

inserted, CW operation was limited to 20 MV/m. The gun exhibited good control of microphonics, had negligible dark current, and had a  $Q_0 > 3 \times 10^9$  at 4K. Bunch charges of  $\sim 100$  pC have been delivered and first preliminary beam measurements were made at a lower cathode gradient of 12 MV/m for cryogenic load reasons. In 2016, the gun was shipped to SLAC for further studies.

The BNL gun was successfully tested with a gradient of up to 20 MV/m on the cathode [Pinayev, 2016]. In that experiment, 1 nC bunches were generated with measured transverse emittances of  $0.5 \mu\text{m}$  horizontally and  $1.5 \mu\text{m}$  vertically for 0.5 ns bunch length. These early tests were very encouraging and studies of this type of SRF gun will continue.

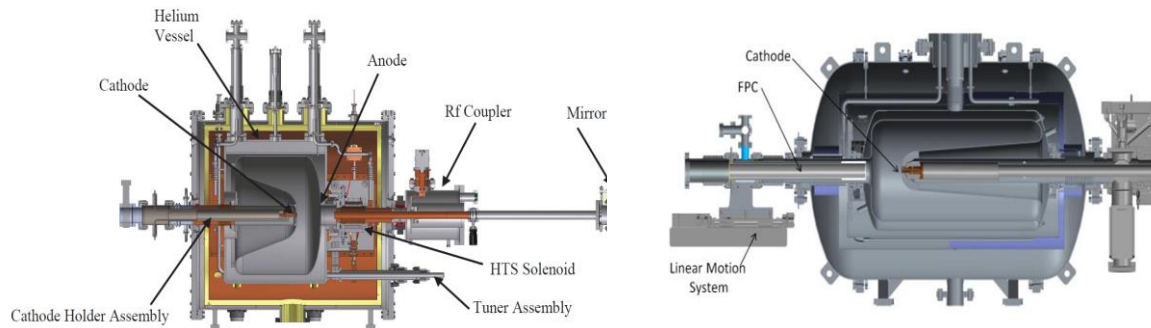


Figure 3-9: Drawing of the WiFEL SRF gun, left, and BNL SRF gun, right. Reprinted with permission from [Legg, 2012] and [Pinayev, 2016], respectively.

From the beam dynamics point of view, a VHF-type gun allows a beam with a relatively long pulse duration (many tens of ps), and therefore reduced transverse beam emittance for a fixed beam charge. Higher gradient allows extraction of higher current density from the cathode, thus potentially reducing intrinsic emittance. Also, improved gradient and output energy is critical to control space-charge-driven degradation of the beam phase space in the gun.

Preliminary layout optimizations of a VHF SRF gun-based injector (using the WiFEL gun as a starting point) showed a factor of 1.8 improvement in beam emittance compared with the LCLS-II baseline using the APEX gun. Figure 3-10 shows the injector layouts and the simulated emittance-bunch length Pareto front for the two cases. By switching to a better cathode, the emittance will drop below  $0.1 \mu\text{m}$  at 100 pC.

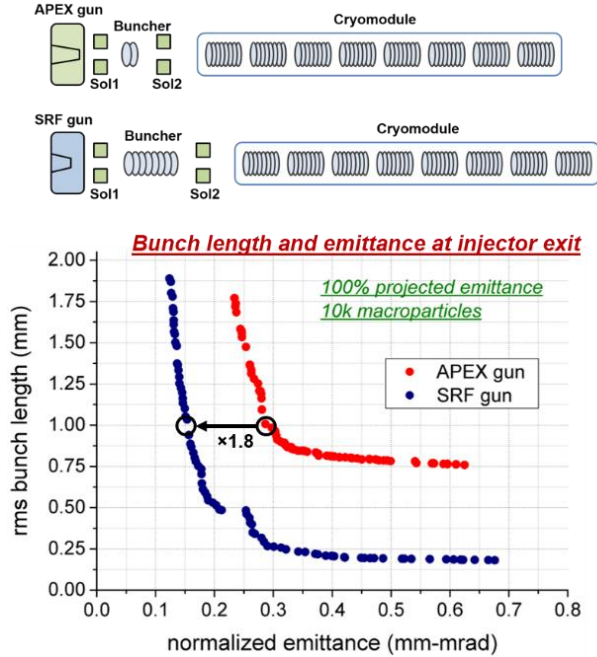


Figure 3-10 Simulated emittance and bunch length Pareto front of APEX and SRF gun-based injectors, with a conservative assumed intrinsic emittance of 1.0  $\mu\text{m}/\text{mm}$  rms spot size. Courtesy of SLAC.

### 3.3.2. Summary and research plan

The proposed SRF gun system has the potential to meet all the requirements for future FEL facilities. Initial optimizations show that it is possible to reach 0.1  $\mu\text{m}$  emittance at 100 pC (with 10-20A peak currents) for gun gradients approaching 40 MV/m. The next step is proving that high gradients can be maintained when cathodes are inserted and retracted.

Recent results from the BNL gun are promising (>500 pC, 0.5  $\mu\text{m}$  emittance), suggesting that a VHF SRF gun could provide a stable, high brightness source for UEM, where 6D brightness is important. Such a gun could enable fs-MeV electron energy loss spectroscopy.

The panelists believe that all types of guns need to develop methods for particle-free cathode insertion, so that RF parameters achieved without a cathode can be maintained after cathode insertion.

The panel proposes a three-pronged research plan to advance the capabilities of VHF SRF guns:

- (1) Using existing equipment, test a cathode with RF to full power and then conduct beam tests, with the goal of verifying the RF and beam simulations. Use the equipment as an environment to test cathodes under moderately high field conditions, and study

development of particle free cathode growth, insertion and load lock techniques, with improved RF joints.

- (2) Carry out full system optimization of an injector based on a quarter-wave SRF gun. Optimize the gun geometry, RF properties, mechanical properties, magnet locations, and beamline layout. Include longitudinal beam dynamics theory, multi-frequency ideas, and new solenoid designs.
- (3) Construct a new cavity and load-lock based on optimization and particle-free insertion techniques. Perform beam tests to confirm reliability and simulations.

### 3.4. DC Electron Guns

Although DC guns are a relatively mature technology and do not warrant attention as a PRD for development of CW sources, ongoing developments are worth pointing out. DC guns are a good choice for many applications, particularly for high average currents at moderate bunch charges. DC guns can provide up to 500 kV operating voltages and cathode gradients in the 5 to 10 MV/m range. The main drawbacks of DC guns are the relatively low accelerating gradient and the resulting lower total beam energy. Significant reduction in the intrinsic emittance is required to overcome the effects of the low acceleration gradient. One of the proposed techniques for intrinsic emittance reduction is to shift the laser wavelength close to the photocathode bandgap, where the QE is lower, but the mean transverse energy (MTE) is near room temperature ( $\sim 25$  meV). For alkali-type cathodes, one can expect a 4X reduction in MTE [Cultrera, 2015], or a 2X reduction in thermal emittance, simply by changing the laser wavelength. Further reduction could be achieved by cooling the cathode, or with an increased cathode gradient.

At high voltages, the gradient (or equivalently, the anode-cathode gap distance) cannot be maintained at the same levels as at lower voltages (see Figure 3-11). One way around the problem is to construct an electrode system with at least two stages. Consider the geometry sketched in Figure 3-12. Inserting an intermediate electrode close to the cathode, at a reduced voltage, takes advantage of the better behavior of the gradient curve at low voltages. For instance, measurements with a pair of flat, stainless steel plates demonstrated that 120 kV DC can be sustained with a 4-mm gap, an equivalent gradient of 30 MV/m.

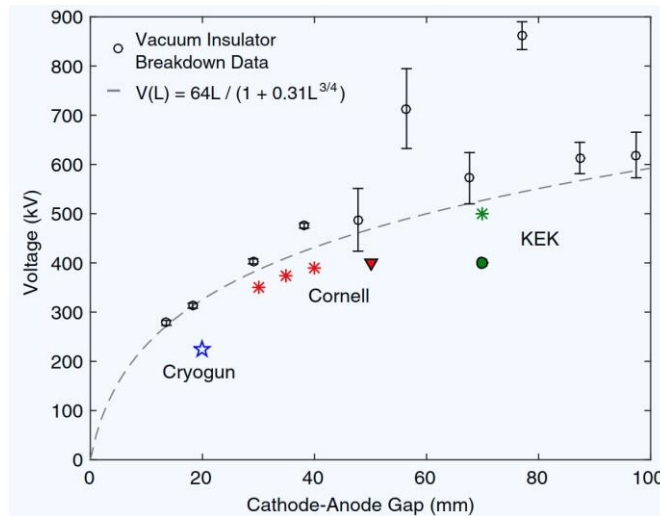


Figure 3-11: Measured values of breakdown voltage versus cathode-anode gap, reprinted with permission from [Gulliford, 2016].

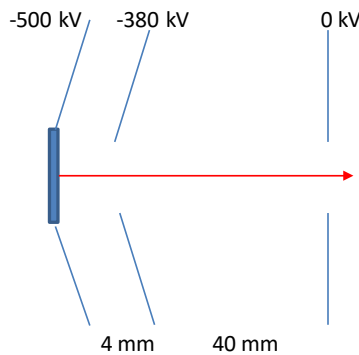


Figure 3-12: A sketch of a gun geometry with an intermediate electrode. Courtesy of KEK and JAEA.

Using a segmented insulator geometry (see Figure 3-12), it may be possible to support such an intermediate electrode, and build a gun with 3X higher cathode gradient while maintaining a total voltage of 500 kV [Nishimori, 2016]. Such a device could reach up to 1 MV total energy, but the cathode loading system would have to be mounted on the high voltage end of the gun.

A team at Jefferson Lab (JLab) has continued to work on DC guns, both as FEL drivers and for polarized electrons. A major problem with the ~500 kV guns described so far is that there is a large surface area of material at high voltage, increasing the probability for breakdown. To reduce this, the JLab team used an industrial insulator in conjunction with a HV cable, reducing

the surface area substantially [Adderly, 2010]. The resulting guns operate at ~200 kV with pA levels of dark current. JLab scientists are continuing work on these devices to make larger insulators and cables for higher voltages. The guns are very compact and are compatible with all cathode types.

Two 500 kV photoemission DC guns have been developed in Japan (see Figure 3-13). These DC guns operate at 500 kV, and can generate a beam corresponding to the requested beam parameters for CW EUV-FEL.

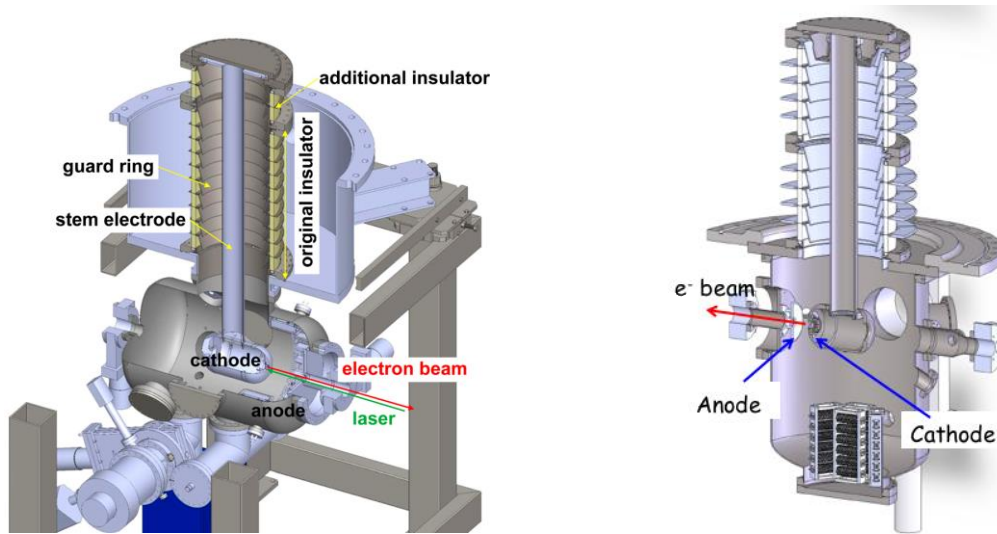


Figure 3-13: Two 500 kV photoemission DC guns, the compact ERL gun developed at JAEA (left) and the second DC gun developed at KEK (right). Courtesy of KEK and JAEA.

During the high-voltage DC gun development, they found a way to maintain stable high voltage [Yamamoto, 2016]. This fact indicates that the DC discharge process in UHV is closely related to ion generation that originated from ESD molecules at the anode. From this point of view, applying lower ESD material and surface treatment for the anode should improve the discharge voltage, and these methods could be applied at higher voltages (>500 kV) and fields (>10 MV/m).

Another method to improve the ability of the anode to handle high voltage is to make the anode ‘transparent’ and to use very low-Z, high thermal conductivity materials, like Be. In that case, field emitted electrons from the cathode will mostly pass by the anode and will strike in a shielded area where the secondary emission effects can be contained. In practice, the anode and

anode support are made from a mesh with a small fill factor. This approach is being tested now at Cornell.

There is no compelling case for R&D to reach substantially higher gradients with DC guns in order to reach the desired  $0.1 \mu\text{m}$  emittance at 100 pC at this time. DC guns are already excellent platforms for high average current, low emittance sources for many applications, but obtaining the  $0.1 \mu\text{m}$  level needed for future FELs seems unlikely.

## 4. PANEL 3: PULSED RF PHOTOCATHODE GUNS

---

### 4.0. Overview

Normal-conducting, pulsed, RF photoinjectors can achieve the highest peak brightness of all conventional electron sources because they access the highest accelerating gradients and output energies. The current generation of pulsed RF guns is largely based on the highly optimized 1.6-cell gun originally developed for the first generation of SASE FEL experiments [Palmer, 1998] and then optimized for the LCLS at SLAC [Akre, 2008]. This injector can achieve peak electric fields at the cathode approaching 120 MV/m and output energy  $> 5$  MeV. The normalized transverse emittance is about  $1 \mu\text{m}$  at 1 nC bunch charge, and has been measured as low as 140 nm at 20 pC. To maximize the acceleration gradient and energy gain from the gun, normal-conducting RF guns are typically operated at somewhat lower repetition rates (typically in the hundred Hz range). The following describes the motivation leading to this panel's recommendations for addressing PRD #3, "High-gradient R&D for next generation electron sources" and current status on key physical and technological issues (computation, stability, and diagnostics) that are critical to realize the potentially dramatic benefit from this research.

The electric field applied to the electron bunch as it is launched from the photocathode is one of the most important parameters in determining the quality of the electron beam from an electron source. Depending on the regime of operation of the injector (aspect ratio of the laser on the cathode), the transverse beam brightness  $B$  of the source, scales with launch field  $E_z$  as  $B \propto \frac{(E_z)^n}{k_B T}$  where  $n$  varies from 1 to 2. Assuming all downstream beam quality dilution can be suppressed, this relation illustrates that there are two ways of increasing the beam's brightness: decrease the excess energy of the emitted electron,  $k_B T$ , or increase  $E_z$ . The former method relies on improvements in the cathode intrinsic emittance and was discussed in the Panel 1 chapter of the report.

Maximizing  $E_z$  is another feasible and promising avenue for increasing the initial beam brightness. Leading-edge methods have already been developed to increase this field by a factor of four, corresponding to a factor of sixteen increase in intrinsic beam brightness for high-charge applications such as FELs or a factor of eight increase for lower-charge applications, such as UED. The high launch field also naturally leads to the possibility of a higher beam energy at the

exit of the gun, thus making the beam more rigid and less sensitive to space charge effects during acceleration and transport, suppressing beam quality dilution after its creation in the source. Given these factors, the panel believes that development of higher gradient photoinjectors should be a primary focus for the pulsed RF gun community.

The path toward higher performance pulsed RF guns requires generating the highest possible brightness bunch at the cathode and then propagating this bunch out of the gun while preserving its quality. Based on this observation, the panel identified two primary research focus areas for pushing the performance of the pulsed RF gun: (1) Developing higher gradient guns, and (2) Tailoring the injector design to match the application.

Developing higher-gradient guns will enable electron sources to generate significantly brighter beams at the cathode and to produce higher energy bunches at the gun exit.

The second idea for improving the performance of the pulsed RF gun is to optimally tailor the injector design to match its intended application. This covers both novel applications such as UED/UEM and established applications such as XFELs with newly identified working points. Importantly, the 1.6-cell gun developed for the LCLS was optimized for a working point of 1 nC, very far from the requirements for novel applications (as low as tens of fC). Even for XFEL working points near the 1-nC design point (e.g., 100 to 250 pC), it has been shown that a simple optimization of the laser profile and beamline produces a significant improvement in beam brightness [Zhou, 2012]. A factor of two in beam emittance improvement is possible. There is a potentially enormous benefit in matching the injector design to the application if it is done carefully. This is not a simple task as it requires detailed considerations of many deleterious effects in the RF gun (e.g. solenoid spherical and chromatic aberrations, quadrupole RF field components, etc.). Fortunately, the orders-of-magnitude improvement in simulation capabilities that has occurred over the last decade makes this task possible now.

Computational modeling is central to the research focus areas, and the electron source community should capitalize on the recent progress that has been made in computational tools (e.g., multi-objective optimization, 3D electromagnetic solvers, point-to-point space charge algorithms, etc.). Researchers are now in a stronger position than ever to be able to create optimized injector designs carefully tailored to advanced DOE/BES application requirements. Further improvements in these tools are still needed, driven by the electron source community's desire for ever colder beams. For example, improvements can be made for simulating the laser

profile and detailed cathode photo-response (including transverse and longitudinal thermal energies). Smooth potential-field models (with frame-of-reference slices) are accurate enough for modeling beams with the emittances and energy spread levels of current interest, and will continue to be sufficient in the near-term. However, as one approaches lower energy spread levels, it becomes necessary to simulate individual electron-electron interactions. Intrabeam scattering (Boersch effect) can be included in 3D accelerator simulations with two-particle pair statistics or heroic point-to-point simulations. For very cold beams, the random spacing of electrons leads to induced thermal motion, similar to nonlinear free energy on a microscopic level [Reiser, 1994], and therefore simulations need to include point-by-point models of this disorder-induced heating. Fast pairwise algorithms may be able to reduce the number of needed calculations to order  $N \log N$  for  $N$  electrons [Maxson, 2013]. Fortunately, disordered-induced heating is critical for those applications bunches with relatively few particles, on the order of  $10^6$  particles/bunch, so this problem should be tractable with exascale computing and advanced algorithms.

Lower repetition rate injectors, like pulsed RF guns, present challenges to beam stability, since feedback systems are limited to relatively small bandwidths. Stability requirements are application-specific. Beam energy stability and timing are strongly affected by RF amplitude and phase fluctuations. The state-of-the-art values for pulsed RF guns in operation as sources for XFELs are typically 100 fs rms and 0.05% energy jitter at the exit of the gun, with the largest contributions to jitter coming from the laser-to-RF timing stability and high voltage stability of the klystron modulator. Figure 4-1 shows an example plot of world-leading shot-by-shot beam energy and phase stability, with rms relative mean energy jitter of about 0.020% to 0.025%.

UED experiments usually require higher temporal resolution, and hence better time stability, than XFEL applications. Further, energy jitter also leads to timing jitter due to the time-of-flight between the cathode and sample (target). For a standard 100 fs time resolution UED system, 50 fs (rms) timing stability and relative energy stability on the order of  $10^{-4}$  is needed. The stability requirements for future 10-fs UED systems will be proportionally more stringent. The current approach to this outstanding issue is to record every pulse (time-stamping), and to post-process the data using a time-of-arrival correlation monitor to take out the jitter. A plethora of techniques have been proposed for both X-ray and electron beam time-of-arrival measurement, most of which rely on the measurement of ultrafast optical modulation of a

material due to the presence of the electron probe beam [Cesar, 2015; Hartmann, 2014]. Many research opportunities exist in this area, including material selection and optimal experimental geometry, as well as strategies for measuring any small modulation signals induced by the low charge UED electron beam excitation.

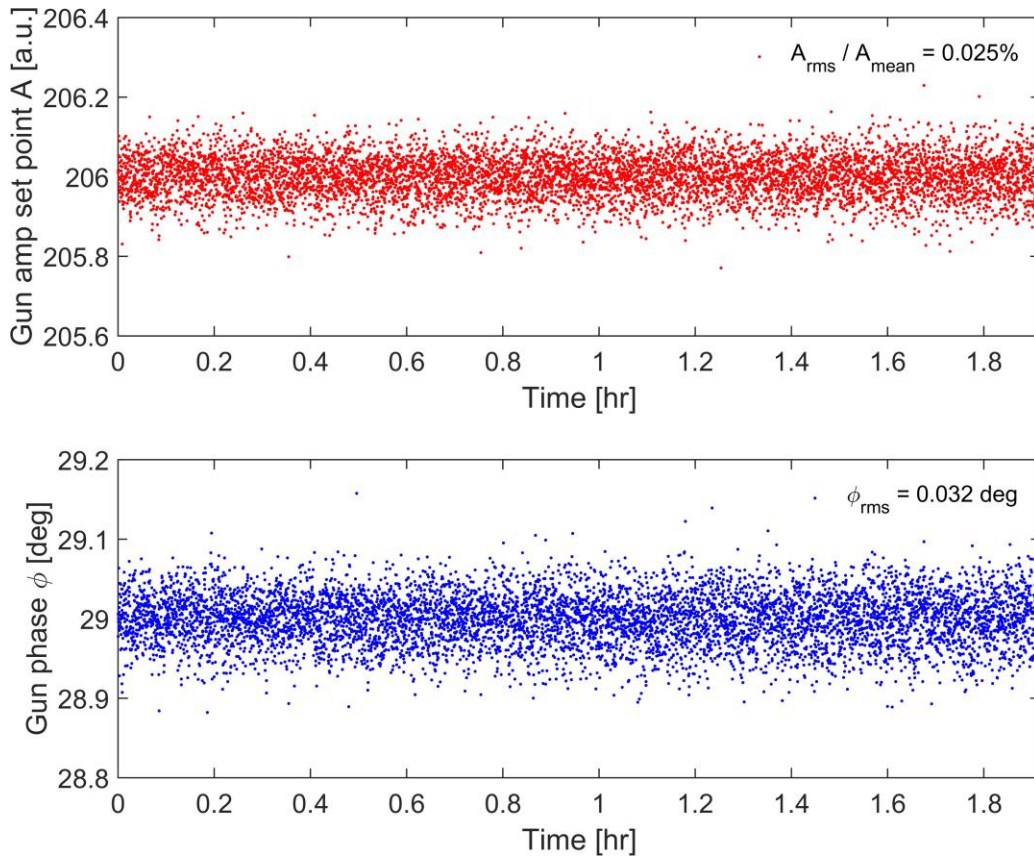


Figure 4-1: Shot-by-shot beam energy and phase stability from SLAC MeV-UED facility. Courtesy of SLAC.

As the beam brightness reaches higher values, beam characterization and diagnostics need equal development. Low-charge beams for UEM/UED applications at relativistic energies from normal conducting RF (NCRF) guns challenge the state of the art in spatial and temporal resolution. Current S-band guns operating at low charge working points can achieve geometric emittances at the few nanometer level, and with strong solenoidal focusing may achieve rms spot sizes as small as a few micrometers. Traditional scintillator crystals can be used at this level with high optical magnification, but care must be taken to balance the spatial resolution limit caused by a thicker crystal with the low photon-yield of a thinner one. Alternatively, commercial direct electron detectors have excellent spatial resolution with pixel sizes of approximately 5  $\mu\text{m}$ ,

negating the need for conversion to optical detectors. A further improvement can be obtained by using shorter wavelength light (e.g., via novel transition radiation diagnostics in the EUV [Murokh, 2016]) and innovative techniques to maximize numerical aperture in the optical system.

Future relativistic UED sources will aim for temporal resolution in the few-femtosecond regime. Diagnostics such as deflection cavities operating at very high voltage ( $>500$  kV) may be employed in this bunch length range [X. Wang, 1999], but these apply relatively large deflection momentum to the beam. Therefore, experiments need to perform a thorough analysis of inherent cavity vertical defocusing, intra-cavity bunch lengthening due to the applied energy spread, and higher order nonlinearities to ensure the validity of the measurement [Floettmann, 2014]. Here, deflecting structures that use high frequency, like conventional X-band (and higher frequency) cavities, as well as deflection structures based on THz [Kealhofer, 2016], laser-driven optical [Plettner, 2009], or plasma-based cavities [Dornmair, 2016] should be considered, due to the linear scaling of the streaking resolution with the field frequency.

## 4.1. Very high gradient injector R&D

The accelerating gradient ( $E_z$ ) in state-of-the-art pulsed RF guns, operating in XFEL or UED beamlines, ranges from 60 MV/m (e.g., European XFEL RF gun) to 120 MV/m (e.g., LCLS photoinjector). The panelists agreed that increasing  $E_z$  is the most promising avenue for (1) generating a beam with high intrinsic brightness and (2) propagating a beam without emittance dilution, by virtue of its higher beam energy at the exit of the gun. A factor of two increase of the gradient yields at least a factor of two decrease of the initial source emittance. The actual goal of this research is to reduce the initial emittance by more than a factor of two in the next 3-5 years. The following strategies were identified for achieving these goals. They are grouped into three research thrusts.

### 4.1.1. Frequency and short RF pulse width

Pulsed RF guns have been operated from 433 MHz [Dowell, 1993; Dowell, 1995] up to 17 GHz [Brown, 2001]. The vast majority of pulsed RF guns operate at S-band frequencies [Akre, 2008], followed by L-band [Feldman, 1991; Krasilnikov, 2012], with a few at X-band [Marsh, 2012; Limborg, 2016] and at C-Band [Taira, 2014]. Stable, high-gradient fields ( $> 80$

MV/m) can be sustained in pulsed RF guns at various frequencies (L to Ku Band) [Doebert, 2004].

The high-gradient research program carried out by SLAC, CLIC, and KEK shows that breakdown rates tend to be related to the RF pulse length  $\tau$  such that  $|B \times E|^n \tau^{1/3}$  or  $|B \times E|^n \tau^{1/4}$  is nearly constant ( $n > 1$ ) [F. Wang, 2008]. As an example, the dependence of the maximum gradient in a high frequency accelerator on the RF pulse duration is shown in Figure 4-2 (left) for X-band structures. The data follows a  $G \sim \tau^{-1/6}$  dependence, where  $G$  is the accelerating gradient. It is interesting to note that a 30 GHz copper cavity at CERN measured at 16 ns matches the trend in terms of surface field (see Figure 4-2 (right)). Pulse length dependences following a  $G \sim \tau^{-1/4}$  law have been reported by other experiments. These data suggest that pulsed heating is the main source responsible for this dependence. Surface pulsed heating stresses the material at the surfaces, ultimately leading to breakdown. Therefore, shortening the RF pulse length could be a viable method for reaching higher gradient operation, as it reduces the RF surface pulsed heating.

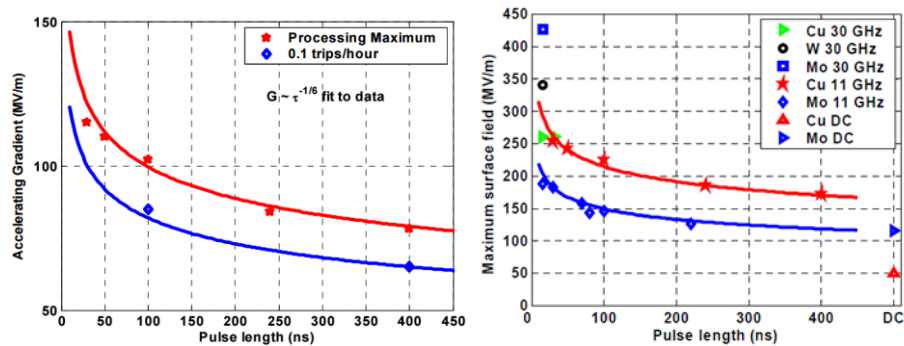


Figure 4-2: Pulse length dependence of the achievable gradient in X-band structures (left). Pulse length dependence of the maximum surface field for different materials (right). Reprinted with permission from [Doebert, 2004].

Increasing the RF frequency ( $f$ ) helps achieve high gradient, since the natural scaling of fill time as  $\sim f^{3/2}$  permits short RF pulses, and the power needed to drive a structure of scaled geometry is also smaller by  $\sim f^{3/2}$ . Nevertheless, experimental validation of the predicted scaling in terms of RF frequency is scarce. Predicted beam characteristics have been recently demonstrated on the two original X-band guns [Marsh, 2012; Limborg, 2016], but the full potential of X-band guns remains to be demonstrated. Advanced designs in C-band for a traveling-wave (TW) photocathode gun [Schaer, 2016], and also in X-band for a standing-wave (SW) photocathode gun are being developed in different laboratories with promising simulation results.

#### 4.1.2. Cryogenic operation of copper structures and hard copper alloys

As discussed above, breakdown can be systematically avoided by diminishing the pulse heating and importantly by strengthening the material. In experiments with single-cell standing-wave (SW) structures at SLAC it has been consistently found that, after initial conditioning, the breakdown rate is reproducible for structures of the same geometry and material, and that the breakdown rate depends more on the peak magnetic fields, through pulsed heating and related phenomena, than on peak surface electric fields [F. Wang, 2008]. Recent studies show that the breakdown rate correlates with peak pulse surface heating and peak-modified Poynting vector, although the research doesn't explain the microscopic mechanism determining the breakdown rate [Higo, 2013]. This is illustrated in Figure 4-3, which summarizes experiments performed on single cell X-band accelerating structures of a modified pill-box design close to that employed in photoinjectors. This research has revealed two promising pathways to very high gradient pulsed RF guns: cryogenic operation of copper structures or fabrication of structures with hard copper alloys (CuAg).

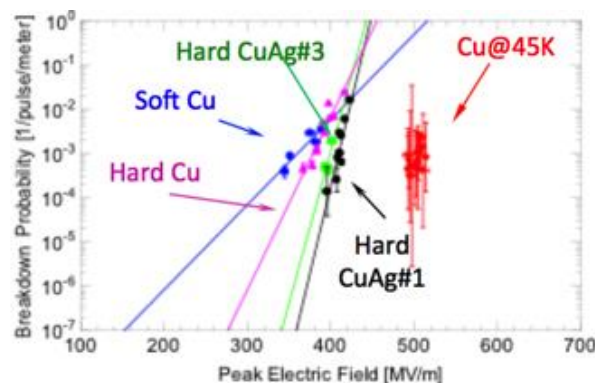


Figure 4-3: Breakdown probability as a function of peak electric field in single cell X-band accelerating structure tests. The introduction of a harder alloy improves the breakdown as predicted; the effect of operation at 45 K permits surface electric fields of 500 MV/m. Reprinted with permission from [Rosenzweig, 2017].

The effect of operation at 45 K is dramatic, permitting surface electric fields of 500 MV/m at short RF pulse length. This remarkable immunity to breakdown is due to both the increased yield strength and the lowering of surface heating due to the diminished surface resistivity. The lowered resistivity and concomitant increased quality factor  $Q$  must be calculated, accounting for the anomalous skin effect. Recent experiments at S-band frequencies by a UCLA-SLAC-INFN team [Rosenzweig, 2017; Cahill, 2017] show the behavior of the

surface resistance and  $Q$  as a function of temperature (see Figure 4-4). A flattening of the surface resistivity is observed below 40 K, with a factor of  $\sim 4.7$  increase in  $Q$  compared to measurements at room temperature. As such, operation of a device such as a pulsed RF photoinjector should be at temperatures below this knee, in order to mitigate possible dynamic changes in RF response due to surface heating and attendant temperature rise. A further advantage of cryogenic operation is found in photocathode physics, as it may provide a path to significantly lower the intrinsic emittance.

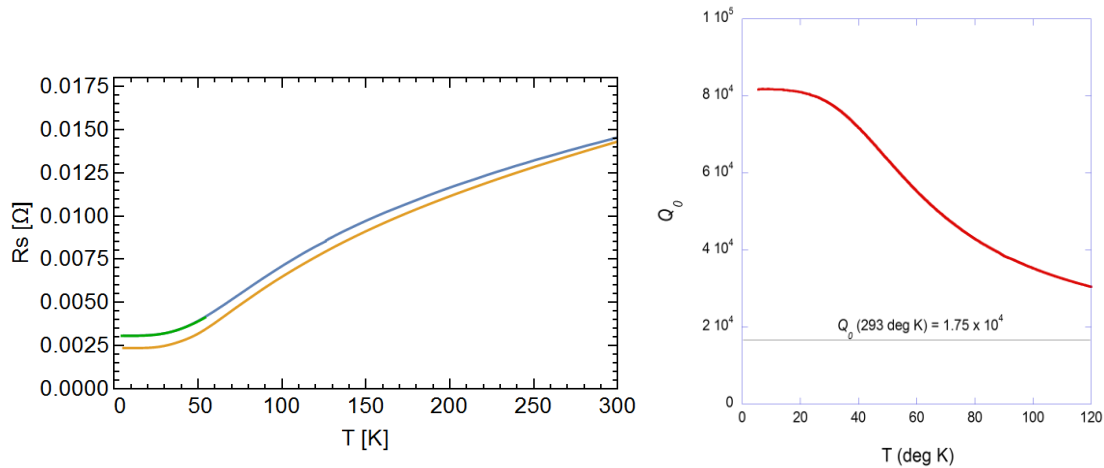


Figure 4-4: (left) RF surface resistance of two different S-band test cavities, manufactured at SLAC (blue) and UCLA (green). (right) Quality factor in SLAC test cavity. Reprinted with permission from [Rosenzweig, 2017].

Progress has been made in the S-band cryogenic gun simulation studies, demonstrating the possibility of very high field operation for a pulsed RF photoinjector. In this case, researchers used a 1.45 cell gun at 250 MV/m, with a 10.5 MeV output energy, conducting detailed studies for both FEL and in UED/UEM applications. The results are given for two limiting cases: a low charge (1.67 pC) UEM-oriented scenario, and a 100 pC FEL scenario. The results of these studies are summarized in Table 4-1. For the hard X-ray FEL case, the charge and current are similar to that given by a recent optimization of the room temperature LCLS photoinjector, while the emittance is lowered from 110 nm-rad to 40 nm-rad, improving the brightness by a factor of 7.5. New optimization approaches were used to obtain these simulated parameters, including using collimation to remove beam tails that contribute to the rms emittance, but not the total beam charge.

Table 4-1: Beam parameters obtained from S-band cryogenic photoinjector simulation studies, for UEM and FEL scenarios.

Scenario	Charge $Q$	Pulse Length $\sigma_t$	RMS emittance $\epsilon_n$	Final energy
Low charge UEM	1.67 pC	0.35 psec	6.5 nm-rad	10.5 MeV
Nominal X-ray FEL	100 pC	3 psec	40 nm-rad (95%)	155 MeV (post-compensation)

This new approach to photoinjectors will require R&D in multiple areas: (1) optimized RF designs for UEM and XFEL applications, (2) studies of the response to very high field RF in actual structures, (3) beam production and diagnosis from such structures, (4) possible cryogenic enhancements of photocathode performance (as discussed in the photocathode panel section of this report), (5) dark current mitigation schemes, (6) cryogenic cooling systems for high repetition rate facilities, and (7) amelioration of coherent synchrotron radiation effects through either narrow conducting boundaries in the chicane [Nodvick, 1954], or by avoiding full bunch compression, relying on innovative ideas such as eSASE [Zholents, 2005].

#### 4.1.3. Multi-frequency guns

A multi-frequency cavity [Kuzikov, 2010] may operate at higher gradients than a single frequency cavity for two reasons: the reduced length of time that cavity surfaces are exposed to high-fields and the so-called “anode-cathode” phenomenon [Kuzikov, 2012]. On a cavity surface, cathode fields (fields oriented so that field-emission is possible) and anode fields (fields that prohibit field-electron emission) are not equal. Therefore, assuming that field emission is responsible for the onset of breakdown, higher gradient operation with less dark current may be possible in multifrequency cavities. Preliminary simulations were carried out on a three-mode, 1.5 cell, RF photocathode gun [Kuzikov, 2012] using four RF feeds and three modes: 0.65 GHz, 1.3 GHz, and 2.6 GHz, (Figure 4-5). These properties may enable bunch energies as high as 3–5 MeV after the first half cell.

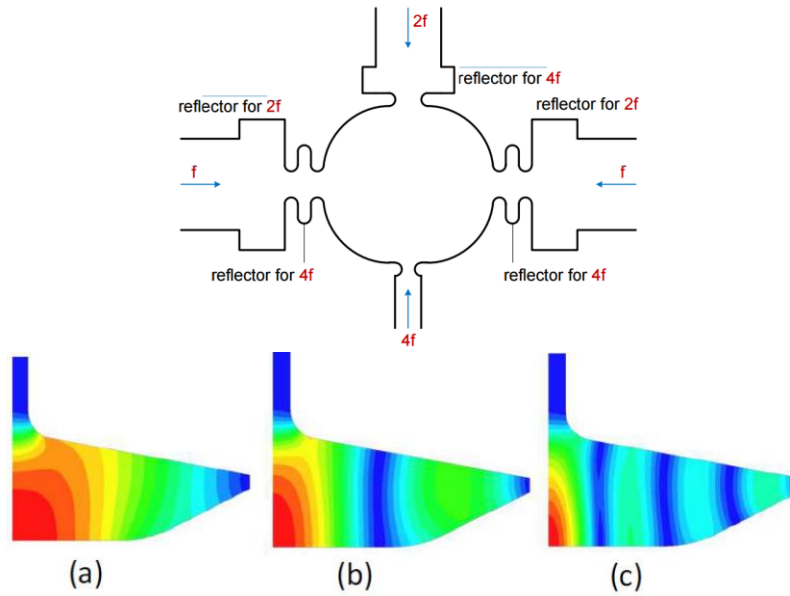


Figure 4-5: Feeding of injection gun by external RF sources (top) and E-field structures of modes in three-mode RF gun cavity : a) 0.65 GHz, b) 1.3 GHz, c) 2.6 GHz. (bottom). Reprinted with permission from [Kuzikov, 2011].

## 4.2. Injector design and demonstration for advanced applications

The second research focus for pushing the performance of the pulsed RF gun involves designing the injector to match both novel applications (e.g. UED/UEM) and established applications with newly identified working points (e.g. XFEL at 100 pC). Optimized injector design is not a simple task, as it requires careful consideration of many deleterious effects in the RF gun (e.g. solenoid spherical and chromatic aberrations, quadrupole RF field components, etc.). The actual goal of this research is to mitigate the RF and beam optics effects and reduce the emittance by more than a factor of two in the next 3-5 years. The strategies for achieving this are grouped into four research thrusts. Note that innovations in injector design also may confer significant advantages on the schemes discussed in Section 4.1.

### 4.2.1. Reducing emittance for hard XFEL applications

There is strong demand to reduce the injector emittance from  $0.4 \mu\text{m}$  to  $<0.1 \mu\text{m}$  at a nominal working point of 200- 250 pC for future harder XFEL application. The panelists believe that a few evolutionary steps can accomplish this:

- (1) Re-optimizing drive laser parameter and beamline layout with reduced thermal emittance
- (2) Controlling the laser spatial profile
- (3) Applying circular collimation to the electron beam.

### Re-optimizing laser parameters and beamline layout

Simulations show that the injector emittance is dominated by the space charge for nominal bunch charge of 250 pC with a 4-ps FWHM drive laser but can be reduced to 0.2  $\mu\text{m}$  (100% particles) with a longer laser pulse of  $\sim 11$  ps. Further simulation studies show that the emittance for 200 pC can be reduced to  $\sim 0.1$   $\mu\text{m}$  (100% particles) [Qian, 2016] by combining a few evolutionary steps including re-optimized beamline layout and reduced thermal emittance of 0.5  $\mu\text{m}/\text{mm}$ , as shown in Figure 4-6.

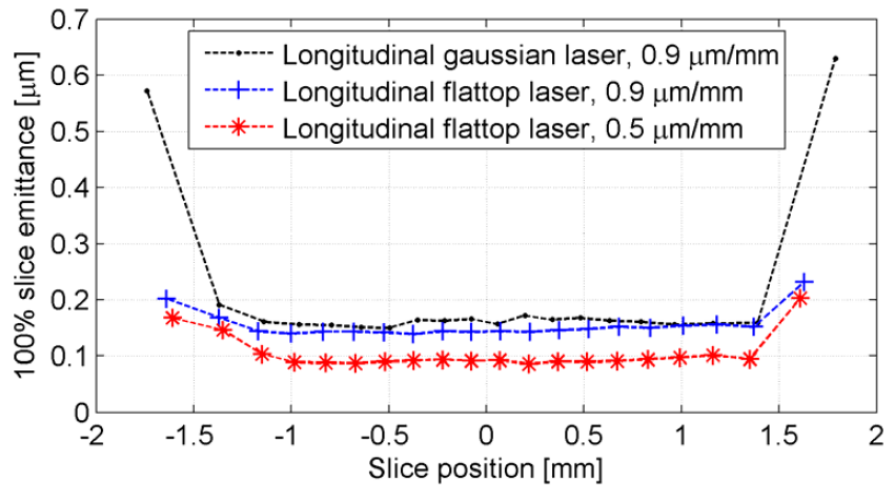


Figure 4-6: Comparison of slice emittance of 200 pC beam with 20 A peak current for different laser distributions and thermal emittance. Reprinted with permission from [Qian, 2016].

### Circular collimation for the electron beam

Beam collimation has been employed in TEM extensively to control and improve the electron beam brightness. Both simulation and experiments [Weathersby, 2015] show that the injector emittance can be reduced by about 40% with 200  $\mu\text{m}$  circular collimation for the electron beam at low energy in the injector beamline. Attaining this reduction requires control of three factors: (1) the wakefield effect from the collimator must not cause a large emittance

growth, (2) the transverse beam jitter must be less than  $\sim 15 \mu\text{m}$  rms, and (3) the collimator pitch/yaw alignment must be controlled with tens of  $\mu\text{rad}$  precision.

#### 4.2.2. New injector designs based on TW/hybrid

*Traveling-wave (TW) photoinjector:* RF traveling-wave photocathode guns have the potential to achieve very high gradient due to the short filling time of the S-band TW gun ( $< 100$  ns), and to provide more rigid electron beams with higher brightness [Schaer, 2016]. A previous study showed the brightness of the SwissFEL photoinjector could be improved by a factor two to four, considering all the machine constraints. The higher brightness is mainly due to doubling of the peak current, by creating a shorter bunch, which relaxes the overall compression factor along the FEL machine. Figure 4-7 shows the mechanical concept that is currently being developed at the Paul Scherrer Institute (PSI).

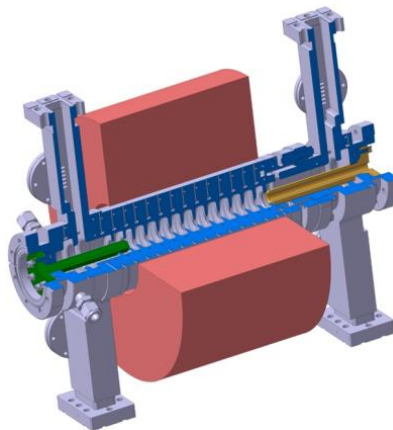


*Figure 4-7: Mechanical concept for TW photoinjector : the cathode (green) and the output coaxial section (yellow) are not brazed to the main gun body (blue) to make the system compatible with the load-lock concept and to allow the mounting of the solenoid, respectively. Reprinted with permission from [Schaer, 2016].*

*X-band Hybrid photoinjector:* The advantages of using the X-band hybrid for UED are based on high fields, which give low emittances, and on velocity bunching, which gives impressively short pulses. The hybrid concept has been proven in S-band at UCLA [Fukasawa, 2014]. Rosenzweig [2011] designed an X-band hybrid photoinjector, an integrated structure consisting of initial standing wave gun cells connected at the input coupler to a traveling wave section. Studies showed that for a gradient at cathode of  $200 \text{ MV/m}$  and a  $6.75 \text{ pC}$  charge, the photoinjector could produce an electron beam with  $80 \mu\text{m}$  (rms) length and  $60 \text{ nm}$  normalized emittance.

### 4.2.3. Multi-mode guns

To date, most RF photoinjectors have been designed to use a single RF mode to capture and accelerate the beam from the photocathode. Combining integer or fractional multiple RF modes within a single cavity can provide additional control over the phase space of the beam emitted from a photocathode. Adding transverse-magnetic (TM) modes can provide additional control over the longitudinal phase space [Dowell, 2004] and shift the peak of the combined RF field relative to the zero-crossing for improved beam dynamics from a field-emission cathode [Lewellen, 2005]. Figure 4-8 illustrates this effect.

While this multimode approach has generally been successful in terms of improving beam quality in simulations, fully 3D designs and experimental explorations have lagged. Implementing a multi-mode architecture offers significant additional challenges in cavity power coupling, tuning, and field control, but the potential benefits have not outweighed the perceived development and implementation costs. However, the push towards ultra-high density phase space and ultra-low energy spread warrants reexamination of multimode techniques in light of the requirements for precise control of beam phase-space evolution. Fully 3D RF cavity modeling and beam dynamics simulation techniques have both improved considerably since gun-based multimode concepts were first proposed, which should substantially reduce the R&D cost of successful implementation.

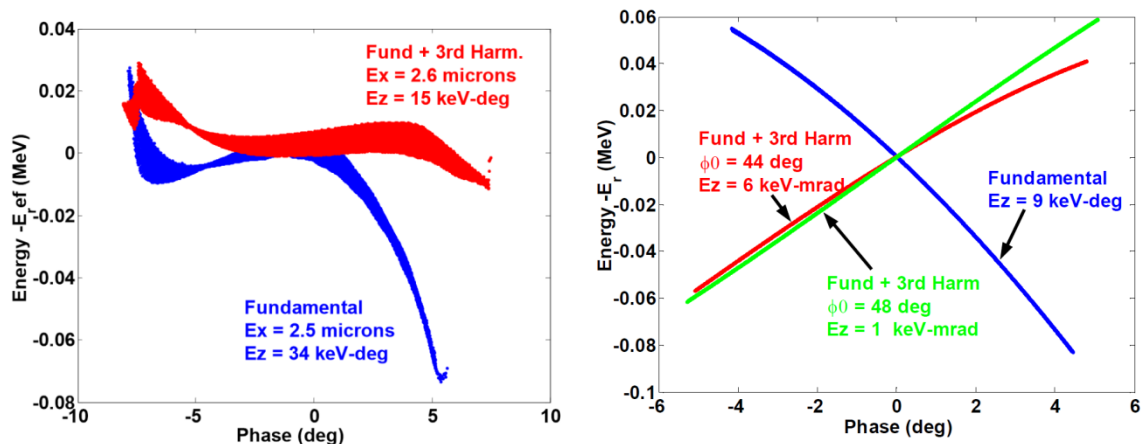


Figure 4-8: Longitudinal phase space control in a 1.5-cell S-band photoinjector: higher-order term reduction at high bunch charge (left); chirp control at low bunch charge (right). Reprinted from [Dowell, 2004] with permission from Elsevier.

#### 4.2.4. Geometry

Even though the canonical 1.6 cell s-band photoinjector gun was designed for the generation of nC bunch charges and mm-mrad emittances, it has also found much success as the source of high brightness beams at low bunch charge (and hence low emittance) for time-resolved electron scattering experiments such as UED. These applications require multiple orders of magnitude reduction in charge, emittance, and bunch length compared to the canonical design parameters. Therefore, the geometry of an UED-optimized source might differ significantly from guns optimized for high charge, while still capitalizing on the high gradient and maturity of pulsed normal conducting RF technology. Figure 4-9 shows a 1.4 cell gun [R. Li, 2014] that provides an example of an improved geometry.

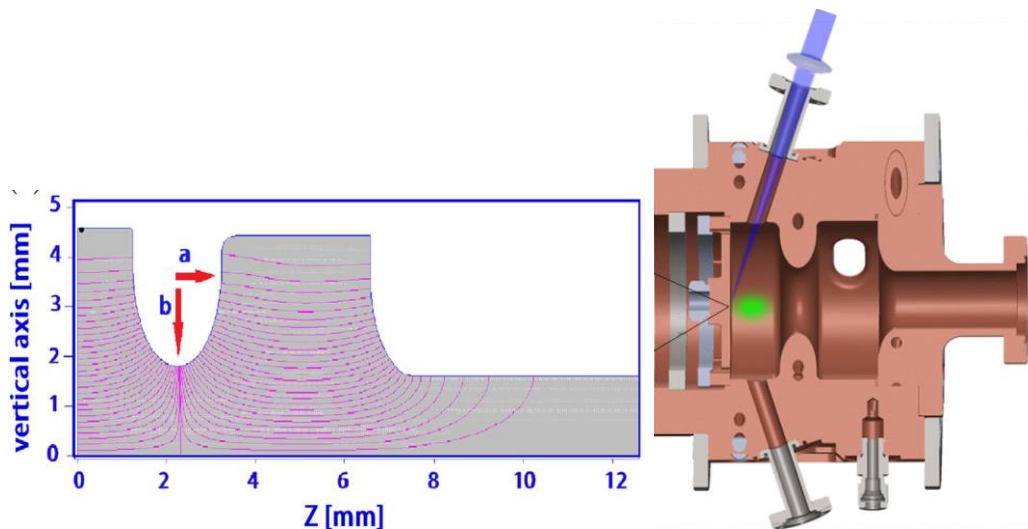


Figure 4-9: 1.4 cell RF gun Cavity profile (left). Reprinted from [Pirez, 2016] with permission from Elsevier. Schematic of oblique incidence laser illumination with final focus lens in the 1.6 cell gun (right), Courtesy of BNL.

Creation of single nm transverse emittances requires new geometries for coupling the laser to the photocathode. Both UCLA and SLAC UED working points currently utilize the 72-degree oblique incidence port of the 1.6 cell gun, which allows the placement of focusing optics much closer to the photocathode than when using normal incidence, thereby enabling smaller (few micron range) source sizes. New geometries, such as the use of shorter, wider oblique laser ports with higher numerical aperture (NA), or the use of rear-illumination photocathodes, may offer advantages in the creation of smaller source sizes.

## 5. PANEL 4: NOVEL ELECTRON SOURCES

---

### 5.0. Overview

Advances in high-brightness electron source technology have enabled the expansion of the scientific capabilities of X-ray and electron scattering instruments, providing opportunities in discovery science. Evolutionary advances in the existing electron gun paradigm will provide increased beam brightness, extending the reach of existing X-ray and electron instruments. However, order-of-magnitude, or greater, improvements in electron beam brightness will require novel techniques outside the present electron gun paradigm. Panel 4 of this Workshop surveyed potential novel electron sources to identify their possible impact and readiness for BES applications. This research supports PRD #4, “R&D in advanced accelerator and beam manipulation concepts.”

On-going research in electron sources can be categorized into several areas of focus: (1) ultra-high-gradient ( $>GV/m$ ) acceleration from rest to relativistic energies, (2) advanced beam manipulation concepts, and (3) electron sources approaching quantum degeneracy. Each of these approaches are discussed, including the status, the required R&D over the near-term (one to three years) and longer-term (five to ten years), and the potential impact on future electron source capabilities.

Several of these novel electron-source concepts are in the early stages of development and only sustained research of these novel techniques, over the next five to ten years, will enable them to advance sufficiently to provide science opportunities for future X-ray and electron scattering instrumentation.

### 5.1. Ultra-high gradient ( $>GV/m$ ) acceleration

The quality of the electron beam from a photoinjector is fundamentally set by the achievable accelerating gradients in the structures. For example, the transverse brightness of an electron bunch is expected to scale linearly with the peak electric field at the point of emission, due to the increased charge density. As the electric field increases, achievable source peak current increases significantly due to the reduced impact of space charge from the increased electric field gradient and the reduced wavelength. These traits can combine to provide

significant improvement in the brightness of electron beams by employing ultra-high gradient (>GV/m) acceleration.

There are, at present, two leading approaches to achieving ultra-high accelerating gradients. The first approach is to drastically increase the frequency of operation of photoinjectors into the THz frequency range, enabling THz guns with >GV/m surface electric fields. Such guns have the potential to increase the brightness of electron beams by two orders of magnitude. THz guns can be powered by pulses derived from laser-driven THz sources. These THz sources hold a broad appeal due to their widespread availability and potential for improved synchronization between the electron beam and an optical laser.

The second approach is to use plasma acceleration. In this approach, relativistic plasma waves are excited by either an intense short-pulse laser or a particle beam to achieve accelerating gradients on the order of 10-100 GV/m. Background plasma electrons trapped in the plasma wave then create an electron beam. The background ions cause rapid acceleration and shielding, greatly reducing the impact of space charge.

The beam quality is determined by the method of electron injection into the plasma wave, with laser-triggered injection offering the potential to increase the beam brightness by orders of magnitude, compared to conventional sources. Plasma accelerators driven by lasers also offer the secondary advantage of compactness, making them deployable at existing facilities where space is at a premium. They also provide intrinsic synchronization to an optical laser driver (and derivative particles and radiation) for pump-probe applications.

### **5.1.1. THz Guns**

High-brightness THz guns could take one of two forms: resonant structures similar to conventional RF photoinjectors, or broadband structures with transient pulses. Broadband structures are inherently compatible with well-developed single/few-cycle optical THz sources [Huang, 2016; Fallahi, 2016].

Photoinjectors operating at THz frequencies can leverage established design principles and require lower peak power than broadband structures (see Figure 5-1). Such THz guns provide several advantages: (1) improved transverse emittance and brightness with the increased electric field strength on the cathode, (2) decreased electron bunch length due to rapid acceleration from rest and reduced impact of space charge forces, (3) higher repetition rates in

the tens of kHz range, and (4) improved synchronization with pump probe experiments. A single laser system can produce a UV pulse for photo-emission, a THz pulse for acceleration and the pump laser pulse necessary to investigate dynamical effects in a sample under study (e.g. in an ultra-fast electron-diffraction setup).

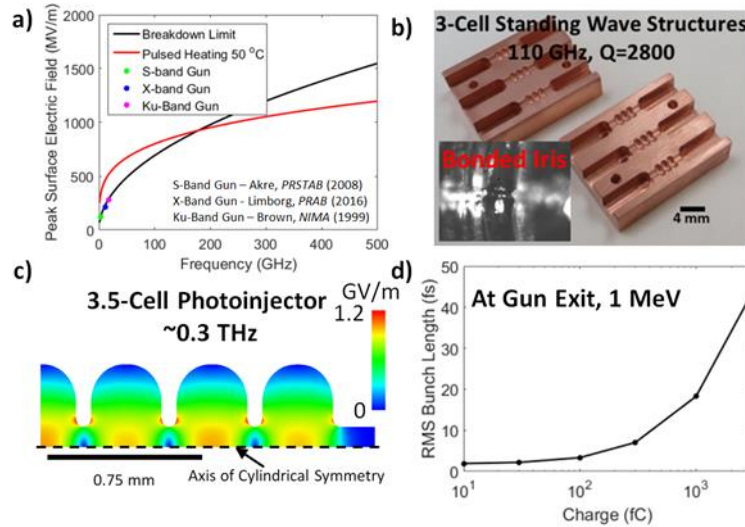


Figure 5-1: Performance of and structure of photoinjectors. a) Achievable surface electric field as a function of frequency in RF photoinjectors, b) Standing wave structures in the mm-wave/THz frequency range. c) Frequency-scaled photoinjector designed at  $\sim 0.3$  THz for 1 MeV electron bunches, d) Performance of photoinjector when powered with 1 MW, 2 ns pulses. For 100 fC, a 4-fs electron bunch is accelerated with normalized transverse emittance 7 nm-rad,  $\sigma_x=14$   $\mu\text{m}$  and 0.02% energy spread. Courtesy of SLAC.

Researchers have recently achieved key experimental milestones that answer fundamental questions about the potential impact for accelerating structures in the THz frequency range. These experiments have demonstrated operation with up to GV/m surface electric fields [Wimmer, 2014; Huang, 2016; Dal Forno, 2016], and acceleration and compression of electron bunches using single-cycle THz pulses [Nanni, Huang, 2015; Kealhofer, 2016].

Near-term technological developments will require fabrication of photoinjectors operating in the THz frequency range and characterization of electron bunches produced with GV/m gradients. Such experiments for resonant structures could commence in 2017 with either accelerator-driven sources, such as THz FELs or wakefield structures, or MW-class pulsed gyrotron oscillators. These experiments have the potential of generating MeV electron beams. Single-cycle sources are also approaching the required few mJ pulse energies for producing MeV

beams, and testing could continue with broadband structures at increasing gradients and energies [Vicario, 2014].

Longer-term R&D for high-power THz sources over the next five to ten years needs to focus on approaches that are efficient and scalable to high repetition rates (tens of kHz) to maximize the impact of THz guns. Novel beam-driven and optical methods for THz generation to produce mJ pulses suitable for powering these photoinjectors need to be explored. Higher charge schemes for producing tens of pC electron bunches for FEL applications should also be investigated.

The proposed research will result in a purely THz accelerator driven with integrated laser systems. These would produce femtosecond MeV electron bunches in mm-scale structures with performance parameters that meet or exceed the requirements set forth by the 2014 DOE BES Workshop for the Future of Electron Scattering and Diffraction [Hall, 2014]. This would make THz guns ideal for addressing the future research needs of the ultrafast science community.

### **5.1.2. Plasma acceleration**

Plasma acceleration is relevant for two BES applications: X-ray light sources, which require GeV-class electron beams, and ultrafast electron diffraction (UED) experiments, which require MeV electron beams.

#### **Plasma acceleration for X-ray light source applications**

Plasma structures with densities of  $10^{16}$ - $10^{18}$   $\text{cm}^{-3}$  can sustain electric fields of order 10 to 100 GV/m [Esarey, 2009]. The plasma density dictates the size of the accelerating buckets (of order 10-100  $\mu\text{m}$ , equivalent to 3-30 THz). The plasma wave forming these accelerating buckets can be excited either by a 100 TW-class laser or a 1 nC, 100 fs-class ultra-relativistic electron beam. Due to the high field gradients, injected electrons behind the driver reach ultra-relativistic energies within millimeters of propagation, limiting emittance degradation from space charge. It is therefore possible to produce electron beams at GeV energies with 10 nm emittance. These beams are few-fs in duration, contain 10-100 pC, and typically have percent-level energy spreads. With these characteristics, a beam brightness of one or two orders of magnitude better than current RF-based accelerators is expected. Injection techniques, acceleration control, and plasma out-coupling are critical to achieving and maintaining the excellent beam quality. For

laser-driven plasma structures, the compact high-quality electron source is intrinsically synchronized to the drive laser and can be deployed at scientific end stations, providing complementary pump/probe capabilities. Figure 5-2 shows a schematic of a laser-plasma accelerated electron beam driving an FEL.

The highest quality plasma-based electron beams have been produced with some form of assisted, or triggered, injection from the background plasma into the accelerating bucket. Triggered injection may take one of several forms: (1) down-ramp injection, which localizes the injection to a sharp density transition [Thompson, 2004; Schmid, 2010], (2) colliding laser pulse injection, where intersecting lasers trap background electrons [Rechatin, 2009], or (3) injection in a partially-ionized gas, time-gating ionization near the peak of the plasma wave driver [Pak, 2010]. While energy spread ( $\sim 5\%$ ), charge (10-100pC), and divergence ( $\sim$ mrad) have been well characterized by the community at large, the emittance ( $\sim 200$  nm) and beam duration ( $\sim 3$ -5 fs) have only been obtained in select experiments [Plateau, 2012; Weingartner, 2012; Buck, 2011]. Based on these numbers, the brightness can be expected to be comparable to state-of-the-art RF accelerators. The repetition rate of the plasma drivers is currently limited to  $\sim 10$  Hz.

Near-term R&D is aimed at implementing electron injection schemes that are technologically accessible at existing plasma accelerator facilities, where the electron beam transverse emittance is predicted to be reduced to the 10-nm level, thus dramatically enhancing the electron beam brightness. For example, a laser pulse can be used to inject electrons in the plasma accelerating bucket via ionization [Hidding, 2012; Yu, 2014]. Owing to the electron beam characteristics, improved methods are required to measure the slice emittances at the 10-nm level.

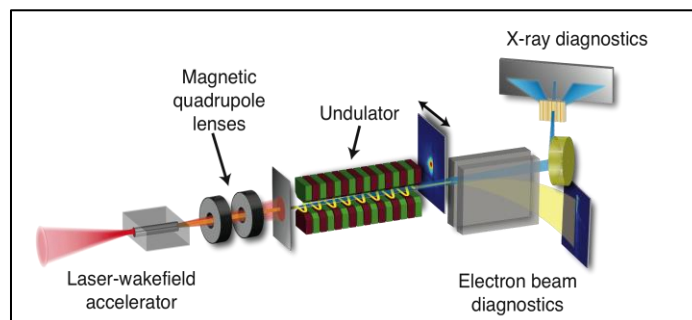


Figure 5-2: Schematic of an X-ray FEL driven by a laser-plasma accelerated electron source. Courtesy of LBNL.

Several institutions are developing kHz 100-TW-class lasers, and laser technology advances will be applied to plasma-based acceleration drivers in five to ten years. It is critical that proof-of-principle concepts developed in the near-term be adapted to the stringent stability and reproducibility requirements that future accelerator facilities demand. The plasma driver must be stabilized and controlled in the spatio-temporal domain and stable plasma profiles need to be created, to ensure accelerator robustness.

### **Ultrafast electron diffraction applications**

Laser-driven plasma acceleration poses a potential solution to some of the challenges facing RF-based ultrafast electron diffraction (UED) experiments and may be able to enable exotic operation modes, such as energy-chirp control or multi-pulse, multi-color beams. MeV electron beams can theoretically mitigate the impact of space charge, and an optical driver can eliminate the jitter between RF and pump lasers that presently limits the time resolution in such experiments.

The goal is to use ultra-short, kHz, mJ laser systems to produce 1-10 MeV electron beams that are transported, without degrading the energy spread and duration, onto samples of interest for UED experiments. Suitable laser systems have only recently become available and researchers have not yet been able to produce MeV electron beams with sufficient quality and stability for UED experiments.

MeV electron beams for UED applications need to reach sub-10 fs duration at a kHz repetition rate, a goal that has not yet been demonstrated on laser-driven plasma accelerator systems. Both solid target-laser interactions and the self-modulated regime of laser-wakefield acceleration can produce copious amounts of MeV electron beams, but the large energy spreads and poor quality hinder the prospect of using these for UED experiments. The bubble regime of laser-plasma acceleration (i.e., using highly-nonlinear plasma waves driven by short, intense laser pulses [Esarey, 2009]) has the potential to generate ultra-short pulses with significant charge and high beam quality. Scaling laws suggest that MeV class beams with sub-10 fs duration can be produced using state-of-the-art, kHz, 5 mJ, 5 fs laser systems. MeV-scale electron beams have been demonstrated in the bubble regime with mJ, fs systems. Early research produced beams at the 20 MeV level, which is too high for practical UED experiments [Schmid, 2009], and more recently at 100 keV [He, Hou, 2013]. In the 100 keV electron beam

experiments, a proper beam transport system was incorporated with the laser-plasma accelerator, permitting the demonstration of static electron diffraction on aluminum thin films [He, Thomas, 2013].

Since few-cycle laser systems operating at a few mJ and a few kHz are now available with 5 fs time resolution, it is expected that in the next few years, kHz electron beams with sub-10 fs duration and fC charge will be produced at the 1-10 MeV level [Faure, 2016; Beaurepaire, 2014].

The longitudinal distribution of the beam needs to be preserved during beam transport from the source to the target, over several tens of centimeters. UED experiments require ~100  $\mu\text{m}$  spots with transverse coherence lengths on the order of a few nanometers. Producing such a beam is essential to demonstrate the utility of laser-plasma acceleration for UED. Source stability needs to improve over the next five to ten years to move beyond R&D projects to create “turn-key” user facility systems.

## 5.2. Advanced beam-manipulation concepts

An electron source produces beams with specific beam parameters driven by the emission process and triggering mechanism (e.g., photoemission). Often the achieved parameters do not match the front-end application. Therefore, particle accelerators commonly incorporate manipulation schemes that include transport and transverse focusing of the beam, along with techniques to enhance the beam peak current, to match requirements imposed by the final application. In the last decade, researchers have developed a wide range of novel techniques to efficiently manipulate electron beams or tailor their phase space to a given requirement.

The panel identified two emerging techniques as especially promising: (1) the coupling of an intense laser pulse to an electron bunch [Hemsing, 2014] and (2) the development of phase space manipulation between two degrees of freedom [P. Emma, 2006; Sun, 2010]. The former class of manipulation techniques has enabled precise control of longitudinal distributions, as demonstrated by various FEL-based seeding schemes or bunching schemes for UED applications. The latter class of techniques was proposed to re-partition the beam emittance of FELs and make use of the injector 6D brightness by redistributing emittances to increase the beam slice energy spread while decreasing the transverse emittance. The method was eventually

combined with transverse shaping techniques to create bunches with tailored temporal distributions [Graves, 2012].

### 5.2.1. Laser-based manipulations

Several proposals suggest using all-optical methods, either infrared (IR) or visible light, to manipulate electron pulses and compress them to durations of a few femtoseconds, or even into the attosecond domain [Wong, 2015; Vartak, 1995; Hilbert, 2009]. These optical techniques all rely on the ponderomotive force, which describes how charged particles are influenced by optical fields [Batelaan, 2007]. A properly synthesized intense laser pulse interacting with electron pulses that have dispersed to durations of  $\sim 1$  ps can accelerate and decelerate the spatially dispersed electron pulse [Hilbert, 2009]. This results in an electron pulse that has faster electrons trailing and slower electrons leading, which after propagation results in pulses that can be compressed to the attosecond range (see Figure 5-3).

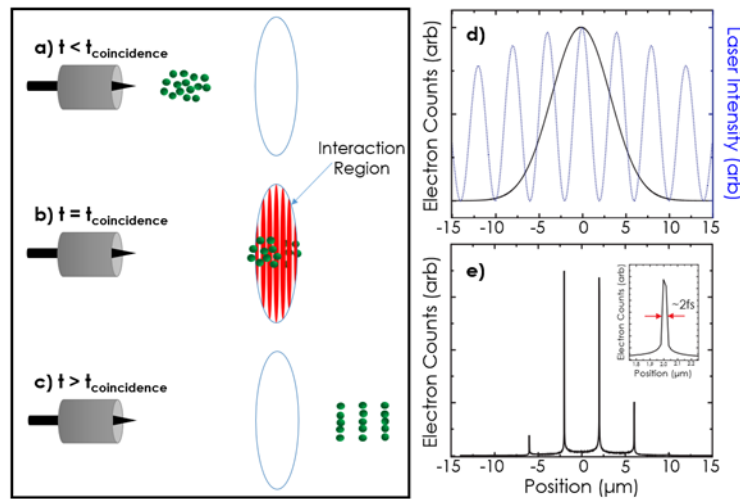


Figure 5-3: Laser pulse interacting with electron pulses. a) A dispersed electron packet of variable velocities is emitted and directed towards the interaction region and sample. b) The electron packet passes through the interaction region, during which time it is subjected to the standing wave. This compresses the packet. c) The electron packet moves away from the interaction region, and towards the sample. d) An electron pulse is overlapped with a standing wave (intensity) formed by the pulsed laser. e) After 2.8 ps, the electrons have reached maximum compression, represented by the narrow peaks. The inset in e) shows a magnified view of one of the peaks. Reprinted with permission from [Dahal, 2016].

These all-optical compression techniques promise advantages over the more widespread use of microwave technology to compress pulses [Walbran, 2015], primarily because they do not require electronic timing equipment. Since femtosecond optical pulses are used to both create the

electron pulses and to compress them, the timing between the two only requires the use of optical delays, which can be controlled with femtosecond accuracy [Walbran, 2015]. In principle, this method allows precise control and delivery of attosecond pulses on arbitrary targets with sufficient temporal precision.

Recent experiments have demonstrated that pulsed THz fields created by the optical rectification of femtosecond IR pulses can be used to compress free electron pulses from  $\sim 1$  ps to 75 fs, a compression factor of 12 [Kealhofer, 2016]. Such short pulses have already been used to image electromagnetic waveforms created in a split ring resonator, providing detailed information on the field vectors, polarization, and amplitudes of the THz laser excited fields and showing the promise of all-optical compression [Ryabov, 2016]. While it may be possible to compress electron pulses to the attosecond regime using multiple THz compression stages [Kealhofer, 2016], this can be accomplished directly in a single stage by using an all-optical compression based on IR or visible light [Hilbert, 2009].

The panel believes that demonstration experiments can be completed in the next one to three years, showing that lower energy (100 eV – 100 keV) electron pulses can be compressed to the few femtosecond range and delivered onto a target. These all-optical compression methods need to be modeled in all three spatial dimensions with realistic electron pulses. Most current work has only examined the effects of compression in the propagation direction, but full 3D models need to be created to use the compressed electron pulses for imaging, diffraction, and spectroscopy. It is possible that this compression technique will eventually be in use in both low energy ( $\sim$ sub-1-keV) pulsed point projection electron microscopes and in ultrafast electron microscopes (UEM) based on commercially available transmission electron microscopes, greatly increasing their respective temporal resolutions [Barwick, 2015]. This development will likely take five to ten years.

The potential impact of the successful demonstration and development of purely optical compression schemes will be significant. Existing UED/UEM instruments are limited to the  $\sim 100$  fs range for temporal resolution, which is sufficient for the investigation of structural dynamics in a variety of condensed matter, material science, and structural biological systems. However, by attaining attosecond temporal resolution in these UEM's, *electronic* dynamics will become accessible. This has the promise of advancing knowledge in the fields of plasmonics and

nanoscale optics. Being able to visualize near-fields and their dynamics will aid in optimization and control of next generation plasmonic devices [Barwick, 2015].

### ***5.2.2. Transverse-to-longitudinal phase-space exchange***

Phase space manipulations between two degrees of freedom, such as the technique of nanopatterning, can produce a coherent hard X-ray seed to generate fully coherent FEL output. The impact of this capability is significant, since it may enable chirped pulse amplification, allowing long X-ray pulses to be compressed to sub-femtosecond duration with peak power exceeding 1 TW. Two-color experiments using bi-periodic gratings for phase-locking, providing attosecond synchronization of the pulses, present another application.

Nanopatterning refers to creating a periodic current modulation at the X-ray wavelength needed for FEL seeding. Nanopatterning produces a deterministic phase relationship so the output is fully coherent, unlike SASE, which lacks longitudinal coherence and suffers from significant instability in power, bandwidth, and frequency. Nanopatterned beams produce a deterministic seed (i.e., every shot the same), enhancing stability in X-ray FEL pulse energy, wavelength, and pointing stability.

Novel approaches to nanopatterning may be more effective than existing methods. For example, one promising approach creates a spatial (transverse) nanopattern by diffracting an electron beam through a patterned grating and a crystal (see Figure 5-4), and then transferring the pattern into the longitudinal dimension through emittance exchange between the transverse and longitudinal phase spaces [Nanni, Graves, and Moncton, 2015; Graves, 2012; Nanni, 2014]. Although a nanopatterned electron beam itself could be considered exotic, it is important to realize that the proposed technologies and methods have been proven in other contexts and therefore are not individually risky.

Recent theoretical and simulation work indicates that nanopatterns can be generated at the appropriate scale and that emittance exchange can swap emittances [Nanni, Graves, 2015] with ratios as high as 10,000:1 when correcting for aberrations. Recent experiments [Nanni, 2016] have shown that the diffracting crystal can survive at least 8 hours without damage (a year of operation with damage less than 1% is predicted), and that the full electron beam is transmitted through the crystal without loss of brilliance.

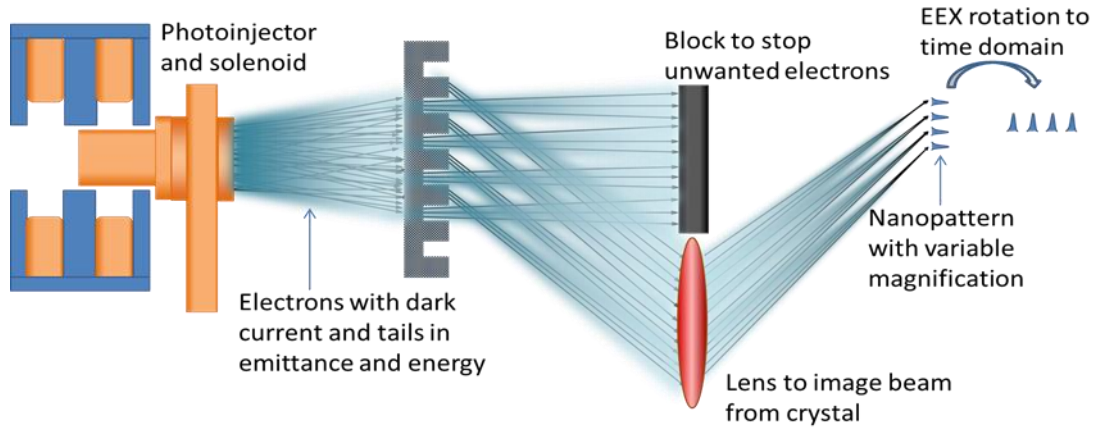


Figure 5-4: Electrons diffracted in grating to produce nanopatterned beamlets. Emittance-exchange is used to rotate pattern to longitudinal plane. Courtesy of Arizona State University.

Experiments aimed at forming the transversely-modulated pattern will be possible at UED facilities within three years. Researchers will investigate resolution limits in transverse patterning, along with the ability to continuously tune the magnification as required for continuous FEL wavelength tuning. Planned experiments aim to demonstrate that knock-on damage to the grating is minimal over long run periods. Additionally, further theoretical development will be required to investigate the ultimate limits of the method. These studies will involve improved simulation tools to model nanometer-scale space-charge effects and demonstrate that the nanopattern can survive subsequent acceleration.

Experimental research over the next five to ten years needs to investigate limits in the generation, transport, and emittance exchange of nanoscale patterns. Eventually, the formed nanopattern should be used to produce coherent X-rays via inverse Compton scattering from a laser or THz structure. This requires development of laser techniques to provide an undulator-like laser field profile, and perhaps development of THz undulator structures and high power THz sources. Successful development of the nanopatterning method should lead to demonstration of seeding at an X-ray FEL facility.

### 5.3. Sources approaching quantum degeneracy

The smallest phase-space volume occupied by an un-polarized beam composed of  $N$  electrons is  $\Gamma \simeq N\lambda_c^3/2$ , where  $\lambda_c$  is the Compton wavelength [Chattopadhyay, 1998]. In conventional electron-emission sources, this quantum limit is never reached. The phase space

occupancy is characterized in terms of a degeneracy parameter which, in the classical limit, can be written as  $\mathcal{D} = \Gamma/\varepsilon_6$ . Here  $\varepsilon_6$  is the emittance for the combined three degrees of freedom (DOF) which, for uncoupled motion, can be written as the product of the emittance values associated with each DOF,  $\varepsilon_6 = \varepsilon_x\varepsilon_y\varepsilon_z$ . The degeneracy factor is bounded to  $\mathcal{D} \leq 1$ . Conventional electron sources have degeneracy parameters  $\mathcal{D} \ll 1$ .

At the present time, the highest brightness electron sources in operation are field emitters using nanotips. The degeneracy parameter for such sources is  $\mathcal{D} \sim 10^{-4}$ , and the high-current photo-injectors typically used in accelerators have  $\mathcal{D} \sim 10^{-11}$ . These are surprisingly low numbers, especially given that inside a metal cathode the electrons occupy almost all available quantum states and thus should yield a beam with degeneracy  $\mathcal{D} \sim 1$  when extracted from the cathode. The mechanism used to extract the electrons from the source, and in large part the electron-electron scattering after extraction, are among the main phenomena that quickly degrade  $\mathcal{D}$  to many orders of magnitude below unity. In recent years, there has been renewed interest in developing electron sources capable of forming quantum-degenerate beams (that is, beams with degeneracy parameter close to unity). These sources include ionization of cold atoms [Luiten, 2007], ionization of high-Rydberg-state atoms [Zolotarev, 2007], and development of high brightness field-emission tips [Jarvis, 2010].

### **5.3.1. Cold atom sources**

Electrons extracted from an ultra-cold plasma produced from a laser-cooled cloud of neutral atoms hold great promise as a source for quantum-degenerate beams. Researchers initially explored the concept over 40 years ago [Gallagher, 1974], but it has generated renewed interest and development more recently [Claessens, 2005]. In this scheme, neutral atoms are trapped and cooled in a magneto-optical trap. A fraction of the cold-atom cloud is locally excited to an intermediate state with a quasi-continuous laser pulse. A pulsed laser beam propagating orthogonally to the excitation laser subsequently ionizes the excited atoms contained within the volume where the two lasers overlap, thereby forming a local, ultra-cold plasma. The electrons contained in this ultra-cold plasma are extracted by applying a pulsed electric field, as shown in Figure 5-5.

When this concept was tested, the transverse beam emittance was found to be on the same order as that produced in photoemission RF guns. The measured emittance corresponds to

electron temperatures around 100 K, well above the ultra-cold plasma temperature ( $<10$  K). This significant temperature increase is attributed to disorder-induced heating during the emission process. Another interesting application of such sources is the precise control over the electron-beam distribution via shaping of the excitation laser distribution [McCulloch, 2011]. The sources developed at the University of Eindhoven in the Netherlands and at the University of Melbourne in Australia have subsequently been used in UED experiments [Speirs, 2015; van Mourik, 2014].

There is currently no group developing cold-atom electron sources in the U.S. The panel concluded that such a lack of effort is unfortunate and should be vigorously pursued, building on the successful international efforts. The short-term investigations should focus on understanding the electron-beam heating that prevents transfer of the ultra-cold plasma temperature to the electron bunch and devising possible mitigation mechanisms. In the longer term, the opportunity to tailor the beam distribution and possible emittance partitions should be investigated.

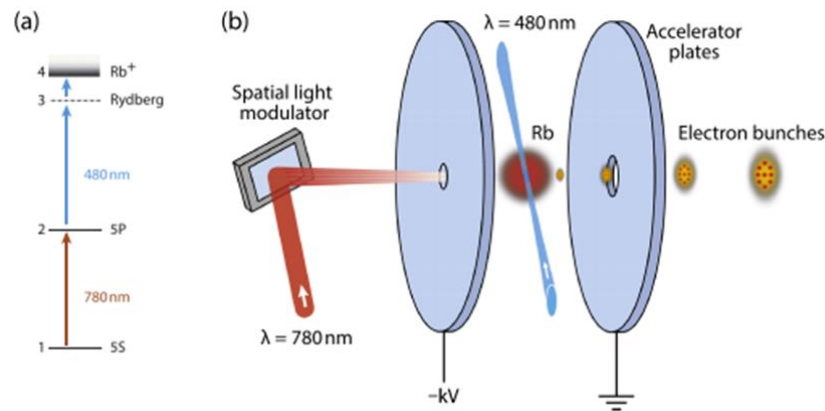


Figure 5-5: Principle of the cold-atom electron source. (a) Photo-excitation/ionization level structure for  $85\text{Rb}$ . (b) Cold-atom electron source based on a cloud of laser-cooled rubidium atoms ( $\text{Rb}$ ) located between two accelerator plates (trapping lasers not shown); Reproduced from [McCulloch, 2016] with permission of IOP Publishing.

### 5.3.2. Sources using high-Rydberg-state atoms

Electrons excited from the ground state into a high Rydberg state close to the ionization energy are extremely sensitive to the influence of external fields and therefore are suitable candidates as sources for quantum degenerate beams. Figure 5-6 shows an example using a source of neutral cesium atoms that are heated and sent to an ionization chamber containing three lasers. Two CW and one pulsed laser overlap to create an interaction region where the Cs atoms can be excited one at a time into a high Rydberg state,  $\sim 10^{-5}$  eV below ionization. Short-pulsed

voltage is applied to ionize the atom, which is then accelerated up to the desired energy. The full cycle can be repeated with  $\sim 10$  MHz repetition rate, generating an average current of  $\sim 1$  pA.

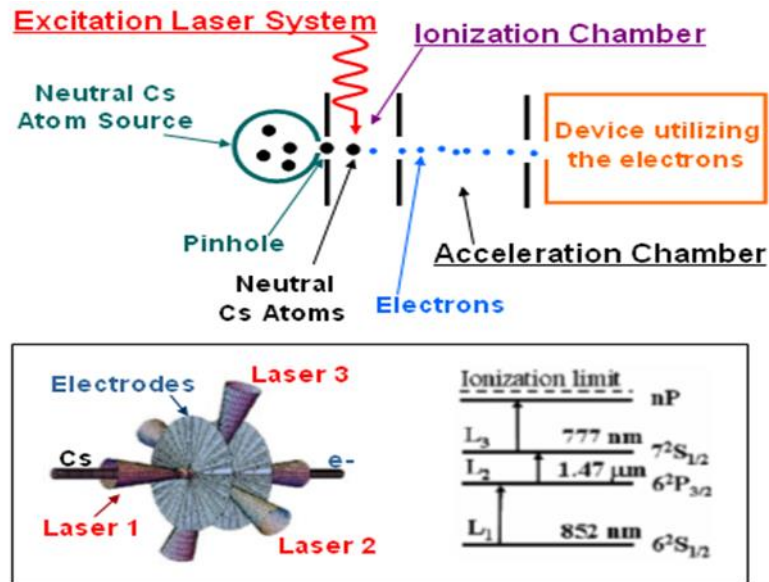


Figure 5-6: Principle of a quantum-degenerate electron source based on ionization of Cs atoms in a high Rydberg state. Courtesy of LBNL.

The described scheme eliminates the Coulomb interaction between electrons since each cycle produces a single electron, and properly controls the interaction between the electron and the parent and residual ions. Calculations from a proof of concept experiment at LBNL show that this approach produces a degeneracy parameter approaching the quantum limit.

This revolutionary source brightness would allow for diffraction patterns with record high visibilities, scanning electron microscopes with  $\text{\AA}$  resolution at low electron energies, and experiments with energy resolution down to  $\sim 10^{-4}$ – $10^{-5}$  eV. The large number of coherent electrons per second will allow for the collection of high-quality diffraction and real space images within seconds. Improved time resolution can be obtained by rotating the longitudinal phase space, trading time versus energy resolution.

### 5.3.3. Field emission sources

The development of extremely bright field emission tips opens opportunities in coherent electron microscopy. These cathodes already provide simple sources of extremely bright beams

with the potential to greatly simplify the control of UEM and UED devices and allow fast gating of the electron pulses so the pulse duration can be varied.

Researchers from several institutions are investigating field emission from single tips and arrays of tips. Recent investigations have demonstrated the formation of spatially localized and ultra-short electron bunches with a high degree of coherence [Ehberger, 2015]. Materials for these emitters include tungsten [Hommelhoff, 2006], molybdenum [Schwoebel, 2005], copper [Singh, 2013], and various forms of carbon [Kang, 1995]. For example, multi-walled carbon nanotubes have been observed to exhibit a nearly quantum degenerate beam with  $\mathcal{D} = 0.25$  [Jarvis, 2010]. The field emission can be triggered with an ultra-short frequency laser or RF fields.

Diamond field-emission arrays (DFEAs), arrays of doped-diamond pyramids with exquisitely sharp tips, are especially promising. These DFEAs are formed using a mold-transfer process [Kang, 1996], patented by Vanderbilt University (see Figure 5-7), but now used in labs around the world. Because this technique uses standard silicon wafer processes to pattern the array, DFEAs can be formed with a very wide range of base length and pitch, and can be created with 1, 2, or 4 peaks per pyramid. DFEAs are robust to exposure to air, emit in poor or good vacuum conditions, and can be easily conditioned to emit uniformly over the whole array [Jarvis, 2009]. Because the tips are diamond, they are chemically inert and have excellent thermal conductivity, allowing them to sustain high per-tip emission current without catastrophic failure modes. To date, the maximum single tip current measured was  $18 \mu\text{A}$ , corresponding to  $>1 \text{ A/mm}$  for a dense array, with an energy spread of  $0.3 \text{ eV}$  for a single tip [Jarvis, 2010], and maximum transverse emittance of  $1 \text{ mm-mrad}$  for an array [Jarvis, 2012].

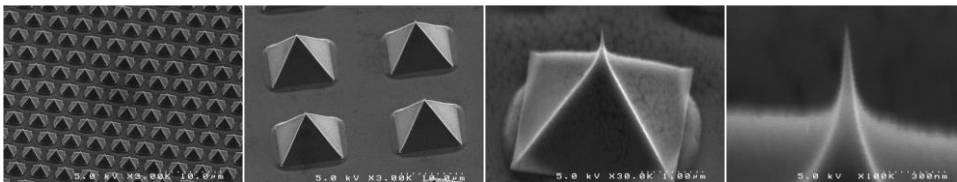


Figure 5-7: SEM images of DEFA samples fabricated at Vanderbilt University shown at four different magnifications. Reproduced from [Kang, 1996], with the permission of the American Vacuum Society.

While single array elements are easy to fabricate, the transverse emittance for a single tip has not been measured. During energy-spread investigations, adsorbates were observed attaching to and departing from the sharpened tips, enhancing emission by an order of magnitude. This directly increases beam brightness, as the adsorbates do not affect the energy spread of the beam.

The primary research effort over the next three years should focus on characterizing beams emitted by single tips, along with ways of stabilizing emitted current. It is necessary to measure total current, emittance, and energy spread and to explore methods to stabilize and maximize the emitted current over a reasonable time span (at least a few hours). The main mechanism for controlling current stability is controlling adsorbate binding, either by heating or cooling the tips or changing the surface termination.

Field emission tips could eliminate the need for a laser in UEM and UED experiments, as well as the need to float heating systems at high voltage. When organized as arrays, field-emitter arrays could be combined with emittance-exchange techniques to support beam nanopatterning [Graves, 2012].

## REFERENCES

---

- “Neutron and X-ray Detectors,” *Report of the Basic Energy Sciences Workshop on Neutron and X-ray Detectors*, Gaithersburg, MD, August 1-3, 2012.
- “X-ray Optics for BES Light Source Facilities,” *Report of the Basic Energy Sciences Workshop on X-ray Optics for BES Light Source Facilities* Potomac, MD, March 27-29, 2013.
- Adderley, P.A., et al., “Load-locked dc high voltage GaAs photogun with an inverted-geometry ceramic insulator,” *Phys. Rev. STAB* **13**, 010101 (2010).
- Akrap, A., et al., “Magneto-Optical Signature of Massless Kane Electrons in  $\text{Cd}_3\text{As}_2$ ,” *Phys. Rev. Lett.* **117**, 136401 (2016).
- Akre, R., et al., “Commissioning the Linac Coherent Light Source injector,” *Phys. Rev. STAB* **11**, 030703 (2008).
- Alexander, A., N. A. Moody, P. R. Bandaru, “Enhanced quantum efficiency of photoelectron emission, through surface textured metal electrodes,” *J. Vac. Sci. Tech. A* **34**, 021401 (2016).
- Altarelli M., et al. (Eds.), “The European X-Ray Free-Electron Laser. Technical Design Report,” Preprint DESY 2006-097, DESY, Hamburg (2006).
- Armstrong, M. R., “Practical considerations for high spatial and temporal resolution dynamic transmission electron microscopy,” *Ultramicroscopy* **107**, 356 (2007).
- Armstrong, M. R., B. Reed, B. Torralva, N. Browning, “Prospects for electron imaging with ultrafast time resolution”, *Appl. Phys. Lett.* **90**, 114101 (2007); doi: 10.1063/1.2712838.
- Bartnik, A. et al, “Operational experience with nanocoulomb bunch charges in the Cornell photoinjector,” *Phys. Rev. ST Accel Beams* **18**, 083401 (2015).
- Barwick, B., A. H. Zewail, “Photonics and Plasmonics in 4D Ultrafast Electron Microscopy,” *ACS Photonics* **2** 1391-1402 (2015).
- Batelaan, H., “Colloquium: Illuminating the Kapitza-Dirac effect with electron matter optics,” *Rev. Mod. Phys.* **79**, 929 (2007).
- Batson, P. E., N. Dellby, O.L. Krivanek, “Sub-angstrom Resolution Using Aberration Corrected Electron Optics” *Nature* **418**, 617 (2002).
- Bazarov, I. V., D. G. Ouzounov, B. M. Dunham, S. A. Belomestnykh, Y. Li, X. Liu, R. E. Meller, J. Sikora, C. K. Sinclair, F. W. Wise, and T. Miyajima, “Efficient temporal shaping of electron distributions for high-brightness photoemission electron guns,” *Phys. Rev. STAB* **11**, 040702 (2008).
- Bazarov, I. V., et al, “Maximum Achievable Beam Brightness from Photoinjectors,” *Phys. Rev. Lett.* **102**, 104801 (2009).

- Bazarov, I.V., B. M. Dunham, Y. Li, X. Liu, D. G. Ouzounov, C. K. Sinclair, F. Hannon, T. Miyajima, “Thermal emittance and response time measurements of negative electron affinity photocathodes,” *J. Appl. Phys.* **103**, 054901 (2008).
- Beaurepaire, B., A Lifschitz, J Faure, “Electron acceleration in sub-relativistic wakefields driven by few-cycle laser pulses,” *New J. Phys.* **16**, 023023 (2014).
- Berger, J.A., B.L. Rickman, T. Li, A.W. Nicholls, and W.A. Schroeder, “Excited-state thermionic emission in III-antimonides: Low emittance ultrafast photocathodes,” *Appl. Phys. Lett.* **101**, 194103 (2012).
- BESAC, “BESAC Report on Facility Upgrades,”  
[https://science.energy.gov/~media/bes/besac/pdf/Reports/BESAC\\_Facility\\_Upgrade\\_Assessment\\_Approved\\_June\\_9\\_2016.pdf](https://science.energy.gov/~media/bes/besac/pdf/Reports/BESAC_Facility_Upgrade_Assessment_Approved_June_9_2016.pdf) (2016).
- BESAC, “Challenges at the Frontiers of Matter and Energy: Transformative Opportunities for Discovery Science,”  
[http://science.energy.gov/~media/bes/besac/pdf/Reports/CFME\\_rpt\\_print.pdf](http://science.energy.gov/~media/bes/besac/pdf/Reports/CFME_rpt_print.pdf) (2015).
- Bisognano, J., et al., “Wisconsin SRF Electron Gun Commissioning” *Proc. PAC2013*, Pasadena, CA (2013).
- Bonifacio, R., C. Narducci, C. Pellegrini, “Collective instabilities and high-gain regime in a free electron laser,” *Opt. Commun.* **50**, 373 (1984).
- Bostedt, C., et al., “Linac Coherent Light Source: The first five years,” *Rev. Mod. Phys.* **88**, 015007 (2016);  
 10.1103/RevModPhys.88.015007.
- Bradley, D.J., et al. “The transverse energy of electrons emitted from GaAs photocathodes,” *J. Phys. D: Appl. Phys.* **10**, 111 (1977).
- Brinkmann, R., et al, “A low emittance, flat-beam electron source for linear colliders,” *Phys. Rev. STAB* **4**, 053501 (2001).
- Brown, W. J., S. E. Korbly, K. E. Kreisler, I. Mastovsky, and R. J. Temkin, “Low emittance electron beam formation with a 17 GHz RF gun,” *Phys. Rev. STAB* **4**, 083501 (2001).
- Browning, N.D., et al, “Recent developments in dynamic transmission electron microscopy”, *Current Opinion in Solid State and Materials Science* **16**, 23 (2012).
- Buck, A., M. Nicolai, K. Schmid, C. M. S. Sears<sup>1</sup>, A. Savert, J. M. Mikhailova, F. Krausz, M. C. Kaluza, L. Veisz, “Real-time observation of laser-driven electron acceleration,” *Nature Physics* **7**, 543 (2011).
- Burrill, A., et al., “First Horizontal Test Results of the HZB SRF Photoinjector for bERLinPro,” *IPAC 2015*, Richmond, VA, USA, (2015).
- Cahill, A., “RF Design for the TopGun Photogun: A Cryogenic Normal Conducting Copper Electron Gun”, *Nucl. Instrum. Meth. A*, submitted for publication (2017).

- Camino, B., et al., "Photoemission simulation for photocathode design: theory and application to copper and silver surfaces," *Comp. Mat. Sci.* **122**, 331–340 (2016).
- Cao, J., H. Ihee, A.H. Zewail, "Ultrafast electron diffraction: determination of radical structure with picosecond time resolution", *Chem. Phys. Lett.* **290**, 1 (1998).
- Carbone, F., et al., "A perspective on novel sources of ultrashort electron and X-ray pulses," *Chem. Phys.* **392**, 1 (2012).
- Carlsten, B. E., "New photoelectric injector design for the Los Alamos National Laboratory XUV FEL accelerator," *Nucl. Instrum. Meth. A* **285**, 313 (1989).
- Cesar, D., "Ultrafast gating of a mid-infrared laser pulse by a sub-pC relativistic electron beam," *J. Appl. Phys.* **118**, 234506 (2015).
- Chaloupka, H., et al., "A proposed superconducting photoemission source of high brightness," *Nucl. Instr. Meth. A* **285**, 327 (1989).
- Chapman, H. N., et al., "Femtosecond X-ray protein nanocrystallography," *Nature* **470**, 73 (2011).
- Chattopadhyay, S., "Photon-Electron Interaction and Condense Beams," *Advanced ICFA Beam dynamics workshop on Quantum Aspects of Beam Physics*, Ed. P.Chen, 153 (World Scientific, 1998).
- Claessens, B. J., S. B. van der Geer, G. Taban, E. J. D. Vredenburg, O. J. Luiten, "Ultra-cold electron source," *Phys. Rev. Lett.* **95**, 164801 (2005).
- Cornacchia, M. and P. Emma, "Transverse to longitudinal emittance exchange," *Phys. Rev. STAB* **5**, 084001 (2002).
- Cultrera, L., C. Gulliford, A. Bartnik, H. Lee, I. Bazarov, "Ultra low emittance electron beams from multi-alkali antimonide photocathode operated with infrared light," *Appl Phys Lett.* **108**, 134105 (2016).
- Cultrera, L., S. Karkare, H. Lee, X. Liu, I. Bazarov, B. Dunham, "Cold electron beams from cryocooled, alkali antimonide photocathodes," *Phys. Rev. STAB* **18**, 113401 (2015).
- Dahal, P. A. Mudvari, A. Basnet, P. Brown, B. Barwick, "Ultrafast electron microscopy for investigating fundamental physics phenomena," *Proc. SPIE Ultrafast Nonlinear Imaging and Spectroscopy IV* **9956**, 995604 (2016).
- Dal Conte, S., et al., "Snapshots of the retarded interaction of charge carriers with ultrafast fluctuations in cuprates", *Nature Physics* **11**, 421 (2015).
- Dal Forno, M., et al, "Experimental measurements of rf breakdowns and deflecting gradients in mm-wave metallic accelerating structures," *Phys. Rev. Accel. Beams* **19**, 051302 (2016).
- Dei-cas, R., et al., "Status report on the low-frequency photo-injector and on the infrared FEL experiment (ELSA)," *Nuc. Instr. Meth. A* **296**, 209 (1990).

- di Bona, A., et al., “Auger and x-ray photoemission spectroscopy study on Cs<sub>2</sub>Te photocathodes,” *J. Appl. Phys.* **80**, 3024 (1996).
- Ding, Y. et al., “Measurements and Simulations of Ultralow Emittance and Ultrashort Electron Beams in the Linac Coherent Light Source,” *Phys. Rev. Lett.* **102**, 254801 (2009).
- Doebert, S., “Gradient limitations for high-frequency accelerators,” *Proc. LINAC 2004*, Lubeck, Germany, p. 513 (2004).
- Dornmair, I., et al., “Plasma-driven ultrashort bunch diagnostics,” *Phys. Rev. STAB* **19**, 062801 (2016).
- Dowell, D. H., et al., “Cathode R&D for future light sources,” *Nucl. Instrum. Meth. Phys. Research A* **622**, 685 (2010).
- Dowell, D. H., “Sources of Emittance in RF Photocathode Injectors: Intrinsic emittance, space charge forces due to non-uniformities, RF and solenoid effects,” arXiv:1610.01242v1 [physics.acc-ph] (2016).
- Dowell, D. H., et al., “A two-frequency RF photocathode gun,” *Nucl. Instrum. Meth. A* **528**, 316 (2004).
- Dowell, D. H., et al., “First operation of a photocathode radio frequency gun injector at high duty factor,” *Appl. Phys. Lett.* **63**, 2035 (1993).
- Dowell, D. H., S.Z. Bethel and K.D. Friddell, “Results from the average power laser experiment photocathode injector test,” *Nucl. Instrum. Meth. A* **356**, 167 (1995).
- Droubay, T. C., et al., “Metal-Insulator Photocathode Heterojunction for Directed Electron Emission,” *Phys. Rev. Lett.* **112**, 067601 (2014).
- Dunham, B., et al., “Record high-average current from a high-brightness photoinjector,” *Appl. Phys. Lett.* **102**, 034105 (2013).
- Duris, J. P., Murokh A. and Musumeci, P. “Tapering enhanced stimulated superradiant amplification,” *New J. Phys.* **17**, 063036 (2015).
- Ehberger, D., J. Hammer, M. Eisele, M. Krüger, J. Noe, A. Högele, P. Hommelhoff, “Highly Coherent Electron Beam from a Laser-Triggered Tungsten Needle Tip,” *Phys. Rev. Lett.* **114**, 227601 (2015).
- Emma, C. et al, “Terawatt x-ray free-electron-laser optimization by transverse electron distribution shaping,” *Phys. Rev. STAB* **17**, 110701 (2014).
- Emma, P., et al., “First lasing and operation of an angstrom-wavelength free-electron laser”, *Nature Photonics* **4**, 641 (2010).
- Emma, P., Z. Huang, K.-J. Kim, P. Piot, “Transverse-to-longitudinal emittance exchange to improve performance of high-gain free-electron lasers,” *Phys. Rev. STAB* **9**, 100702 (2006).

- Erni, R., et al, "Atomic-Resolution Imaging with a Sub-50-pm Electron Probe," *Phys. Rev. Lett.* **102**, 096101 (2009).
- Esarey, E., C. B. Schroeder, W. P. Leemans, "Physics of laser-driven plasma-based electron accelerators," *Rev. Mod. Phys.* **81**, 1129 (2009).
- Ewbank, J. D., et al, "Electron diffraction instrumentation at the University of Arkansas from continuous beams to picosecond pulses: 1983 to 1998", Proc. SPIE 3516, 23rd International Congress on High-Speed Photography and Photonics, 596 (June 22, 1999); doi:10.1117/12.350539; <http://dx.doi.org/10.1117/12.350539>
- Fallahi, A., et al., "Short Electron Bunch Generation Using Single-Cycle Ultrafast Electron Guns," *Phys. Rev. Accel. Beams* **19**, 081302 (2016).
- Faure, J., B. van der Geer, B. Beaupaire, G. Gallé, A. Vernier, A. Lifschitz, "Concept of a laser-plasma-based electron source for sub-10-fs electron diffraction," *Phys. Rev. Accel. Beams* **19**, 021302 (2016).
- Feldman, D., et al., "Performance of the Los Alamos HIBAF accelerator at 17 MeV, *Nucl. Instrum. Meth. A* **285**, 313 (1991).
- Feng, J., et al., "Thermal limit to the intrinsic emittance from metal photocathodes," *Appl. Phys. Lett.* **107**, 134101 (2015).
- Feng, J. et al, "Near atomically smooth alkali antimonide photocathode thin films," *J. Appl. Phys.* **121**, 044904 (2017); doi: <http://dx.doi.org/10.1063/1.4974363>.
- Ferrario, M. et al, "HOMDYN Study for the LCLS RF Photo-Injector," SLAC-PUB-8400 (2001).
- Filippetto, D., H. Qian, "Design of a high-flux instrument for ultrafast electron diffraction and microscopy," *Journal of Physics B: Atomic, Molecular and Optical Physics* **49**, 104003 (2016).
- Filippetto, D., P. Musumeci, M. Zolotarev, G. Stupakov, "Maximum current density and beam brightness achievable by laser-driven electron sources," *Phys. Rev. STAB* **17**, 024201 (2014).
- Floettmann, K., V. Paramonov, "Beam dynamics in transverse deflecting rf structures," *Phys. Rev. STAB* **17**, 024001 (2014).
- Fraser, J. S., et al, "Photocathodes in Accelerator Applications," *Proc. 1987 Particle Accelerator Conf*, Washington, DC, Mar. 16-19, p.1705 (1987).
- Fukasawa, A., et al., "Progress on the Hybrid Gun Project at UCLA," *Physics Procedia* **52**, 2, doi: 10.1016/j.phpro.2014.06.002 (2014).
- Gallagher, A. C., G. York, "A photoionization source of mono-energetic electron," *Rev. Sci. Instrum.* **45**, 662 (1974).

- Grassellino, A., et al., “Nitrogen and argon doping of niobium for superconducting radio frequency cavities: a pathway to highly efficient accelerating structures Supercond,” *Sci. Technol.* **26**, 102001 (2013).
- Graves, W. S., F. X. Kaertner, D. E. Moncton, “Intense Superradiant X Rays from A Compact Source using a Nanocathode Array and Emittance Exchange,” *Phys. Rev. Lett.* **108**, 263904 (2012).
- Graves, W. S., et al., “Compact x-ray source based on burst-mode inverse Compton scattering at 100 kHz,” *Phys. Rev. STAB* **17**, 120701 (2014).
- Gulliford, C., A. Bartnik, I. Bazarov, “Multiobjective optimizations of a novel cryocooled dc gun based ultrafast electron diffraction beam line,” *Phys. Rev. STAB* **19**, 093402 (2016).
- Hall, E., S. Stemmer, H. Zheng, Y. Zhu, G. Maracas, *Workshop on Future of Electron Scattering & Diffraction*, DOE-BES Report, Feb 25-26, 2014, Rockville, MD USA, [http://science.energy.gov/~media/bes/pdf/reports/files/Future\\_of\\_Electron\\_Scattering.pdf/](http://science.energy.gov/~media/bes/pdf/reports/files/Future_of_Electron_Scattering.pdf/) (2014).
- Hartmann, N., et al., “Sub-femtosecond precision measurement of relative X-ray arrival time for free-electron lasers,” *Nature Photonics*, **8**, 706–709 (2014).
- He, Z.-H., A. G. R. Thomas, B. Beaurepaire, J. A. Nees, B. Hou, V. Malka, K. Krushelnick, J. Faure, “Electron diffraction using ultrafast electron bunches from a laser-wakefield accelerator at kHz repetition rate,” *Appl. Phys. Lett.* **102**, 064104 (2013).
- He, Z.-H., B. Hou, J. A. Nees, J. H. Easter, J. Faure, K. Krushelnick, A. G. R. Thomas, “High repetition-rate wakefield electron source generated by few-millijoule, 30 fs laser pulses on a density downramp,” *New J. Phys.* **15**, 053016 (2013).
- Helfenstein, P., A. Mustonen, T. Feurer, S. Tsujino, “Collimated Field Emission Beams from Metal Double-Gate Nanotip Arrays Optically Excited via Surface Plasmon Resonance” *Appl. Phys. Express* **6**, 114301 (2013).
- Hemming, E., G. Stupakov, D. Xiang, A. Zholents, “Beam by design: Laser manipulation of electrons in modern accelerators,” *Rev. Mod. Phys.* **86**, 897 (2014).
- Hidding, B., G. Pretzler, J. B. Rosenzweig, T. Konigstein, D. Schiller, D. L. Bruhwiler, “Ultracold Electron Bunch Generation via Plasma Photocathode Emission and Acceleration in a Beam-Driven Plasma Blowout,” *Phys. Rev. Lett.* **108**, 035001 (2012).
- Higo, T., T. Abe, Y. Arakida, S. Matsumoto, T. Shidara, T. Takatomi, M. Yamanaka, Y. Higashi, A. Grudiev, G. Riddone, and W. Wuensch, “Comparison of high gradient performance in varying cavity geometries,” *Proc. IPAC2013*, Shanghai, China, WEPFI018 (JACoW, Shanghai, China), 2741 (2013).
- Hilbert, S., C. Uiterwaal, B. Barwick, H. Batelaan, A. H. Zewail, “Temporal lenses for attosecond and femtosecond electron pulses,” *Proc. Natl. Acad. Sci.* **106**, 10558 (2009).

- Hommelhoff, P., C. Kealhofer, M. A. Kasevich, “Ultrafast Electron Pulses from a Tungsten Tip Triggered by Low-Power Femtosecond Laser Pulses,” *Phys. Rev. Lett.* **97**, 247402 (2006).
- Huang Z., I. Lindau, “Free-electron lasers: SACLA hard-X-ray compact FEL”, *Nature Photonics* **6**, 505 (2012).
- Huang, W. R., et al., “Terahertz-driven, all-optical electron gun,” *Optica*, accepted for publication, arXiv:1605.06667 (2016).
- Ihee, H., et al, “Direct imaging of transient molecular structures with ultrafast diffraction,” *Science* **291**, 458 (2001).10.1126/science.291.5503.458.
- J. Hao et al., “Development of DC-SRF injector at Peking University,” *Proc. IPAC 2015*, Richmond, VA, (2015).
- Jarvis, J. D., B. K. Choi, A. B. Hmelo, B. Ivanov, C. A. Brau, “Emittance measurements of electron beams from diamond field emitter arrays,” *J. Vac. Sci. Technol. B* **30**, 042201 (2012).
- Jarvis, J. D., et al., “Resonant tunneling and extreme brightness from diamond field emitters and carbon nanotubes,” *J. Appl. Phys.* **108**, 094322 (2010).
- Jarvis, J. D., H. L. Andrews, C. A. Brau, B. K. Choi, J. Davidson, W.-P. Kang, Y.-M. Wong, “Uniformity conditioning of diamond field emitter arrays,” *J. Vac. Sci. Technol. B* **27**, 2264 (2009).
- Jensen, K. L., “Scattering and the relationship between quantum efficiency and emittance,” *J. Appl. Phys.* **113**, 056101 (2013).
- Jensen, K. L., E. Montgomery, D. W. Feldman, P. G. O’Shea, J. Harris, J. Lewellen, and N. Moody, “Multiple scattering effects on quantum efficiency and response time for cesiated metal photocathodes,” *J. Appl. Phys.* **110**, 034504 (2011).
- Jensen, K. L., N. A. Moody, D. W. Feldman, E. J. Montgomery, P. G. O’Shea, “Photoemission from metals and cesiated surfaces,” *J. Appl. Phys.* **102**, 074902 (2007).
- Jiao, Y., et al, “Modeling and multidimensional optimization of a tapered free electron laser,” *Phys. Rev. STAB* **15**, 050704 (2012).
- Kang, W. P., et al., “Micropatterned polycrystalline diamond field emitter vacuum diode arrays,” *J. Vac. Sci. Technol. B* **14**, 2068 (1996).
- Kang, W. P., J. L. Davidson, M. Howell, B. Bhuvu, D. L. Kinser, Q. Li, J. F. Xu, *Proceedings of International Vacuum Microelectronics Conference, IVMC*, Portland, OR, 4 August 1995, 287–291 (1995).
- Karkare, S., and I. V. Bazarov, “Effect of nanoscale surface roughness on transverse energy spread from GaAs photocathodes,” *Appl. Phys. Lett.* **98**, 094104 (2011).
- Karkare, S., et.al., “Ultrabright and Ultrafast III–V Semiconductor Photocathodes” *Phys. Rev. Lett.* **112**, 097601 (2014).

- Karkare, S., I. V. Bazarov, “Effects of Surface Nonuniformities on the Mean Transverse Energy from Photocathodes,” *Phys. Rev Applied* **4**, 024015 (2015); .
- Karkare, S., L. Boulet, A. Singh, R. Hennig, I. Bazarov, “Ab initio studies of Cs on GaAs (100) and (110) surfaces,” *Phys. Rev. B.* **91**, 035408 (2015).
- Kealhofer, C., W. Schneider, D. Ehberger, A. Ryabov, F. Krausz, P. Baum, “All-optical control and metrology of electron pulses,” *Science* **352**, 429 (2016).
- Kim, K. J., “RF and space-charge effects in laser-driven RF electron guns,” *Nucl. Instrum. Methods A* **275**, 201 (1989).
- Konomi, T., et al., “Design, fabrication and performance of SRF-Gun cavity,” *Proc. IPAC 2015*, Richmond, VA, (2015).
- Krasilnikov, M., et al., “Experimentally minimized beam emittance from an L-band photoinjector,” *Phys. Rev. STAB* **15**, 100701 (2012).
- Kuwahara, M., Y. Takeda, K. Saitoh, T. Ujihara, H. Asano, T. Nakanishi, N. Tanaka, “Development of spin-polarized transmission electron microscope,” *J. Phys.: Conf. Ser.* **298** 012016 (2011).
- Kuzikov, S. V., et al., “A multi-frequency RF photocathode gun,” 15th Adv. Accel. Concepts Workshop, Austin, TX, *AIP Conference Proceedings* **1507**, 927 (2012).
- Kuzikov, S. V., A. A. Vikharev, “A Multi-Mode RF Photocathode Gun,” *Proc. 2011 International Particle Accelerator Conference IPAC2011*, San Sebastián, Spain, p. 1135 (2011).
- Kuzikov, S. V., S. Yu. Kazakov, Y. Jiang, J.L. Hirshfield, “Asymmetric bimodal accelerator cavity for raising rf breakdown thresholds,” *Phys. Rev. Lett.* **104**, 214801 (2010).
- Lee, H., L. Cultrera, I.V. Bazarov, “Intrinsic emittance reduction in transmission mode photocathodes,” *Appl. Phys. Lett.* **108**, 124105 (2016).
- R. Legg et al., “Status of the Wisconsin RF Gun,” *Proc. 2012 International Particle Accelerator Conference IPAC2012*, New Orleans, LA, USA, p. 661 (2012).
- Lewellen, J., J. Noonan, “Field-emission cathode gating for rf electron guns,” *Phys. Rev. STAB* **8**, 033502 (2005).
- Li, R. K., P. Musumeci, “Single-shot MeV transmission electron microscopy with picosecond temporal resolution,” *Phys. Rev. Appl.* **2**, 024003 (2014).
- Li, R., et al., “Surface-Plasmon Resonance-Enhanced Multiphoton Emission of High-Brightness Electron Beams from a Nanostructured Copper Cathode” *Phys. Rev. Lett.* **110**, 074801 (2013).
- Li, S., et al., “LCLS laser modulation to improve FEL operation efficiency and performance,” *Proc. IPAC 2015*, Richmond, VA, 1813 (2015).

- Li, T., B.L. Rickman, W.A. Schroeder, “Emission properties of body-centered cubic elemental metal photocathodes,” *J. Appl. Phys.* **117** 134901 (2015).
- Limborg, C., et al., “Performance of a first generation X-Band gun”, *Phys. Rev. STAB* **19**, 053401 (2016).
- Lobastov, V. A., R. Srinivasan, and A.H. Zewail, “Four-Dimensional Ultrafast Electron Microscopy,” *Proc. Natl. Acad. Sci.* **102**, 7069 (2005).
- Lozovoy, V. V., et al, “Phase-only synthesis of ultrafast stretched square pulses,” *Optics Express* **23**, 27105 (2015).
- Luiten, O. J., B. J. Claessens, S. B. van der Geer, M. P. Reijnders, G. Taban, E. J. D. Vredenburg, “Ultracold electron sources,” *Int. J. Mod. Phys.* **22**, 3882 (2007).
- Marsh, R., “Modeling and design of an X-band rf photo-injector,” *Phys. Rev. STAB* **15**, 102001 (2012).
- Maxson, J., “Toward Optimal Beam Brightness from High Voltage DC Photoelectron Sources,” Ph.D Thesis, Cornell University (2015).
- Maxson, J., I. V. Bazarov, W. Wan, H. A. Padmore, C.E. Coleman-Smith, “Fundamental photoemission brightness limit from disorder induced heating.” *New Journ. Phys.* **15** 103024 (2013).
- Maxson, J., H. Lee, A. C. Bartnik, J. Kiefer, I. Bazarov, “Adaptive electron beam shaping using a photoemission gun and spatial light modulator,” *Phys. Rev. STAB* **18** 023401 (2013).
- Maxson, J., P. Musumeci, L. Cultrera, S. Karkare, and H. Padmore, “Ultrafast laser pulse heating of metallic photocathodes and its contribution to intrinsic emittance,” *Nucl. Instr. Meth. Phys. Res. A*, in press (2017).
- McCulloch, A. J., B. M. Sparkes, R. E. Scholten, “Cold electron sources using laser-cooled atoms,” *J. Phys. B: At. Mol. Opt. Phys.* **49**, 164004 (2016).
- McCulloch, A. J., et al., “Arbitrarily shaped high-coherence electron bunches from cold atoms,” *Nature Physics* **7**, 785 (2011).
- Miao, J., et al, “Atomic electron tomography: 3D structures without crystals”, *Science* **353**, 2157 (2016). DOI: 10.1126/science.aaf2157.
- Miller R. J. D., “Femtosecond crystallography using ultrabright electron and x-ray sources: Capturing chemistry in action,” *Science* **343**, 1108 (2014).
- Minitti, M.P., et al, “Imaging molecular motion: femtosecond X-ray scattering of an electrocyclic chemical reaction,” *Phys. Rev. Lett.* **114**, 255501 (2015).
- Mourou, G., S. Williamson, “Picosecond electron diffraction,” *Appl. Phys. Lett.* **41**, 44 (1982); doi: <http://dx.doi.org/10.1063/1.93316>.
- Muller, D., “Structure and bonding at the atomic scale by scanning transmission electron microscopy,” *Nature Materials* **8**, 263 (2009).

- Murokh, A., et al., “Extreme ultraviolet transition radiation beam profile monitor,” presented at the 17th Advanced Accelerator Concepts Workshop, National Harbor, MD, July 31 – Aug 5, 2016.
- Nanni, E. A., et al., “Measurements of Transmitted Electron Beam Extinction through Si Crystal Membranes,” *Proc. 2016 International Particle Accelerator Conference IPAC2016*, Busan, Korea, p. 1611 (2016).
- Nanni, E. A., W. R. Huang, et al., “Terahertz-driven linear electron acceleration,” *Nature Commun.* **6**, 8486 (2015).
- Nanni, E. A., W. S. Graves, “Aberration Corrected Emittance Exchange,” *Phys. Rev. STAB* **18**, 084401 (2015).
- Nanni, E. A., W. S. Graves, D.E. Moncton, “Nano-modulated electron beams via electron diffraction and emittance exchange for coherent x-ray generation,” arXiv:1506.07053 (2015).
- Nanni, E. A., W. S. Graves, P. Piot, “Nanometer Scale Coherent Current Modulation via a Nanotip Cathode Array and Emittance Exchange,” *Proceedings of the 2014 International Particle Accelerator Conference IPAC2014*, Dresden, Germany, p. 1952 (2014).
- Nemeth, K., et al., “High-Brightness Photocathodes through Ultrathin Surface Layers on Metals,” *Phys. Rev. Lett.* **104**, 046801 (2010).
- Nguyen, D., et al., “End-point energy measurements of field emission current in a continuous-wave normal-conducting rf injector,” *Phys. Rev. STAB* **14**, 030704 (2011).
- Nishimori N., et al., “A DC Photoemission gun upgrade at the Compact ERL,” *Proceedings of IPAC 2016*, Busan, Korea (2016).
- Nodvick, J. S., and D. S. Saxon, “Suppression of Coherent Radiation by Electrons in a Synchrotron,” *Phys. Rev.* **96**, 180 (1954).
- Öström, H., et al., “Probing the transition state region in catalytic CO oxidation on Ru,” *Science* **347**, 978 (2015).
- Pak, A., K. A. Marsh, S. F. Martins, W. Lu, W. B. Mori, C. Joshi, “Injection and Trapping of Tunnel-Ionized Electrons into Laser-Produced Wakes,” *Phys. Rev. Lett.* **104**, 025003 (2010).
- Palmer, D. T., “The next generation photoinjector”, PhD Thesis, Stanford Univ. (1998).
- Palmer, D.T., et al, “Initial commissioning results of next generation photoinjector,” 7<sup>th</sup> Advanced Accelerator Concepts Conference, Lake Tahoe, CA, USA, 13 - 19 Oct 1996, *AIP Conf. Proc.* **398**, 695 (1997).
- Pavlenko, V., F. Liu, M. Hoffbauer, E. Batista, N. A. Moody, “Kinetics of alkali-based photocathode degradation,” *AIP Advances* **6**, 115008 (2016), [10.1063/1.4967349](https://doi.org/10.1063/1.4967349).
- Pellegrini, C., et al., “The physics of x-ray free-electron lasers,” *Rev. Mod. Phys.* **88**, 015006 (2016).
- Pinayev, I., et al., “Record Performance of SRF Gun with CsK<sub>2</sub>Sb Photocathode,” *Proc. 2016 International Particle Accelerator Conference IPAC2016*, Busan, Korea, p. 2085 (2016).
- Pirez, E., et al, “S-Band 1.4 cell photoinjector design for high brightness beam generation,” *Nucl. Instrum. Methods*

A, in press (2016); doi: 10.1016/j.nima.2016.08.063

- Plateau, G. R., et al., “Low-Emittance Electron Bunches from a Laser-Plasma Accelerator Measured using Single-Shot X-Ray Spectroscopy,” *Phys. Rev. Lett.* **109**, 064802 (2012).
- Plemmons, D.A., et al, “Probing Structural and Electronic Dynamics with Ultrafast Electron Microscopy”, *Chem. Mater.* **9**, 3178 (2015).
- Plettner, T., R. L. Byer, C. McGuinness, and P. Hommelhoff, “Photonic-based laser driven electron beam deflection and focusing structures” *Phys. Rev. STAB* **12**, 101302 (2009).
- Qian, H., et al., “S-band photoinjector investigations by multi-objective genetic optimizer,” *Proc. 2016 International Particle Accelerator Conference IPAC 2016*, Busan, Korea, p. 3979 (2016).
- Rechatin, C., et al., “Controlling the Phase-Space Volume of Injected Electrons in a Laser-Plasma Accelerator,” *Phys. Rev. Lett.* **102**, 164801 (2009).
- Reiser, M., *Theory and design of charged particle beams*, New York: John Wiley & Sons, Inc., page 470 (1994).
- Ropers, C., D. R. Solli, C. P. Schulz, C. Lienau, T. Elsaesser, “Localized Multiphoton Emission of Femtosecond Electron Pulses from Metal Nanotips,” *Phys. Rev. Lett.* **98**, 043907 (2007).
- Rosenzweig, J. B., et al., “Generation of ultra-short, high brightness electron beams for single-spike SASE FEL operation,” *Nucl. Instrum. Methods A* **593**, 39 (2008).
- Rosenzweig, J. B., et al, “Next generation high brightness electron beams from ultra-high field cryogenic radiofrequency photocathode source”, *Phys. Rev. STAB* <http://arxiv.org/abs/1603.01657>, in press (2017).
- Rosenzweig, J. B., et al., “Design and applications of an X-band hybrid photoinjector,” *Nucl. Instrum. Meth. A* **657**, 107 (2011).
- Ruiz-Oses, M., et al., “Direct observation of bi-alkali antimonide photocathodes growth via in operando x-ray diffraction studies,” *APL Materials* **2**, 121101 (2014).
- Ryabov, A., P. Baum, “Electron microscopy of electromagnetic waveforms,” *Science* **353**, 274 (2016).
- Sannibale, F., “Overview of Electron Source Development for High Repetition Rate FEL Facilities”, *Proc.NAPAC16*, Oct. 9-14, 2016, Chicago, IL (2016).
- Sannibale, F., et al., “Advanced photoinjector experiment photogun commissioning results,” *Phys. Rev. STAB* **15**, 103501 (2012).
- Savitzky, B. H., R. Hovden, K. Whitham, J. Yang, F. Wise, T. Hanrath, and L. F. Kourkoutis, “Propagation of Structural Disorder in Epitaxially Connected Quantum Dot Solids from Atomic to Micron Scale,” *Nano Letters* **16**, 5714 (2016).
- Schaer, M., et al., “RF traveling-wave electron gun for photoinjectors,” *Phys. Rev. STAB* **19**, 072001 (2016).

- Schmid, K., et al., “Density-transition based electron injector for laser driven wakefield accelerators,” *Phys. Rev. STAB* **13**, 091301 (2010).
- Schmid, K., et al., “Few-Cycle Laser-Driven Electron Acceleration,” *Phys. Rev. Lett.* **102**, 124801 (2009).
- Schoenlein, R.W., et al., “New Science Opportunities Enabled by LCLS-II X-ray Lasers,” SLAC-R-1053 (2015).
- Schubert, S., et al., “Bi-alkali antimonide photocathode growth: An X-ray diffraction study,” *J. Appl. Phys.* **120**, 035303 (2016).
- Schwoebel, P. R., C. A. Spindt, C. E. Holland, “High current, high current density field emitter array cathodes,” *J. Vac. Sci. Technol. B* **23**, 691 (2005).
- Sciaini, G., R. J. D. Miller, “Femtosecond electron diffraction: Heralding the era of atomically resolved dynamics,” *Rep. Prog. Phys.* **74**, 096101 (2011).
- Sekutowicz, J., “SRF gun development overview,” *SRF 2015*, Whistler, Canada, 2015.
- Serafini, L., J. B. Rosenzweig, “Envelope analysis of intense relativistic quasilaminar beams in rf photoinjectors: a theory of emittance compensation”, *Phys. Rev. E* **55**, 7565- 7590 (1997).
- Shabaev, A., A. L. Efros, “Dark and Photo-Conductivity in Ordered Array of Nanocrystals,” *Nano Letters* **13**, 5454 (2013).
- Singh, A. K., J. Kumar, “Evaluation of field emission parameters in a copper nano-tip based diode,” *J. Appl. Phys.* **113**, 053303 (2013).
- Siwick, B. J., et al, “An atomic-level view of melting using femtosecond electron diffraction”, *Science* **302**, 1382 (2003). 10.1126/science.1090052.
- Smedley, J., et al., “Lead photocathodes,” *Phys. Rev. STAB* **11**, 013502 (2008).
- Speirs, R.W., et al, “Single-shot electron diffraction using a cold atom electron source,” *J. Phys. B: At. Mol. Opt. Phys.* **48**, 214002 (2015).
- Spicer, W. E., A. Herrera-Gomez, “Modern theory and applications of photocathodes,” *Proc. SPIE Int. Soc. Opt. Eng: Photodetectors and Power Meters* **2022**, 18 (1993).
- Sun, Y.-E., et al., “Tunable Subpicosecond Electron-Bunch-Train Generation Using a Transverse-To-Longitudinal Phase-Space Exchange Technique,” *Phys. Rev. Lett.* **105**, 234801 (2010).
- Taira, Y., et al. “Fabrication and Low Power test of C-Band RF Gun,” *Nucl. Instrum. Meth. B* **331**, 27 (2014).
- Teichert, J., et al., “First beam characterization of SRF gun II at ELBE with a Cu photocathode,” *ERL15*, Stony Brook, NY (2015).
- Thompson, M. C., J. B. Rosenzweig, H. Suk, “Plasma density transition trapping as a possible high-brightness electron beam source,” *Phys. Rev. STAB* **7**, 011301 (2004).

- Tomizawa, H., et al., “Development of adaptive feedback control system of both spatial and temporal beam shaping for UV laser light source for RF gun,” Proc. LINAC 2004, Lübeck, Germany, p 207, (2004).
- Trigo, M., et al., “Fourier-transform inelastic X-ray scattering from time- and momentum-dependent phononphonon correlations,” *Nat. Phys.*, **9**, 790 (2013).
- Tsujino, S., et al, “Measurement of transverse emittance and coherence of double-gate field emitter array cathodes,” *Nature Communications* **7**, 24976 (2016); DOI: 10.1038/ncomms13976.
- Tsujino, S., et al., “Static and optical field enhancement in metallic nanotips studied by two-photon photoemission microscopy and spectroscopy excited by picosecond laser pulses,” *Appl. Phys. Lett.* **94**(9), 093508 (2009).
- van Mourik, M. W., W. J. Engelen, E. J. D. Vredenburg, O. J. Luiten, “Ultrafast electron diffraction using an ultracold source,” *Structural Dynamics* **1**, 034302 (2014).
- Vartak, S. D., N. M. Lawandy, “Breaking the femtosecond barrier: a method for generating attosecond pulses of electrons and photons,” *Opt. Commun.* **120**, 184 (1995).
- Vecchione, T., et al., “A low emittance and high efficiency visible light photocathode for high brightness accelerator-based X-ray light sources,” *Appl. Phys. Lett.* **99**(3), 034103 (2011); DOI: 10.1063/1.3612916.
- Vecchione, T., *European Workshop on Photocathodes for Particle Accelerator Applications*, Daresbury, UK (2016).
- Velazquez, D., Ph.D. Thesis, Illinois Institute of Technology (2015); ISBN: 9781321939859.
- Vicario, C., et al., “Generation of 0.9-mJ THz pulses in DSTMS pumped by a Cr:Mg<sub>2</sub>SiO<sub>4</sub> laser,” *Opt. Lett.* **39**, 6632 (2014).
- Walbran, M., A. Gliserin, K. Jung, J. Kim, P. Baum, “5-Femtosecond Laser-Electron Synchronization for Pump-Probe Crystallography and Diffraction,” *Phys. Rev. Applied* **4**, 044013 (2015).
- Wang, F., “Breakdown Characteristics Study on an 18 Cell X-band Structure,” SLAC Technical Report No. SLAC-PUB-13458 (2008).
- Wang, X. J., “Producing and measuring small electron bunches”, *Proc. 1999 Particle Accelerator Conference*, New York, p.229 (1999).
- Wang, X. J., et al, “Efficiency and Spectrum Enhancement in a Tapered Free-Electron Laser Amplifier”, *Phys. Rev. Lett.* **103**, 154801 (2009).
- Wang, X. J., et al, “Experimental observation of high-brightness microbunching in a photocathode rf electron gun,” *Phys. Rev. E* **54**, R3121 (1996).
- Wang, X. J., Z. Wu, and H. Ihee, in *Proceedings of 2003 Particle Accelerator Conference*, IEEE, Portland, OR, USA, p. 420 (2003).

- Weathersby, S. P., et al., “Mega-electron-volt ultrafast electron diffraction at SLAC National Accelerator Laboratory,” *Rev. Sci. Instr.* **86**, 073702 (2015).
- Weiner, A. M., “Femtosecond pulse shaping using spatial light modulators,” *Rev. Sci. Instrum.* **71**, 1929 (2000).
- Weingartner, R., et al., “Ultralow emittance electron beams from a laser-wakefield accelerator,” *Phys. Rev. STAB* **15**, 111302 (2012).
- Wimmer, L., et al., “Terahertz control of nanotip photoemission,” *Nature Physics* **10**, 432 (2014).
- Wong, L. J., B. Freelon, T. Rohwer, N. Gedik S. G. Johnson, “All-optical three-dimensional electron pulse compression,” *New J. Phys.* **17**, 013051 (2015).
- Xiang, D., et al., “Accelerator-based single-shot ultrafast transmission electron microscope with picosecond temporal resolution and nanometer spatial resolution,” *Nucl. Instrum. Meth. A* **759**, 74 (2014).
- Yamamoto, M., N. Nishimori, “High voltage threshold for stable operation in a dc electron gun,” *Appl. Phys. Lett.* **109** 014103 (2016).
- Yang, J. M. Guehr, T. Vecchione, et al., “Diffractive imaging of a rotational wavepacket in nitrogen molecules with femtosecond megaelectronvolt electron pulses,” *Nat. Commun.* **7**, 11232 (2016).
- Yu, L.-L., et al., “Two-Color Laser-Ionization Injection,” *Phys. Rev. Lett.* **112**, 125001 (2014).
- Zhang, H., et al., “An ultrabright and monochromatic electron point source made of a LaB6 nanowire,” *Nature Nanotechnology* **11**, 273 (2016); DOI: 10.1038/NNANO.2015.276.
- Zholents, A. A., “Method of an enhanced self-amplified spontaneous emission for x-ray free electron lasers,” *Phys. Rev. STAB* **8**, 040701 (2005).
- Zholents, A. A., “Method of an enhanced self-amplified spontaneous emission for x-ray free electron lasers’, *Phys. Rev. STAB* **8**, 040701 (2005).
- Zhou, F., et al., “Impact of the spatial laser distribution on photocathode gun operation,” *Phys. Rev. Accel. Beams* **15**, 090701 (2012).
- Zhou, Q. J., et al., “Architecture of the synaptotagmin-SNARE machinery for neuronal exocytosis,” *Nature* **525**, 62 (2015).
- Zhu, P., et al., “Femtosecond time-resolved MeV electron diffraction,” *New J. Phys.* **17**, 063004 (2015).
- Zolotorev, M., E. D. Commins, F. Sannibale, “Proposal for a Quantum-Degenerate Electron Source,” *Phys. Rev. Lett.* **98**, 184801 (2007).

## APPENDIX A: LIST OF PARTICIPANTS

---

### Workshop Co-Chairs

Xijie Wang, SLAC National Accelerator Laboratory

Pietro Musumeci, University of California - Los Angeles

### Invited Speakers

Ivan Bazarov, Cornell University

David Muller, Cornell University

Paul Emma, SLAC National Accelerator Laboratory

Swapan Chattopadhyay, Northern Illinois University

### Panel Co-chairs

Katherine Harkay, Argonne National Laboratory, Panel 1

Alan Fry, SLAC National Accelerator Laboratory, Panel 1

Bruce Dunham, SLAC National Accelerator Laboratory, Panel 2

Jacek Sekutowicz, Deutsches Elektronen-Synchrotron, Panel 2

Bruce Carlsten, Los Alamos National Laboratory, Panel 3

John Power Power, Argonne National Laboratory, Panel 3

Phillipe Piot, Northern Illinois University, Panel 4

Carl Schroeder, Lawrence Berkeley National Laboratory, Panel 4

### Participants, Panel # 1

Howard Padmore, Lawrence Berkeley National Laboratory

Luca Cultrera, Cornell University

Nathan Moody, Los Alamos National Laboratory

John Smedley, Brookhaven National Laboratory

Schroeder Andreas, University of Illinois

Keith Jensen, U.S. Naval Research Laboratory

Markus Babzien, Brookhaven National Laboratory

Fay Hannon, Thomas Jefferson National Accelerator Facility

Siddharth Karkare, Lawrence Berkeley National Laboratory  
Theodore Vecchione, SLAC National Accelerator Laboratory  
Daniele Filippetto, Lawrence Berkeley National Laboratory  
Dave Dowell, SLAC National Accelerator Laboratory

### **Participants, Panel # 2**

Fernando Sannibale, Lawrence Berkeley National Laboratory  
Masahiro Yamamoto, The High Energy Accelerator Research Organization  
Weishi Wan, Lawrence Berkeley National Laboratory  
Andrew Minor, University of California - Berkeley  
Renkai Li, SLAC National Accelerator Laboratory  
Joseph Frisch, SLAC National Accelerator Laboratory  
John Lewellen, Los Alamos National Laboratory  
David Flannigan, University of Minnesota  
Ji Qian, Lawrence Berkeley National Laboratory  
Andre Arnold, Helmholtz-Zentrum Dresden-Rossendorf  
Chad Mitchell, Lawrence Berkeley National Laboratory  
Kwang-je Kim, Argonne National Laboratory

### **Participants, Panel # 3**

James B. Rosenzweig, University of California - Los Angeles  
Yimei Zhu, Brookhaven National Laboratory  
Jared Maxson, University of California - Los Angeles  
Cecile Limborg, SLAC National Accelerator Laboratory  
Steve J. Russell, Los Alamos National Laboratory  
Feng Zhou, SLAC National Accelerator Laboratory  
Zhentang Zhao, Shanghai Institute of Applied Physics  
Paolo Craievich, Paul Scherrer Institute

#### **Participants, Panel # 4**

Mingwei Chen, Johns Hopkins University

William Graves, Arizona State University

Brett Barwick, Trinity College

Emilio Nanni, SLAC National Accelerator Laboratory

Matthias Fuchs, University of Nebraska - Lincoln

Wei Gai, Argonne National Laboratory

Jeroen van Tilborg, Lawrence Berkeley National Laboratory

Juhao Wu, SLAC National Accelerator Laboratory

Felicie Albert, Lawrence Livermore National Laboratory

Heather Andrews, Los Alamos National Laboratory

Karren More, Oak Ridge National Laboratory

Mark Hogan, SLAC National Accelerator Laboratory

#### **DOE Office of Science**

Eliane Lessner, U.S. Department of Energy, Basic Energy Sciences

James Murphy, U.S. Department of Energy, Basic Energy Sciences

Eric Colby, U.S. Department of Energy, High Energy Physics

Manouchehr Farkhondeh, U.S. Department of Energy, Nuclear Physics

# APPENDIX B: WORKSHOP AGENDA

## Basic Energy Science Workshop on Future Electron Sources

September 8-9, 2016, SLAC , Menlo Park, CA 94025, USA

Workshop Co-Chairs: Pietro Musumeci (UCLA) & Xijie Wang (SLAC)

DOE BES contact: Eliane Lessner

### Wednesday, September 7, 2016

06:30 - 08:00 PM *Welcome Reception - SLAC Bldg 53 Lobby and Exhibit Hall*

### Thursday, September 8, 2016

07:30 - 08:30 AM *Registration/Breakfast - SLAC Bldg 53 Panofsky Auditorium Hallway*

### Opening Plenary Session - Bldg. 53 Panofsky Auditorium

08:25 - 08:45 AM **DOE BES Welcome and Workshop Charge**  
E. Lessner / J. Murphy

08:45 - 09:00 AM **Workshop Introduction**  
P. Musumeci / XJ Wang, Co-Chairs

09:00 - 09:40 AM **Plenary 1: Future Needs of Electron Source for X-ray FELs**  
P. Emma, SLAC National Accelerator Laboratory

09:40 - 10:20 AM **Plenary 2: Future Needs of Electron Source for Electron Scattering Instrumentations**  
D. Muller, Cornell University

10:20 - 10:40 AM *Coffee Break*

10:40 - 11:20 AM **Plenary 3: High Brightness Electron Sources**  
I. Bazarov, Cornell University

11:20 - 12:00 PM **Plenary 4: Novel Electron Sources**  
S. Chattopadhyay, Northern Illinois University / Fermilab

12:00 - 01:00 PM *Working Lunch Buffet*

12:40 - 01:00 PM **Panel Introductions - Panel Co-Chairs**

#### Panel 1: Science and Technology of Electron Generation

K. Harkay      Argonne National Laboratory  
A. Fry          SLAC National Accelerator Laboratory

#### Panel 2: CW Electron Sources

B. Dunham      SLAC National Accelerator Laboratory  
J. Sekutowicz    Deutsches Elektronen-Synchrotron

#### Panel 3: Pulsed Injectors

B. Carlsten      Los Alamos National Laboratory  
J. Power          Argonne National Laboratory

#### Panel 4: Exotic Sources: cold atoms, plasma-based, tips, THz guns

P. Piot          Northern Illinois University  
C. Schroeder      Lawrence Berkeley National Laboratory

01:00 - 05:30 PM	<b>Parallel Panel Sessions: BES Facility Needs and Technical Challenges</b> <b>Breakout Rooms</b>  <b>Panel 1:</b> Trinity-A, Rm. 1350-B, Bldg. 53 <b>Panel 2:</b> Trinity-B, Rm. 1350-B, Bldg. 53 <b>Panel 3:</b> Almanor, Rm. 3002, Bldg. 53 <b>Panel 4:</b> Havasu, Rm. 3004, Bldg. 53
03:00 - 03:20 PM	<i>Coffee Break</i>
06:00 - 07:30 PM	<i>Working Dinner Buffet</i> <b>Parallel Panel Sessions: Future Directions and Priority Research Directions</b> <b>Breakout Rooms</b>
07:30 - 08:10 PM	<b>Plenary Session: Panel Reports on <u>BES Facility Needs and Challenges</u></b> <b>Bldg. 53 Panofsky Auditorium</b>
<b>Friday, September 9, 2016</b>	
07:30 - 08:30 AM	<i>Breakfast</i>
08:30 - 09:00 AM	<b>Plenary Session: Workshop Expectations and Report</b> <b>Bldg. 53 Panofsky Auditorium</b>
09:00 - 12:00 PM	<b>Parallel Panel Sessions: Panel Priority Research Directions and Report Outline</b> <b>Breakout Rooms</b>
10:20 - 10:40 AM	<i>Coffee Break</i>
12:00 - 01:30 PM	<i>Working Lunch Buffet</i>
12:30 - 01:30 PM	<b>Plenary Session: Panel Reports on Priority Research Directions</b> <b>Bldg. 53 Panofsky Auditorium</b>
01:30 - 04:00 PM	<b>Parallel Panel Sessions: Workshop Report Writing</b> <b>Breakout Rooms</b>
03:00 - 03:20 PM	<i>Coffee Break</i>
04:00 - 04:30 PM	<b>Closing Remarks</b>
04:30 PM	<b>Workshop Adjourned</b>